TÉCNICO LISBOA

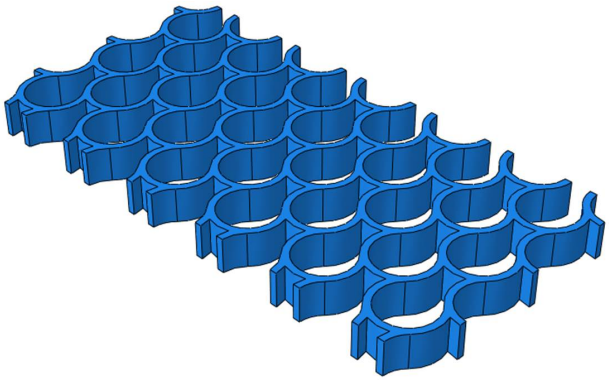

Development and evaluation of new concepts in the design of honeycombs used in composite panels

Jordi Bru Revert

Thesis to obtain the Master of Science Degree in

Engineering and Industrial Management

Supervisors:

Professor Maria de Fátima Reis Vaz

Professor Augusto Manuel Moura Moita de Deus

Examination committee

Chairperson: Professor Ana Isabel Cerqueira de Sousa Gouveia Carvalho

Supervisor: Professor Maria de Fátima Reis Vaz

Member of the committee: Professor Luis Filipe Galrão dos Reis

March 2019

To my family for their unconditional support.

Acknowledgements

First of all, I would like to express my thankfulness to my two supervisors, Professor Maria de Fátima Reis Vaz and Professor Augusto Moita de Deus, for the opportunity to conduct this research, for their help, support, encouragement and dedicated guidance, without them, this dissertation would not have been carried out. Their patience and availability during the whole project is highly appreciated.

Secondly, I would like to thank Professor Nuno Frutuoso and Professor Manuel Sardinha for their help when the specimens were printed by FDM. In addition, I am grateful to the PhD student Pedro Costa for all his kind help and assistance in any problem that I had during my research.

Last but not least, I wish to thank all my family and friends for their unconditional support and understanding during all my period in Lisbon. Specially, I would like to express my extreme gratitude to my elder sister Anna, without her, nothing would have been possible. She was, is and will be my reference. Thanks as well to my youngest sister Laia for brightening my days of darkness. Finally, I would like to thank my girlfriend Julia for her love and patience in all this period.

Abstract

Sandwich panels have been widely used in many engineering applications where saving weight whilst maintaining high strength and stiffness is crucial. The increase in use of these structures highlights the need for a detailed study and development of new structural typologies to upgrade mechanical properties such as stiffness, strength and energy absorption. The sandwich panel cores are man-made cellular materials. The most common core is the two dimensional regular hexagonal cell shape, labelled honeycomb which has been used as the baseline of this study.

Two new bioinspired natural structures were developed to find improvements in the performance of sandwich panel cores, particularly in the in-plane properties. Among all the large amount of structures that nature provides, enamel and bamboo were chosen. The compressive and flexural properties of these two innovative cellular structures were assessed and compared against the classic honeycomb. To carry out this comparison, all the arrangements were numerically simulated with the Abaqus software for different relative densities. Finally, the fused deposition modelling (FDM) technique was used to print some selected samples in polylactic acid (PLA) that were experimentally tested. The ultimate goal of this methodology was to validate the results from the finite elements simulations with experimental data.

Results show that the mechanical properties depend on the core geometry and have a strong reliance on the relative density. Finally, for the same relative density, the bioinspired natural structures compete with the traditional core structures in what concerns to strength and stiffness.

Key-words: Cellular structure, compression test, three point bending test, numerical simulations, FDM.

Resumo

Os painéis em sanduíche têm sido amplamente utilizados em muitas aplicações de engenharia, onde diminuir o peso, mantendo a elevada resistência e rigidez, é crucial. A utilização crescente destas estruturas implica a necessidade de um estudo detalhado e do desenvolvimento de novas topologias que conduzam a uma melhoria das propriedades mecânicas, como rigidez, resistência mecânica e absorção de energia. Os núcleos do painel em sanduíche são, em geral, materiais celulares. A configuração mais comum dos núcleos é o arranjo hexagonal regular designado por honeycomb ou favo de mel, que foi usado como base do estudo.

Duas novas estruturas naturais bioinspiradas foram desenvolvidas de modo a melhorar no desempenho dos núcleos do painel sandwich. Entre toda a gama de estruturas que a natureza oferece, o enamel e o bamboo foram os escolhidos. As propriedades de compressão e flexão dessas duas estruturas celulares inovadoras foram avaliadas em comparação com o honeycomb clássico. Para realizar esta comparação, todas as configurações foram simuladas numericamente com o software Abaqus para diferentes densidades relativas. Finalmente, a técnica de fused deposition modelling (FDM) foi usada para imprimir algumas amostras selecionadas em ácido polilático (PLA) que foram testadas experimentalmente. O objetivo final da metodologia foi comparar os resultados das simulações de elementos finitos com os dados experimentais.

Os resultados mostraram que as propriedades mecânicas dependem da geometria do núcleo e têm uma forte dependência da densidade relativa. Finalmente, para a mesma densidade relativa, as estruturas bioinspiradas competem com as estruturas tradicionais no que diz respeito à resistência e rigidez.

Palavras-chave: Estruturas celulares, compressão, flexão, simulação numérica, FDM.

Contents

List of Figures

List of Tables

Nomenclature

E_s	Young modulus of the solid
ρ_s	Density of the solid
ρ^*	Density of the cellular material
ρ	Relative density
M_s	Solid mass
M_T	Total mass
V_S	Solid volume
V_T	Total volume
t	Cell wall thickness
l	Cell edge length
C_1	Experimental constant
D_1	Experimental constant
h	Dimension of the cell in the ribbon direction
θ	Cell angle
E_2^*	Young modulus in the X2 direction
v_{21}^*	Poisson's ratio in the X2 direction
G_{21}^*	Shear modulus in the X1-X2 plane
$(\sigma_{el}^*)_2$	Plateau stress for elastomeric honeycomb in the X2 direction
$(\sigma_{pl}^*)_2$	Plateau stress for plastic honeycomb in the X2 direction
$(\sigma_{cr}^*)_2$	Plateau stress for brittle honeycomb in the X2 direction
A_{hex}	Hexagonal area
r	Radius of the enamel structure
A_{enamel}	Enamel area
W	Width of the modules
L	Length of the modules
h	Height of the modules
D	Structures with relative density around 0.08
A	Structures with relative density around 0.10
B	Structures with relative density around 0.12
E	Structures with relative density around 0.14
C	Structures with relative density around 0.22
$t_{1,2,3,4}$	Graded thickness of the bamboo structure
σ_{vM}	von Mises stress
K	Initial stiffness
Ea	Absorbed energy
σ_{max}	Maximum stress
ε	Maximum strain

1. Introduction

One of the big targets in mechanical and design engineering is to achieve new load-carrying structures with high strength and stiffness whilst maintaining minimum structural weight. These requirements can be found in the sandwich panels composed by two stiff face sheets separated by some different type of thicker core. The core is a man-made cellular material which can be either honeycomb or foams [1]. The most extensively used core is the regular hexagonal honeycomb.

In the last years, many investigations have been carried out to study and analyse the structural and the mechanical properties of the honeycomb as a core under bending, compression or other loading conditions [1–3].

More recently, new core designs have been developed in order to enhance some properties of the classic honeycomb core [4,5]. Bioinspired natural materials can be an extended source of ideas in order to create new core designs and to mimic natural structures. All these complex shapes can be produced thanks to the additive manufacturing technology.

1.1. Aim of the thesis

The aim of this thesis is to develop new bioinspired cellular honeycomb structures and to study the mechanical properties under compression and three point bending (3PB) tests. The two proposed structures designated by enamel and bamboo will be compared to the baseline honeycomb configuration, which is the most common type of two-dimensional arrangement.

1.2. Background

Sandwich panels have been widely used in a range of applications in mechanical and aerospace engineering with aluminium and Kevlar being the most common materials in honeycomb panels. The increased use of honeycomb cellular structures in composite panels highlights the need for a detailed study and development of new structural typologies to improve mechanical properties such as strength, toughness, stiffness and energy absorption whilst achieving a lightweight component. The developments in additive manufacturing techniques, allows the fabrication of cellular structures with complex shapes.

1.3. Motivation

Within the scope of this dissertation, two new types of honeycomb structures were designed and manufactured based on bioinspired natural materials, enamel and bamboo. The outcome of this research has the potential to improve the performance of composites and introduce new technological advances in the engineering industry, if the new structures exhibit better in plane properties in comparison with honeycombs, formed by regular hexagonal cells.

1.4. Thesis structure

This document is divided into five different chapters. The first one is the current introduction followed by the literature review where the state of the art is discussed. The third chapter is

used to explain the methodology followed throughout the entire project and in the chapter four the results obtained are presented and discussed. Finally, chapter five summarises the conclusions and future work.

2. Literature review

2.1. Cellular materials

Cellular materials are made by an interconnected network of solid struts that form the face and edges of cells. These materials can be divided into two topological distinctions, the two-dimensional structures (honeycombs) and three dimensional structures (foams) [1].

On the one hand, honeycombs (Figure 2.1 (a)) are formed by polygonal cells organised in a horizontal plane and extruded forming a prismatic structure to fill the third spatial direction. This arrangement is simpler than the one of foams and will be the focus of this thesis. On the other hand, foams are made by polyhedral cells packed in three dimensions to fill the space. In addition, foams can be divided into open-cells and closed-cells. Open cells only gather the material on the edges (Figure 2.1 (b)), whilst closed cells have solid faces (Figure 2.1 (c)) [1].

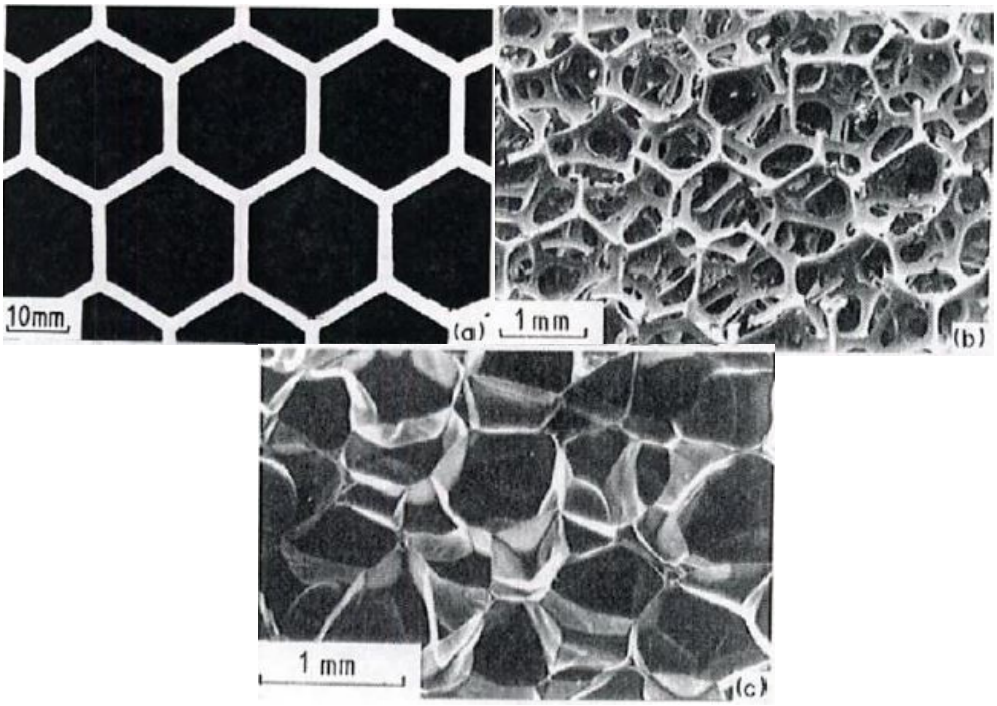

Figure 2.1: Examples of cellular materials. (a)Two-dimensional honeycomb, (b) three-dimensional foam with open-cells, and (c) three-dimensional foam with closed-cells [1].

The cellular solid properties depend mainly on the properties of the solid material that forms the walls and/or the faces (E_s, ρ_s, σ_s…), relative density (ρ^*/ρ_s that represents the volume fraction of the solid), the cell geometry (cell shape, open cell, closed cell…) and the cell size [1].

2.1.1. Relative density

Among all these properties the most important structural parameter is the relative density (ρ^*/ρ_s), which is the ratio of the cellular material density (ρ^*) over the density of the solid that the cell walls are made of (ρ_s) [1].

As it is shown in the following demonstration, the relative density represents a fraction of volume and can be represented as a porosity parameter [1].

$$\rho = \frac{\rho^*}{\rho_s} = \frac{M_s}{V_T} \cdot \frac{V_s}{M_T} = \frac{V_s}{V_T} = (1 - \text{Porosity}) \tag{2.1}$$

where M and V are the mass and the volume respectively with the sub index S and T indicating solid or total.

Gibson and Ashby defined in reference [1] that cellular structures have a relative density below 0.3 while any material with a value higher than this is considered to be a solid that contains isolated pores. Therefore, all the structures designed in this research have less than 0.3 of relative density.

The relative density can be related to the dimensions of the structure. If the cell-wall thickness is t, the cell-edge length is l and $t \ll l$ as shown in Figure 2.2 , then for the honeycombs:

$$\frac{\rho^*}{\rho_s} = C_1 \frac{t}{l} \tag{2.2}$$

where the constant C_1 is determined by experimental measurements. Expression (2.2) is not accurate enough when the relative density is large due to the double-counting problem, as corners are counted twice. In this case, another approach of the relative density is given by (2.3) where D_1 is a different constant that makes the approximation more complicated.

$$\frac{\rho^*}{\rho_s} = C_1 \frac{t}{l} \left(1 - D_1 \frac{t}{l}\right) \tag{2.3}$$

The new added term is important when t/l is large and it makes the relative density go to one when the cell thickness has the value that just causes the cell to fill completely. This happens for regular honeycombs when $t = \sqrt{3}\, l$, giving the following expression.

$$\frac{\rho^*}{\rho_s} = \frac{2}{\sqrt{3}} \frac{t}{l} \left(1 - \frac{1}{2\sqrt{3}} \frac{t}{l}\right) \tag{2.4}$$

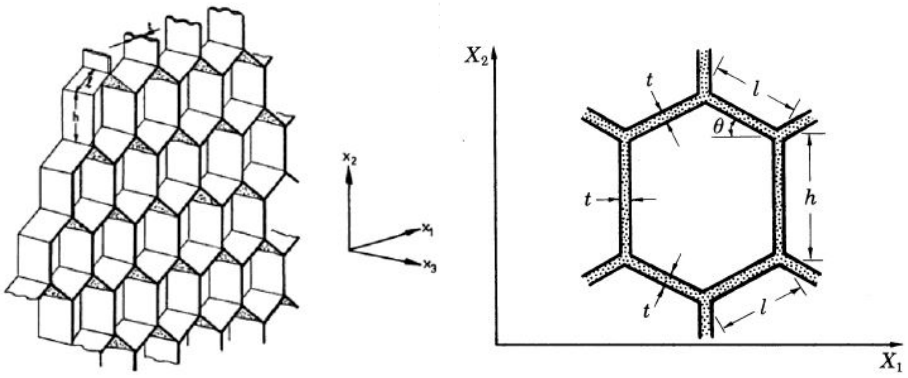

(a) (b)

Figure 2.2: (a) Honeycomb hexagonal cells, and (b) hexagonal unit cell [1].

2.1.2. Mechanical properties of the honeycombs

Honeycomb behaviour depends on which plane the mechanical properties are evaluated in. The in-plane behaviour is defined when the stress is applied in the $X_1 – X_2$ plane and the out-of-plane performance when the stress is applied in the X_3 direction (Figure 2.2). Additionally, in the $X_1 – X_2$ plane, the honeycomb has different properties that rely on the direction where the load is applied [1], and depend on the materials fabrication [6]. The “W” direction (Figure 2.3) is the expansion direction and the “L” direction is the core ribbon direction. The cell size is the distance between two opposite sides of the hexagonal cell [7].

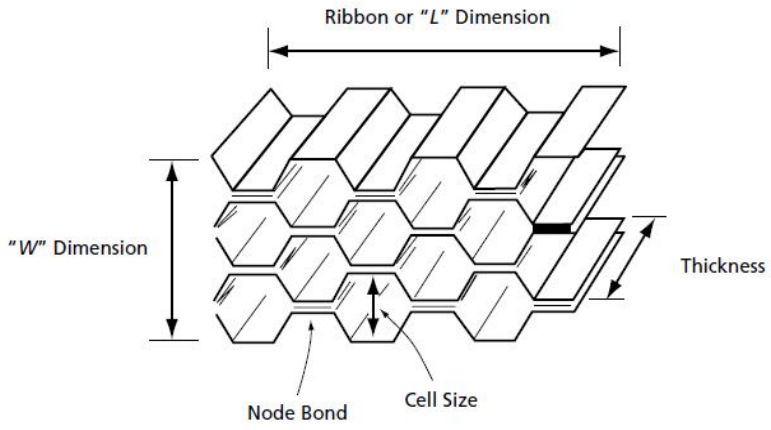

Figure 2.3: Typical terminology of honeycomb [6].

2.1.2.1 In-plane behaviour

In-plane deformation

To understand better the behaviour in this plane, compressive and tensile stress-strain curves are represented in Figure 2.4 for cell wall materials that have elastomeric, plastic and brittle behaviour [1].

Compressive stress-strain curves (Figure 2.4) have three differentiated areas. First of all, there is a linear elastic deformation caused by the cell walls bending. Beyond a critical stress and strain and depending on the cell wall materials, the cells collapse by elastic buckling, plastic yielding or brittle fracture. Finally, there is a densification part that starts when each cell wall is in contact with each other [1].

For the tensile stress-strain curves (Figure 2.4) the first part is the same as in compression, as cell walls bend giving a linear-elastic deformation, but in tension, elastomeric materials do not buckle and the stiffness rises due to cell walls rotation towards the tensile axis. For plastic materials, the behaviour is almost the same than in compression and for the brittle materials, the honeycomb fails [1].

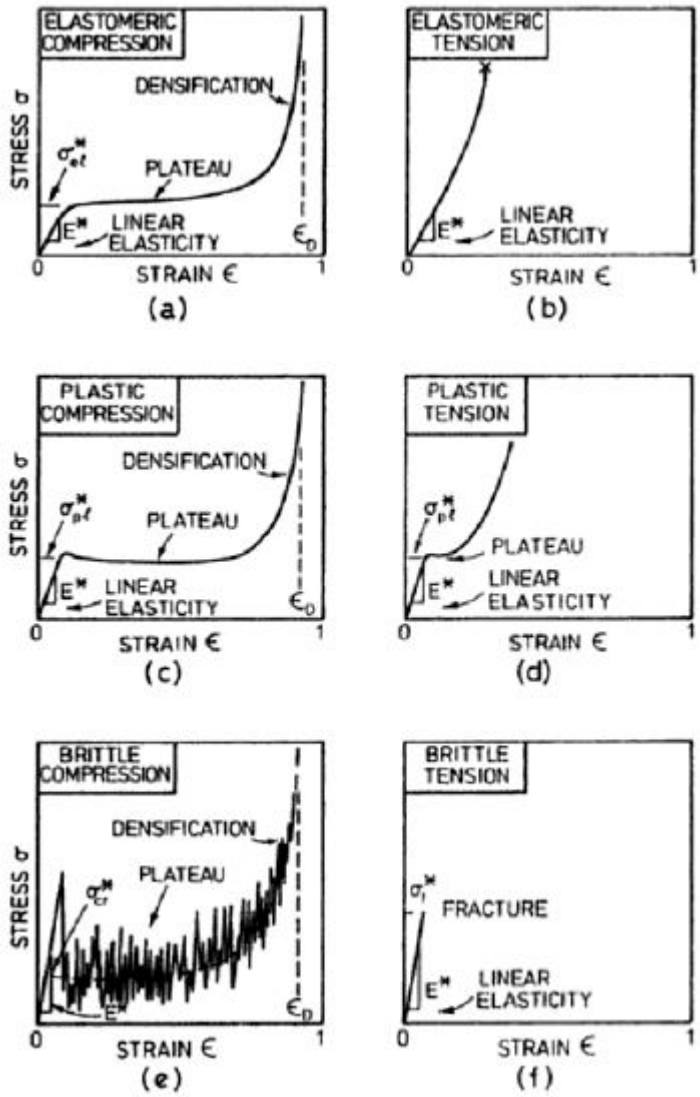

Figure 2.4: Honeycomb stress-strain curves (compression and tension): (a) and (b) for elastomeric material; (c) and (d) for elastic-plastic material; (e) and (f) for elastic-brittle material [1].

An enhancement of the relative thickness of the walls increases the relative density of the honeycombs. Subsequently, the resistance to cell collapse and cell wall bending rise up, giving a higher plateau stress and elastic modulus. As the cell walls are in contact sooner, the densification starts before and produces a reduction of the densification strain. Figure 2.5 shows how the curve stress-strain changes with the increase of the relative density for a honeycomb loaded in the $X_1 - X_2$ plane.

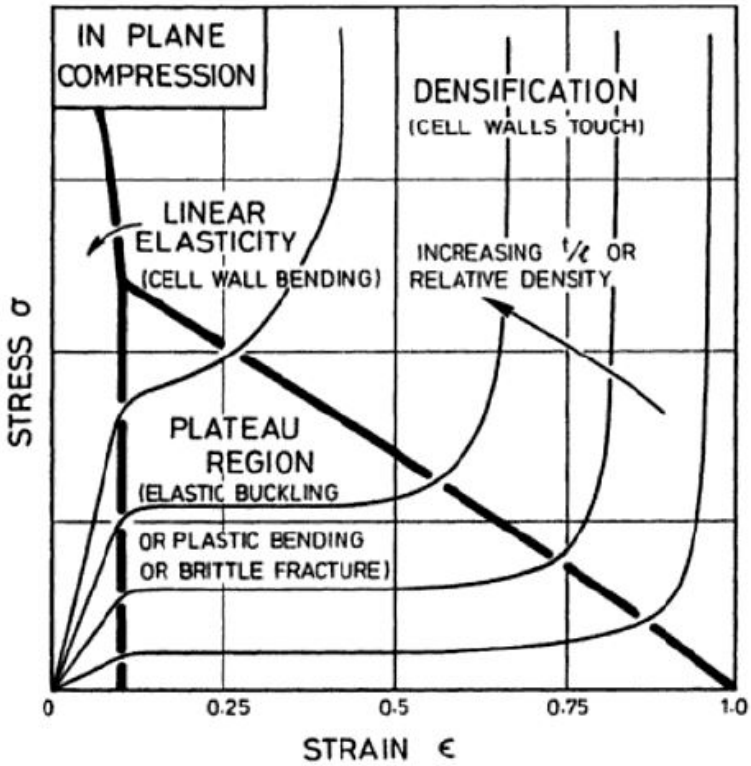

Figure 2.5: Diagram for in-plane compression honeycomb with different relative densities [1].

In-plane properties with uniaxial loading

For a honeycomb with h, l and θ parameters as shown in Figure 2.6 (a), and assuming that changes in the geometry due to deformation can be neglected, the relative density expression could be written as [1]:

$$\frac{\rho^*}{\rho_s} = \frac{{}^{t}/_{l}\,({}^{h}/_{l} + 2)}{2\cos\theta\,({}^{h}/_{l} + \sin\theta)}. \tag{2.5}$$

For regular cells ($h = l;\ \theta = 30°$) the expression reduces to:

$$\frac{\rho^*}{\rho_s} = \frac{2}{\sqrt{3}}\frac{t}{l}. \tag{2.6}$$

a) Linear-elastic deformation

The properties Young's modulus (E_2^*), Poisson's ratio (v_{21}^*) and shear modulus (G_{21}^*) are evaluated when the stress is applied in the X_2 direction as shown in Figure 2.6 (b). This will be the loading type that is analysed in the present work. For the applied stress in the X_1 direction, the expressions are evaluated in detail by Gibson and Ashby [1].

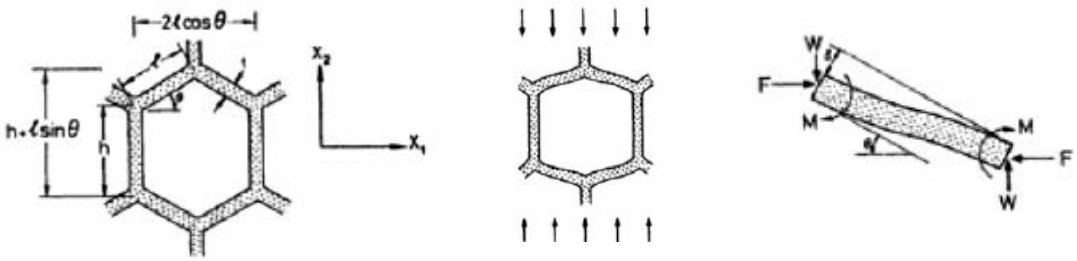

(a) (b)

Figure 2.6: Schematic unit cell, (a) parameters for underformed honeycomb, and (b) bending deformation caused by X_2 stress.

From expression (2.7) one can see that the Young's modulus, E_2^* depends on the solid property (first term), relative density (second term) and cell geometry (third term) [1].

$$E_2^* = E_s \left(\frac{t}{l}\right)^3 \frac{(h/l + \sin\theta)}{cos^3\theta}. \tag{2.7}$$

The reduced expression for regular hexagons with uniform wall thickness is:

$$E_2^* = 2.3\, E_s \left(\frac{t}{l}\right)^3. \tag{2.8}$$

The second characteristic parameter in the linear-elastic part is the Poisson's ratio (v_{21}^*). The following expression shows the dependences that the cell geometry has in the Poisson ratio.

$$v_{21}^* = \frac{(h/l + \sin\theta)\sin\theta}{cos^2\theta}. \tag{2.9}$$

For the regular hexagons the Poisson ratio has a unit value.

The last elastic parameter is the shear modulus (G_{21}^*) for shear in the X_1 – X_2 plane, which depends on the solid property (first term), relative density (second term) and cell geometry (third term).

$$G_{21}^* = E_s \left(\frac{t}{l}\right)^3 \frac{(h/l + \sin\theta)}{(h/l)^2 (1 + 2h/l)\cos\theta}. \tag{2.10}$$

For the regular uniform hexagons the shear modulus has the following expression:

$$G_{21}^{*} = 0.57\, E_s \left(\frac{t}{l}\right)^3 \tag{2.11}$$

b) Non linear elasticity

In the compression test, the second zone behaviour of the stress-strain curves is shown in Figure 2.4, and as it was mentioned before, depends on the material of the honeycomb walls. For this reason, the next section is going to be divided in the three different material behaviours: elastic, plastic and brittle materials. For each case, the expression of the stress will be deduced [1].

1- Plateau stress: elastic buckling

The Plateau stress for elastomeric honeycombs such a rubber, is caused by elastic buckling. There is buckling only in the X_2 direction, as loads parallel to the X_1 direction only cause bending. The expression for the collapse stress $(\sigma_{el}^{*})_2$ is:

$$(\sigma_{el}^{*})_2 = \frac{n^2\pi^2}{24} E_s \left(\frac{t}{l}\right)^3 \frac{1}{(h/l)^2 \cos\theta} \tag{2.12}$$

where the factor n characterizes the rotational stiffness of the nodes that depends on h/l. Gibson and Ashby [1], give more information about this parameter. For regular hexagons $n = 0.69$ and the stress will be calculated as:

$$(\sigma_{el}^{*})_2 = 0.22\, E_s \left(\frac{t}{l}\right)^3. \tag{2.13}$$

2- Plateau stress: plastic yielding

Metals and many polymers have elastic-plastic behaviour. Collapse by plastic yielding occurs when the bending moment in the cell walls reach the entirely plastic moment. The collapse stress expression $\left(\sigma_{pl}^{*}\right)_2$ for the X_2 direction is:

$$\left(\sigma_{pl}^{*}\right)_2 = \sigma_{ys} \left(\frac{t}{l}\right)^2 \frac{1}{2\cos^2\theta}. \tag{2.14}$$

For regular hexagons, the stress is the same for both directions and the expression is:

$$\left(\sigma_{pl}^{*}\right)_2 = \frac{2}{3}\sigma_{ys} \left(\frac{t}{l}\right)^2. \tag{2.15}$$

3- Plateau stress: brittle crushing

Ceramic materials have this kind of behaviour and fail in a brittle manner. Cell wall bending-stress reaches the modulus of rupture (σ_{fs}) and wall fracture occurs. For the X_2 direction, the stress is given by:

$$(\sigma_{cr}^{*})_2 = \sigma_{fs} \frac{1}{3\,cos^2\theta} \left(\frac{t}{l}\right)^2 . \tag{2.16}$$

For regular hexagonal honeycombs the expression reduces to:

$$(\sigma_{cr}^{*})_2 = \frac{4}{9}\sigma_{fs} \left(\frac{t}{l}\right)^2 . \tag{2.17}$$

2.1.2.2. Out-of-plane behaviour

Regarding the out-of-plane properties, cellular materials have a good response when the load is applied in the X_3 direction. Properties such as strength and stiffness are lower in the in-plane than in the out-of-plane because when the stress is applied in the in-plane direction, the cell walls bend as opposed to the cell walls extending or compressing in the out-of-plane case [1].

On the one hand, for the compression in the X_3 direction, the initial phase presents linear-elastic behaviour. Depending on the cell wall materials, the cells collapse by elastic buckling (elastomeric materials) or plastic buckling (metals or polymers). As shown in Figure 2.7 (a), after collapse, there is a densification part where failure occurs as a consequence of the cells crushing.

On the other hand, for the honeycomb panels under tension, the curve presents linear-elastic behaviour until a determinate stress is attained and then, depending on the material, it will plastically yield or fracture, Figure 2.7 (b).

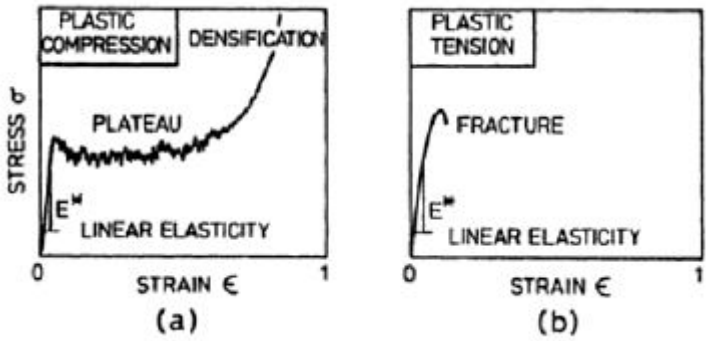

Figure 2.7: Stress-strain curves when the load is applied in the X_3 direction; (a) compression, and (b) tension [1].

Finally, as it happened on the in-plane behaviour, the stress-strain curves depend on the relative density. More detailed information about the expressions can be found in [1].

2.1.3. Honeycomb fabrication methods

Honeycomb structures can be manufactured in five different ways: resistance welding, diffusion bonding, brazing, thermal fusion and adhesive bonding. The first three methods are used for honeycomb structures that need to withstand very high temperatures and their costs are high. The most common fabrication process is adhesive bonding that has two basics techniques, expansion and corrugation method that are explained below [8].

Expansion method

The expansion process is typically used for the low density honeycomb cores ($\leq 160\ kg/m^3$) [7]. In Figure 2.8 there is a representative sketch of the expansion process. The sheets of the roll are cut with specific dimensions and adhesive strips are overlayed in certain areas. Afterwards, the sheets with the adhesive are stacked and cured under high temperature and pressure. Finally, the honeycomb before expansion is sliced with the correct thickness of the core and then, the sliced block is expanded to the proper honeycomb structure [8].

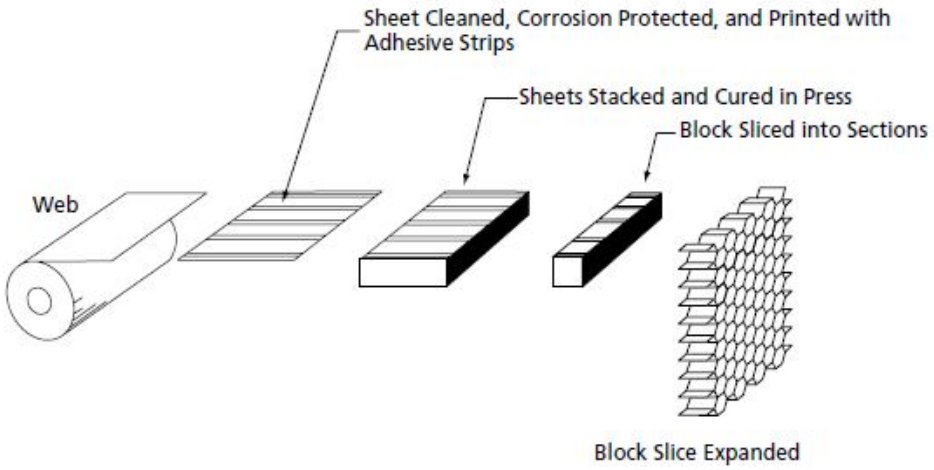

Figure 2.8: Expansion process of a honeycomb [8].

Metallic cores, such as aluminium, maintain their shape after the expansion process because of their plastic deformation, but non-metallic cores, such as aramid or glass, have to be held in the extended position and dipped in liquid epoxy, phenolic, polyester, or polyimide resin, which will be cured before the broadening force can be released. A repetition of dip and cure process times may be required to achieve the desired density [7].

Corrugation method

The corrugation process, illustrated in Figure 2.9, is more expensive than the expansion process and is used for high density honeycomb cores ($\geq 160\ kg/m^3$) as well as for those materials that cannot be made by expansion [7].

In this process, sheets are corrugated with the rolls and cut with a determinate length. Subsequently, adhesive is applied to the nodes of each sheet. Finally, in an oven, the sheets are stacked and cured [8].

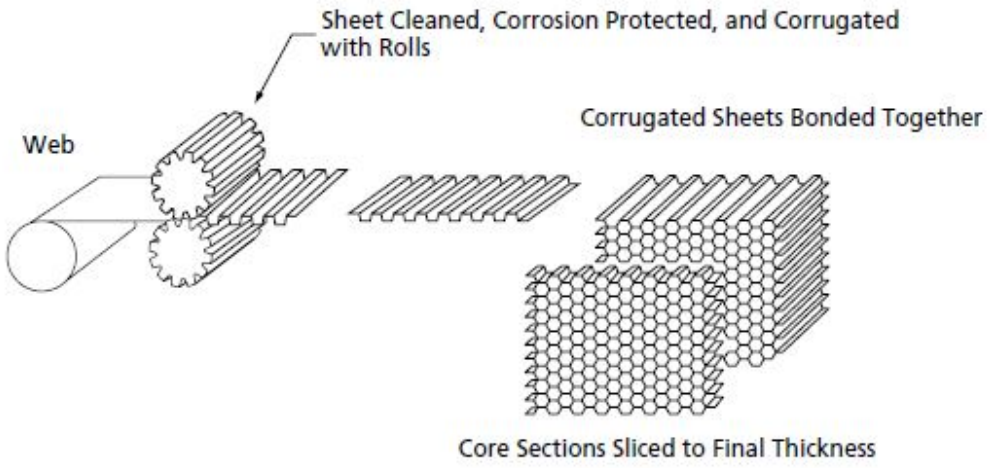

Figure 2.9: Corrugation process of honeycomb [8].

2.1.4. Types of honeycomb configurations

2.1.4.1. Honeycomb cores review

The most common honeycomb structures present a very efficient hexagonal cell shape with an outstanding performance in those applications in which stiffness is a critical property. Moreover, they can further upgrade their strength by reinforcing the cell configuration if longitudinal reinforcements are added in the "L" direction. The main problem of the hexagonal assemblies is the limited formability. They are very complicated to build and repair and have frequently experienced in-service durability problems. In addition, aluminium core structures could suffer from corrosion [7].

The most usual honeycomb cell shapes apart from hexagonal are flexible and square cores. These two configurations have some variations such as underexpanded, overexpanded and reinforced cores [8]. Flexible core was made to give better formability on compound contours without cell wall buckling. Overexpanded core is another configuration to enhance the formability which is a hexagonal core that has been overexpanded in the “W” direction. With this configuration the shear properties in the “W” direction increase while the shear properties in “L” direction decrease in comparison with regular hexagonal core [7].

Other honeycomb configurations, Lotus and Plateau have been recently studied [4,9].

2.1.4.2. Lotus configuration

Lotus configuration (Figure 2.10) can be described also as a quasi-2D material. It is a structure with a solid prismatic porous surface where the pores are prolonged along a single direction [9]. It may be fabricated by the unidirectional solidification of an insoluble gas and a mixture of molten parent material [10].

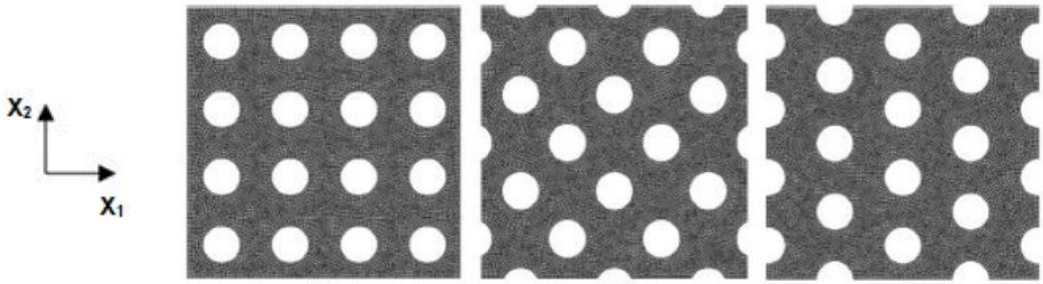

Figure 2.10: Lotus configuration with (a) aligned pores, (b) with 45º orientation, and (c) displaced [10].

2.1.4.3. Plateau configuration

The Plateau configuration, represented in Figure 2.11 is based on the regular hexagonal configuration, with the difference that it has circular edges with a radius of curvature r in the nodes, which are denoted as Plateau borders. The configuration with Plateau borders presents an accumulation of material that decrease the effective length of the struts and may affect the mechanical properties [9].

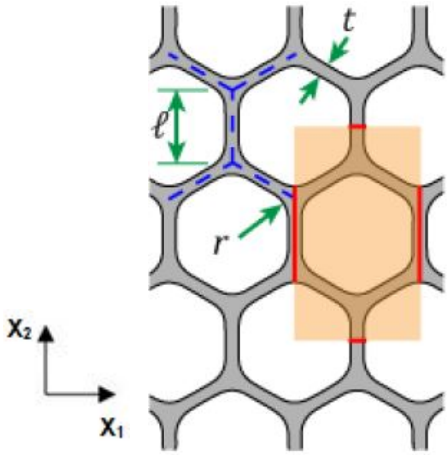

Figure 2.11: Honeycomb configuration with Plateau borders and $r = 0.4l$ [9].

2.1.5. Applications of cellular solids

Cellular solids have a lot of applications that can be divided in four areas: thermal insulation, buoyancy, packaging and structural uses [1]. The first three areas of application are going to be briefly commented in this section, but the fourth category which is structural uses, specifically sandwich panels, is the most relevant for this thesis and for this reason, it will be discussed in the next section.

For **thermal insulation**, there are some materials and structures, such as polymeric and glass foams, that provide a low thermal conductivity and can be used in a wide range of applications in fields such as transport systems, ships or modern buildings. A specific advantage of the ultra-low-temperature foam is the low thermal mass, reducing the refrigerant needed to cool in insulation applications.

Cellular materials are widely used in marine **buoyancy**. Closed-cell plastic foams are really good in damage-tolerance and their elevated water resistance make them ideal for this application, since they do not corrode.

Packaging, it is one of the most common uses of man-made cellular solids. Packages have the function of absorbing the impact energy and avoiding the content from suffering stress damage. Foams in particular are very good in this area.

Other applications of cellular material are filters; car catalyst, water-repellent membranes and some foams possess electrical properties that can be used as attenuation of the magnetic waves.

2.2. Composite materials as sandwich panels

Composite materials are those that use two or more materials possessing better properties together than if the individual components are used separately. The main advantage of composite materials is that they show high strength and stiffness combined with low density when compared with compact or bulk materials [7].

The idea of sandwich panels is very popular amongst all possible design concepts in composite structures due to the development of man-made cellular material as a core material. Sandwich panels are structures composed by two stiff face sheets which are bonded with some different type of lightweight core [1]. Sandwich structures exhibit high stiffness with high strength-to-weight ratios compared to normal plates [7]. The concept of the sandwich panels is that the core carries the shear loads, whereas the faces carry the bending loads (compression and tension). Sandwich panels work as an I beam as shown in Figure 2.12 [6].

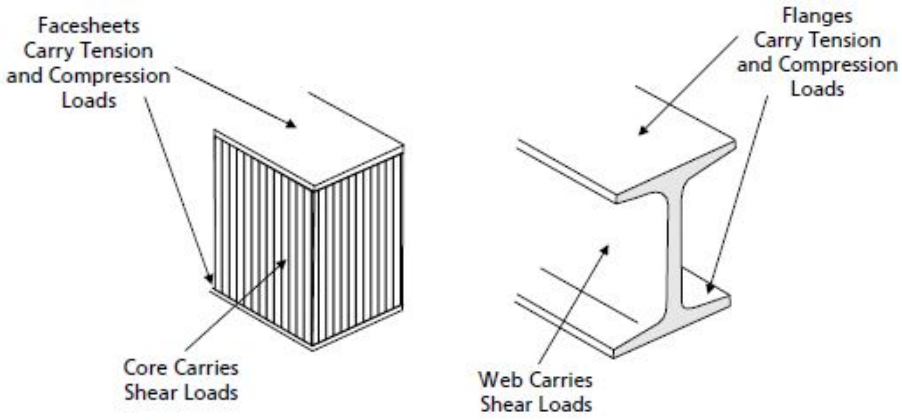

Figure 2.12: Sandwich panel composite compared to an I beam [6].

Table 2.1 shows how efficient honeycomb cores are in sandwich constructions, particularly in stiffness critical applications. The stiffness is multiplied by 7 with only a 3% weight gain when the thickness of the core is doubled. The stiffness is also increased over 37 times with just a 6% weight gain when the thickness is quadrupled. Whenever possible, sandwich constructions are used by structural designers mainly because of the weight saving in aerospace, building constructions, portable buildings or sports equipment [1,6,7].

Table 2.1: Structural efficiency of sandwich panels [6].

	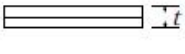	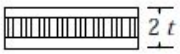	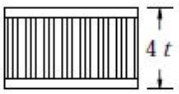
Relative Bending Stiffness	1	7.0	37
Relative Bending Strength	1	3.5	9.2
Relative Weight	1	1.03	1.06

The separation of the face sheets by the core raises the moment of inertia of the panel without a large increase in weight, making an efficient assembly that resists to bending and to buckling loads.

The core and face materials and their geometry determine the mechanical behaviour of the sandwich panels. Honeycomb core composites are lighter than core foams although foams provide thermal insulation besides structural support [1].

2.2.1. Honeycomb core materials

Honeycomb cores can be made of metallic materials, normally aluminium, and from non-metallic materials which include polymers such as aramid polymers (with trade names Kevlar or Nomex), Kraft paper, fiberglass, phenolic resin (which is the most common), epoxy and thermoplastic for toughness applications or polyimide for the high temperature applications [8].

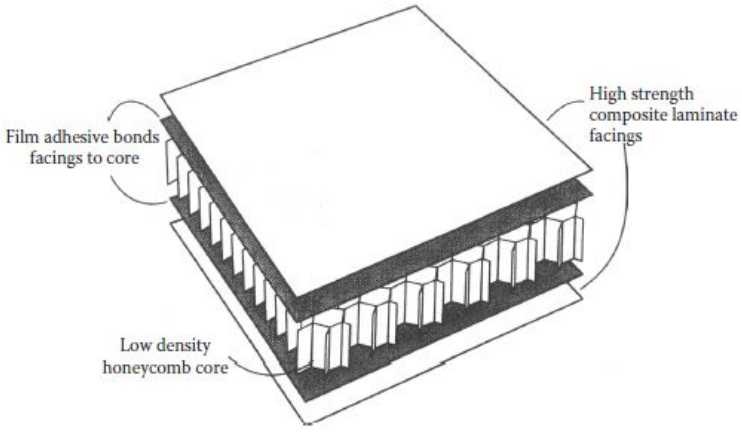

Figure 2.13: Composite sandwich structure with honeycomb core [11].

2.2.2. Foam core

Another type of core structure used in sandwich panels is foam. Foam cores properties are not as good as those of honeycomb cores but provide thermal insulation as well as structural support. Foam panels are widely used in commercial applications such as aircraft, construction or boat manufacturing. Sandwich structures made of foam cores are easier to build than the ones made of honeycomb cells [7].

As aforementioned, foams can be classified as open-cell or closed-cell. For structural applications almost all foams are made of closed cells because of their better mechanical properties in comparison with open cells. The density of the cores ranges from 32 to 640 Kg/m^3.

Foam structures are very different depending on which material is used. Polystyrene cores are lightweight with low cost but are barely used in structural applications because of their low mechanical properties. For moderate mechanical properties polyurethane foams are used. The most common material for sandwich panels is the polyvinyl chloride (PVC) that can be either crosslinked (thermoset) or un-crosslinked (thermoplastic). Un-crosslinked PVC is more damage resistant, tougher and easier to thermoform, whereas the crosslinked has better mechanical properties, temperature resistance and is more resistant to solvents.

Polymethylmethacrylimides (PMI) is used to achieve excellent mechanical properties, good heat resistance and good solvent resistance. These foams are only used for high performance aerospace applications due to the high cost of manufacturing.

2.3. Bioinspired natural materials

Engineers and scientists are fascinated by the qualities and the architectural complexity that natural structures have, which can offer a combination of exceptional mechanical properties with lightweight [12]. Pushed forward by people's concerns in environmental preservation and sustainability, research has been concentrated in the development of ultralight materials and structures based on natural materials which are denoted by bioinspired materials.

In biological systems, the design of structures and materials is closely connected but in synthetic materials, there is a separation between design structures (mechanical engineers) and materials (materials engineers) [13]. In this dissertation, the focus is going to be in the structure or geometry of the honeycomb cores to evaluate the mechanical properties and not in the material itself.

Biomimicry is the research of emulating and mimicking nature to seek sustainable design solutions for different human problems [14]. Mechanical engineering has mimicked many natural forms to create more efficient and better structures for various engineering purposes. However, mimicking the characteristics of natural materials is not easy, this being the biggest challenge that bioinspired natural materials present [12].

The design of bioinspired natural materials is not directly transferable to the engineering designs. There are some differences between the engineering strategies and the nature strategies. One of the main differences is the variety of elements and the manner in which materials are made (Figure 2.14) [15].

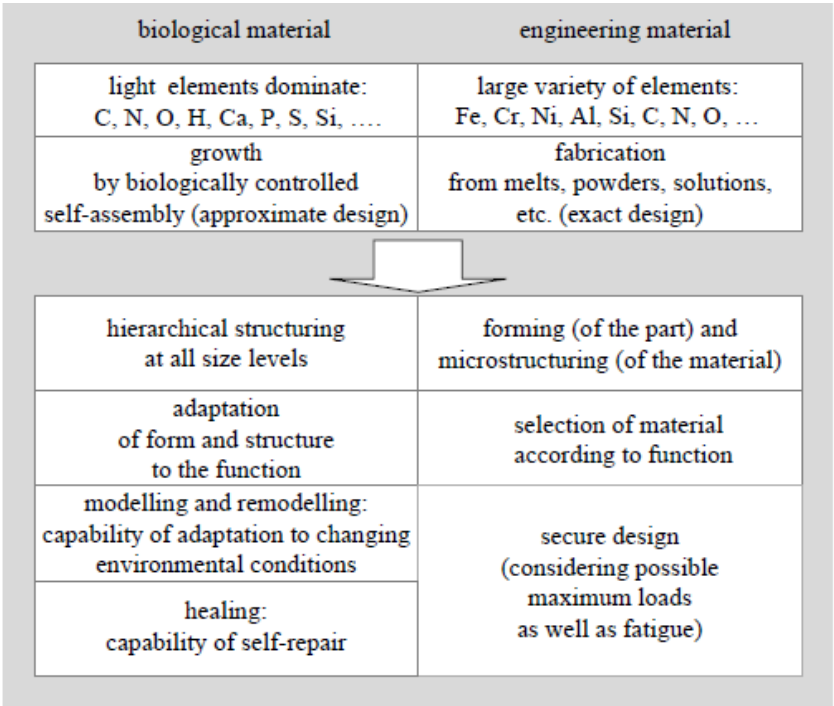

Figure 2.14: Different strategies to accomplish the desired functionality in engineering and in biology [15].

As shown in Figure 2.14, whereas engineers select the material to build a specific design, nature grows using the principle of self-assembling, providing control of the structure at all hierarchical levels [15]. Man-made structures are far from attaining the similar degree of architectural control [12]. In addition, the boundary conditions, that nature is exposed to, are very important for the growth of the contemplated structure. Growth is highly affected by external conditions such a mechanical loading, temperature, water or supply of light. Natural materials are able to adapt to changes in the environmental conditions and over millions of years of adaptation, nature has provided a variety of mechanically efficient materials [15].

Contrary to synthetic systems, another defining feature of natural materials and one of the most remarkable properties is the self-healing ability. Nearly all natural structures can be repaired by themselves after damage [15].

In this dissertation, two new bioinspired structures were designed, evaluated and characterized in order to be used as a replacement of honeycomb cores. Among all natural sources such as wood, enamel, nacre, bamboo, bone, fish scales, birds beak or palm [12], enamel and bamboo were selected to make new designs with the potential to achieve new technological advances in many industrial areas. Some features of enamel and bamboo will be explained in the next sections to understand a bit more of the behaviour of these materials.

2.3.1. Enamel structure

Enamel is the hardest biological tissue known. A tooth is principally formed of an external part called enamel and an internal region called dentin as shown in Figure 2.15. Enamel provides hardness and stiffness to the tooth because of its high degree of mineralization and its hierarchical microstructure. Thanks to enamel teeth are able to withstand a large range of imposed loads [13,16].

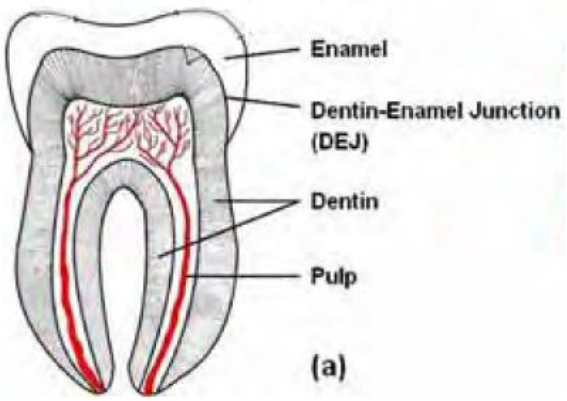

Figure 2.15: Internal parts of a tooth [13].

Enamel is composed by two microstructures, the hydroxyapatite rod (R) unit and the enclosing organic rich sheath structure (IR) (Figure 2.16 (a)). These two microstructures have different mechanical properties and for instance Young's modulus and hardness are higher in the rods than in the sheaths [17,18].

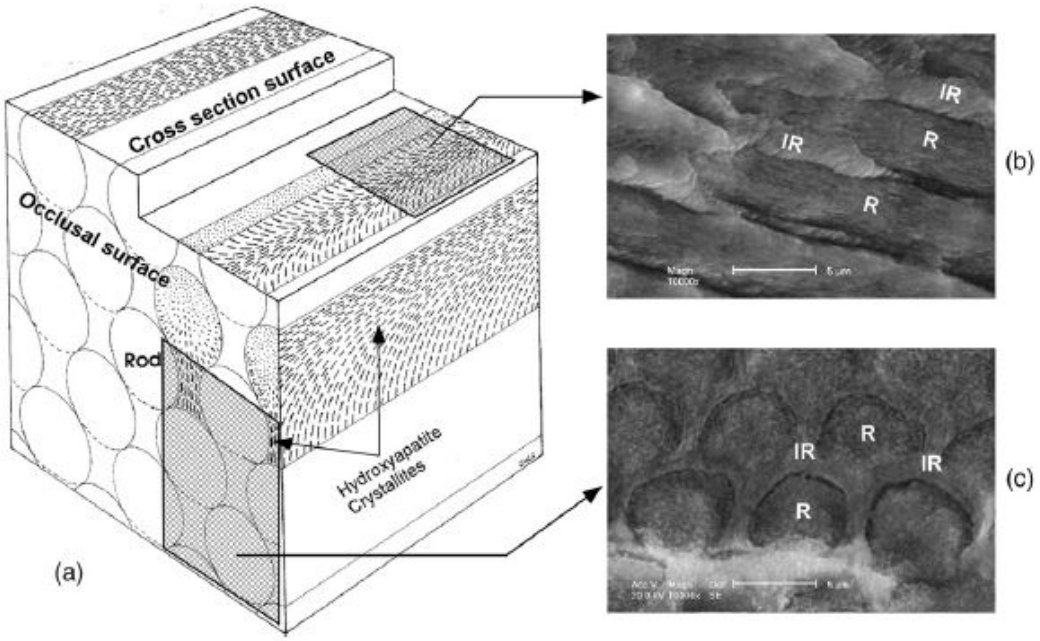

Figure 2.16: (a) Illustration of the enamel hierarchical structure. (b) and (c) scanning electron microscopy (SEM) images of the different faces. R is the rod and IR the inter rod [17].

Due to the anisotropic nature of the enamel, loads applied perpendicular to the occlusal surface (see Figure 2.16) show larger Young's modulus than in cross-section surface [19]. Enamel is really hard but at the same time brittle with a very low toughness. In spite of the fact that enamel is not a damage-tolerant material, it can withstand large forces attaining 1000 N many times per day during mastication [20].

2.3.2. Bamboo structure

Engineers, biologists, architects and material researchers have considered bamboo as a sustainable structural material. In comparison with other construction materials, bamboo presents good advantages because of its high bending capacity, lightness and the low and simple cost of the processing technique. Bamboo is the plant that grows the fastest on the earth as well as it is a renewable natural resource [21]. The potential applications of bamboo structure are developing a new field of investigation which has the capacity to change the manner that a lot of infrastructures are constructed nowadays. However, due to the lack of understanding of the properties and appropriate building codes, the applications of bamboo structures are still limited [22,23].

The main part of the bamboo macrostructure is the culm, a hollow cylindrical shoot that is separated into sections by nodes. The longitudinal spaces between the nodes are the internodes, as shown in Figure 2.17 [24].

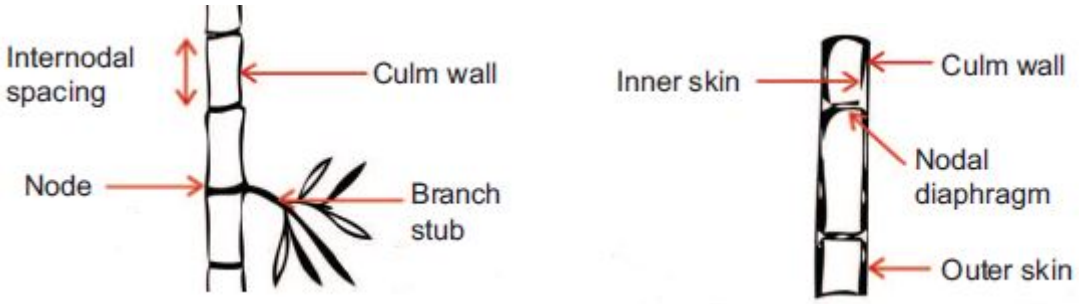

Figure 2.17: Parts of the bamboo macrostructure [25].

Moso bamboo (*Phyllostachys pubescens*), is the most common type of bamboo in which the diameter of the culm and the wall thickness decrease from the ground to the top [21].

In regards to the microstructure, bamboo can be treated as a composite material. It is formed by vascular bundles or fibers embedded in a matrix of lignin with parenchyma cells. Figure 2.18 depicts how the volume fraction of the vascular bundles fibers in the bamboo culm increases across the wall thickness, being this radial increment from the inside towards the outer part. Similarly, the volume fraction of fibers increases from the ground to the top [21].

Figure 2.18: Scanning electron microscopy (SEM) micrograph of wall thickness of Moso bamboo [26].

The increase of the volume fraction of fibers and the fraction of solid, provides a gradient of density in surface across the wall thickness of the bamboo culm. From the inside (low fiber density) to the outside (high fiber density) [21].The vascular bundles fibers are composed of empty vessels enclosed by fibrous sclerenchyma cells, as shown Figure 2.19 [24,27].

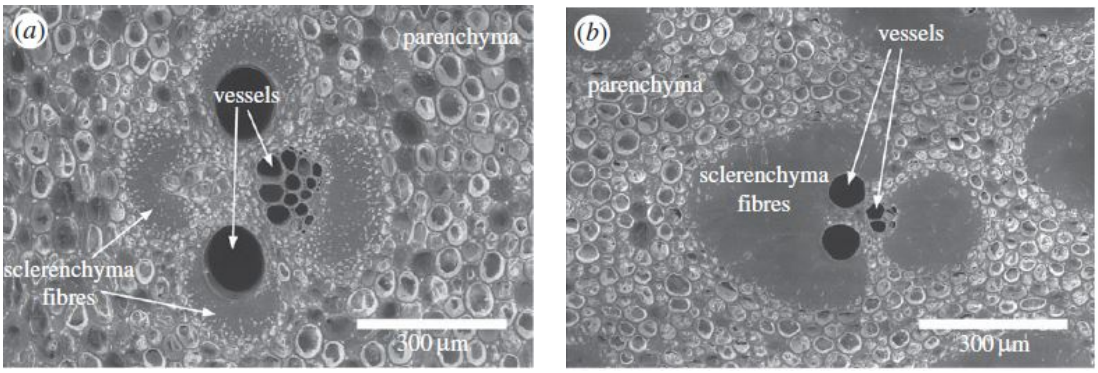

Figure 2.19: SEM micrograph of vascular bundles fibers, (a) inner surface, and (b) outer surface [26].

The volume fraction of solid in the vascular bundles fibers also increases towards the outer surface as the vessel dimensions decrease [21]. This gradation in the radial and longitudinal directions causes the strength to be higher in the outside surface than in the inside surface and as a consequence, bamboo structures tend to break up from the inside to the outside [28].

Figure 2.20, shows another scheme of the bamboo graded hierarchical structure that provides an efficient combination of stiffness and strength to weight ratio [29].

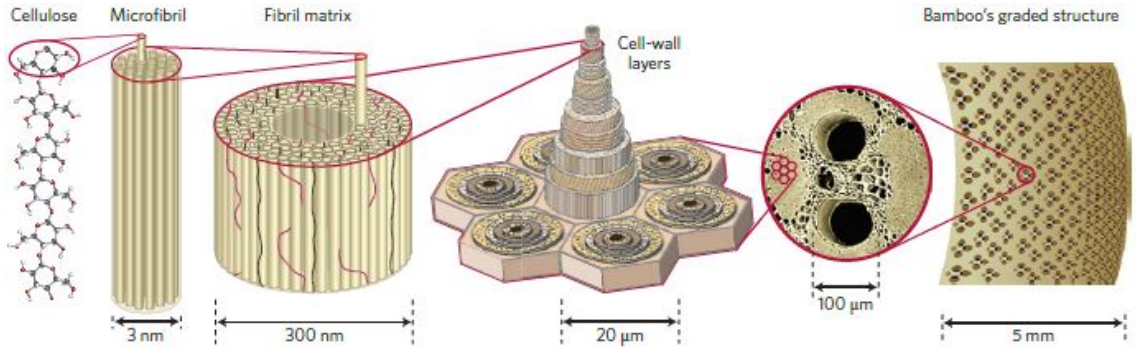

Figure 2.20: Bamboo graded hierarchical structure [12].

As the volume fraction of fibers increases and the dimension of vessels decrease across the thickness of the bamboo culm, from the outside to inside surface, the strength decreases from the outside to the inside, taking lower values at the inner parts.

2.4. Previous work

The present work is inserted into a series of studies performed by the supervisors of the thesis that focus on honeycomb configurations that could provide better properties than the conventional ones.

Recently, in the work published by Araújo et al. [4], new core geometries of sandwich panels were proposed as alternatives to the classic hexagonal honeycomb structure. These new cell configurations were named lotus and hexagonal honeycomb with Plateau borders, (Figure 2.21 (b) and (c)).

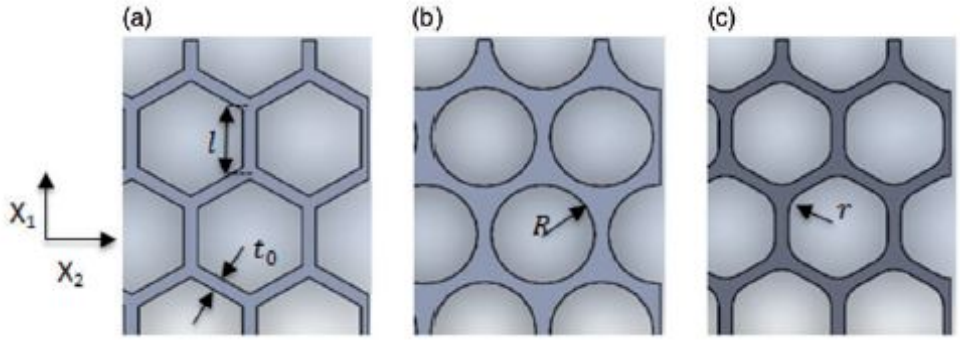

Figure 2.21: Schemes of cellular assemblies: (a) regular hexagonal honeycomb, (b) lotus structure, and (c) hexagonal honeycomb with Plateau borders [4].

Araújo et al. [4] studied the flexural behaviour of these structures with different relative densities.

For a high relative density, lotus has the highest flexural strength and the highest absorbed energy, but honeycomb shows the highest stiffness. However, for lower densities there was no such behaviour. To conclude, it was observed that there is a strong dependency of the relative density but there was not a single structure that gives the best mechanical properties in regards to stiffness, strength and energy absorption. The two proposed configurations provide an effective answer to the needs required for sandwich cores.

2.5. Additive manufacturing

As described by the American Society for Testing and Materials (ASTM), additive manufacturing (AM), is a manufacturing technique of building objects layer by layer using computer-aided design (CAD). Additive manufacturing has the main advantage that offers an effective method to produce complicated structures at a low cost and small investment in manufacturing infrastructure [30]. Nevertheless, this technology cannot be utilized neither to create a larger number of specimens nor large pieces [12].

There are many classifications for AM processes but one clear and intuitive was made by Kruth [31] according to the feedstock material adopted and is represented in Figure 2.22.

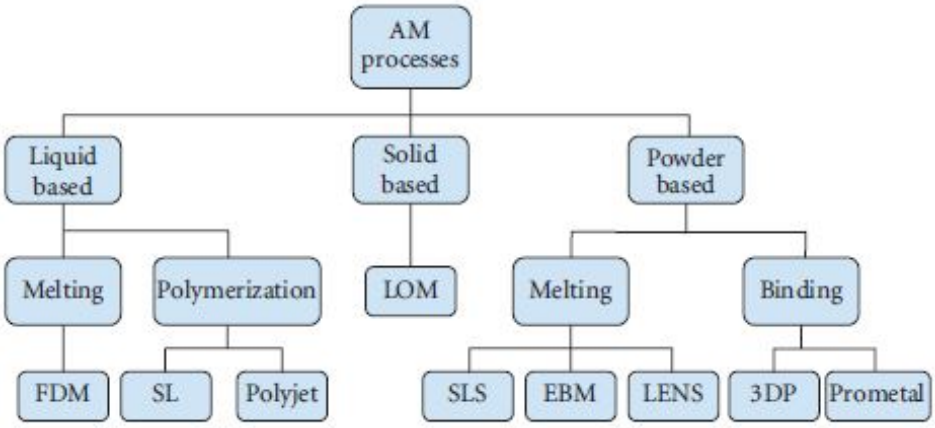

Figure 2.22: Classification of AM processes depending of the feedstock material [31].

Amongst all processes showed in Figure 2.22, fused deposit modelling (FDM) is the most common method. Figure 2.23 helps to explain how this technique works. The filament is fed via a pinch roller mechanism and afterwards, the feedstock is fused in a heated liquifier. The material goes through the print nozzle that is controlled by the software in the horizontal x-y plane. After depositing the material in the plane, the nozzle goes up and the piece accumulates material, in parallel layers in the vertical direction, until the desired thickness is achieved [32].

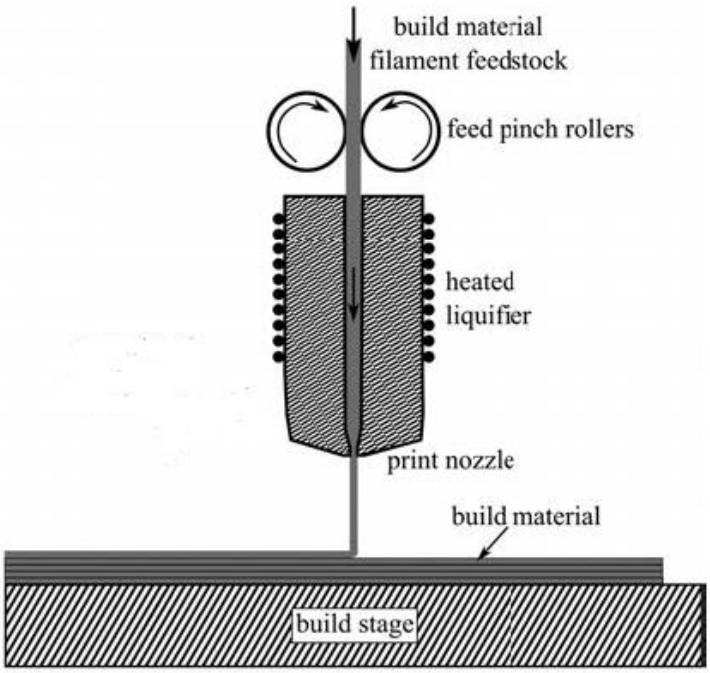

Figure 2.23: Extrusion-based additive manufacturing process fused deposit modelling [32]

The first materials used in additive manufacturing were paper laminates, waxes and polymeric materials. Lately, metals, ceramics and composite materials have been used, and research has been made, in order to improve the mechanical properties of the resulting object [30].

The materials are selected depending on the fabrication technique. For instance, photosensitive polymers such as epoxy, acrylate or hybrid resins are broadly used in photopolymerization-based 3D printing like stereolithography (STL). However, thermoplastic polymers such a polylactic acid (PLA) or acrylonitrile butadiene styrene (ABS), are extensively used for extrusion-based AM like FDM [30].

In regards to the AM applications, FDM parts have been successfully used in medical, automotive and aerospace applications. In the field of composites, AM processes have been widely used to build cellular materials and may give a way forward to manufacturing the future bioinspired natural materials because, it allows to build cost-effective and flexible designs of highly complex shapes [33,34].

3. Methodology

For the purposes of this research, three different cellular structures were designed in order to analyse the effect of the geometry in the mechanical properties of the resulting material by carrying out compression and three point bending tests. Configurations with different relative densities in each group of arrangements were studied through numerical simulations using the finite elements method (FEM) software ABAQUS. Finally, some samples were chosen to be printed with PLA material and subsequently tested in order to compare the results with the ones obtained in the numerical simulations.

3.1. Numerical simulations

3.1.1. Material

The material used in the simulations and in the FDM prototypes of the cells was polylactide or poly lactid acid, more known as PLA. PLA is a high-modulus, high-strength and thermoplastic polymer that can be efficiently manufactured on standard plastic devices to produce molded parts. In addition, PLA is a renewable and biodegradable aliphatic polyester with a wide field of application [35]. The most relevant properties for the current study are summarised in Table 3.1 [36,37], where the mechanical properties were determined previously on FDM printed samples by Fernandes et al. [38].

Table 3.1: PLA properties of samples printed by FDM.

	Amount	Units
Solid density	1252	Kg/m^3
Elastic modulus	1500	MPa
Poisson's ratio	0.36	-
Tensile strength	20	MPa
Elongation at break	7	%

3.1.2. Models

A total of twenty four models, with (four for each of the three configurations, either for bending and to compression tests) were created using the CAD software Autodesk Inventor 2016. The samples were built symmetrically with approximately the same size, when it was possible. For the compression test the dimensions of the specimens were around 136 x 118 x 10 mm^3 and for the 3PB test around 140 x 65 x 10 mm^3.

The first model to study is the classic regular hexagonal honeycomb (just honeycomb for the rest of the document) that was taken as the baseline to compare with the new configurations. Representative cell of this model are shown in Figure 3.1 (a).

For all the samples, the cell edge length l was constant ($l = 10\,mm$) and the cell wall thickness t was the parameter that was changed. For this reason, all the inside holes have the same area that was calculated according to the following expression.

$$A_{hex} = \frac{3\,l^2\sqrt{3}}{2} = 259.81\,mm^2$$

The second structure to analyse is the enamel, a biomimicked natural material. The structure that was proposed in this work was adapted from the enamel microstructure shown previously. The topology of the cell of the enamel model proposed here is represented in Figure 3.1 (b), where $r = 8.145\,mm$ for all the samples and t is the parameter that may be modified. The parameter r was calculated so that the inner cell area was equal to the one of the honeycomb, being $A_{enamel} = 259.81\,mm^2$.

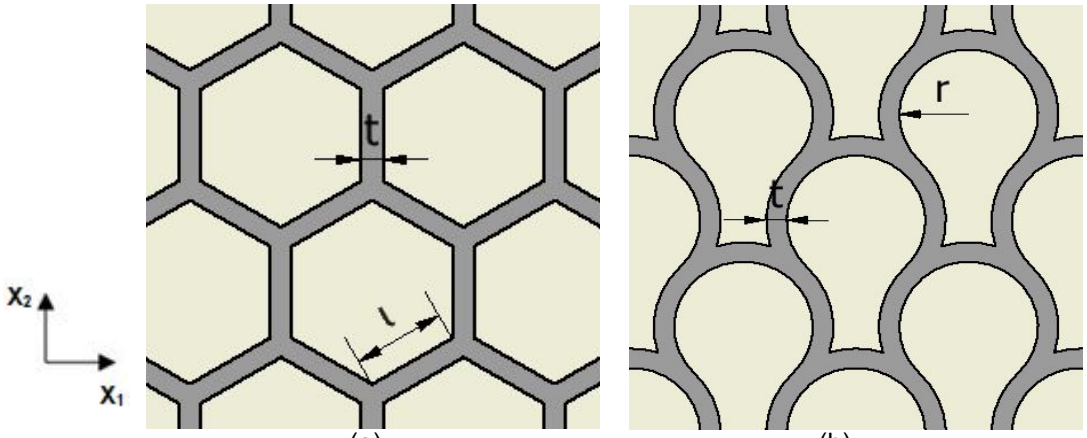

(a) (b)

Figure 3.1: Sketches of cellular assemblies: (a) regular hexagonal honeycomb, and (b) enamel.

Finally, the third configuration studied is the bamboo structure. As it was commented in section 2.3, imitating natural structures is not an easy task and the bamboo structure is an example of this. In this dissertation, based on the regular honeycomb structure it was applied the idea of graded structures, changing the cell wall thickness in order to have different strength of the cells. In this way, the wall-cell thickness increases from the inside to outside surfaces, so outside cells that possess larger thickness also have higher strength.

Two structures were designed to study this characteristic. The first structure, which is denoted by bamboo_1, is shown in the sketch of Figure 3.2. for samples that will be evaluated by bending and by compression. The cells in the middle of the samples have less thickness t_1 than the cells in the periphery t_3 or t_4 which we may consider to be longitudinal grading effect. The colours help to understand the way that the thickness changes.

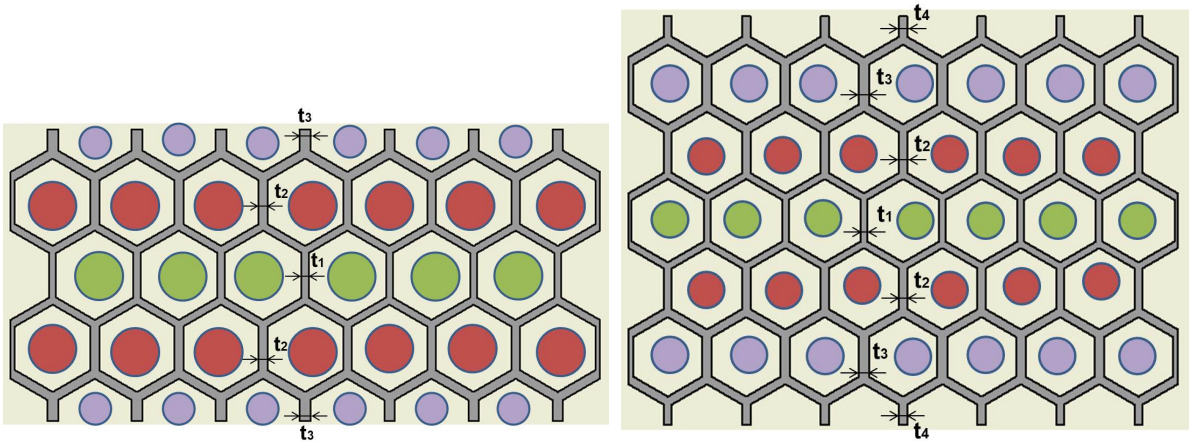

(a) (b)

Figure 3.2: Sketch for the configuration bamboo_1, (a) 3PB test, and (b) compression test.

The second structure named bamboo_2 is shown in Figure 3.3. The structure has a radial increase of the wall-cell thickness being thicker in the outside walls than in the inside walls.

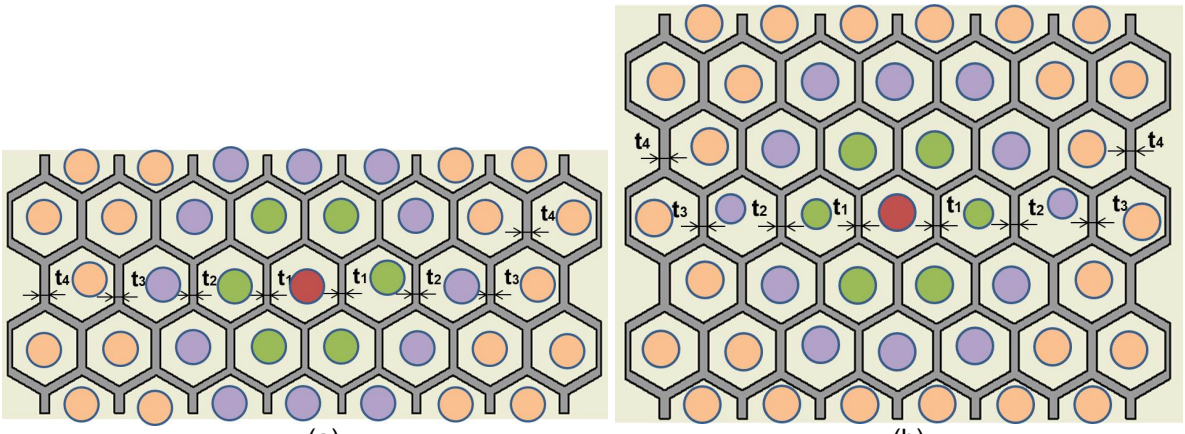

(a) (b)

Figure 3.3: Sketch for the configuration bamboo_2. (a) 3PB test, and (b) compression test.

3.1.2.1. Honeycomb configuration

The samples with the honeycomb configuration with four relative densities, designed either for compression and to bending tests are in this section.

Compression test

The four samples created for the compression test are represented in Figure 3.4 (a), (b) and Figure 3.5 (a), (b) from the lowest to the highest density, denoted by D, A, B and C. Samples have different relative densities, achieved by changing the cell wall thickness, changing from t=0.8 mm (Figure 3.4 (a)) to t=2.4 mm in (Figure 3.5 (b)). The designation A was used for t=1 mm, which was the starting arrangement. In addition, the principal properties of the cells and the whole specimens are summarised in Table 3.2, where V_T is the total volume, V_S is the volume occupied by the solid determined by the software and ρ is the relative density previously defined.

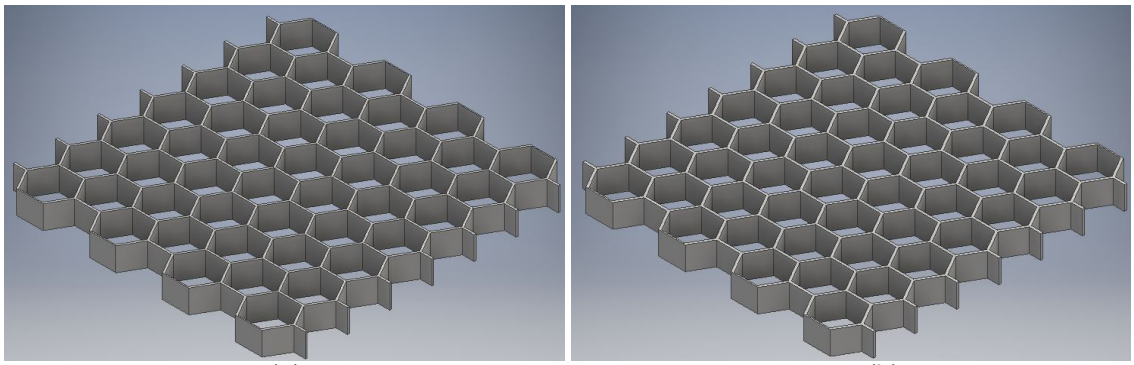

(a) (b)

Figure 3.4: CAD samples for the honeycomb compression test (a) honeycomb D, and (b) honeycomb A.

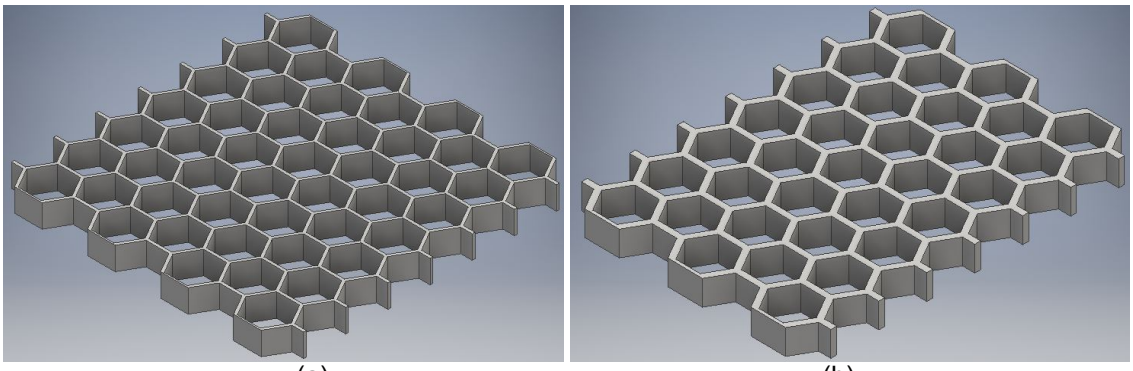

(a) (b)

Figure 3.5: CAD samples for the honeycomb compression test (a) honeycomb B, and (b) honeycomb C.

Table 3.2: Honeycomb compression specimens parameters.

	Cell parameters		Module parameters					
	t (mm)	l (mm)	W (mm)	L(mm)	h (mm)	V_T (mm^3)	V_S (mm^3)	ρ (-)
Honeycomb D	0.8	10	126.84	125.54	10	1.59×10^5	1.37×10^4	0.086
Honeycomb A	1	10	128.24	126.93	10	1.63×10^5	1.73×10^4	0.106
Honeycomb B	1.2	10	129.64	128.31	10	1.66×10^5	2.09×10^4	0.125
Honeycomb C	2.4	10	138.04	102.47	10	1.41×10^5	3.23×10^4	0.229

Three point bending test

The honeycomb samples created to perform the bending tests are illustrated in Figure 3.6 and Figure 3.7. Furthermore, the cell and sample properties are represented in Table 3.3.

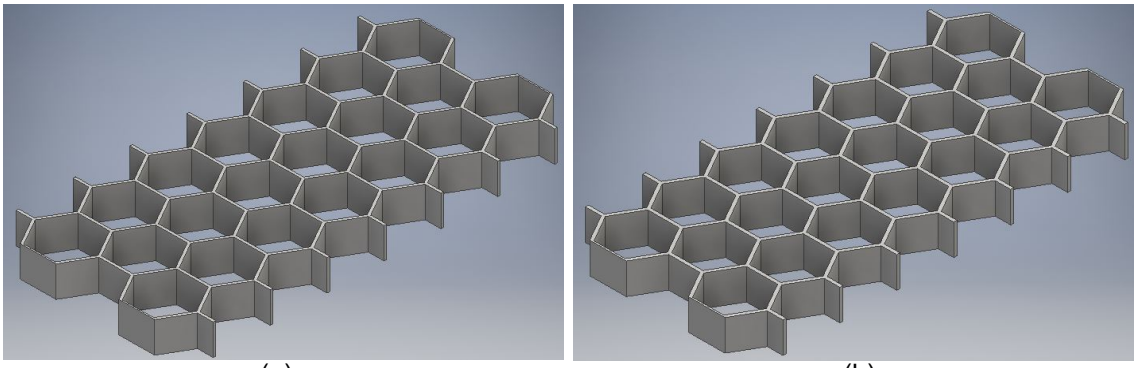

(a) (b)

Figure 3.6: CAD samples for the honeycomb bending test (a) honeycomb D, and (b) honeycomb A.

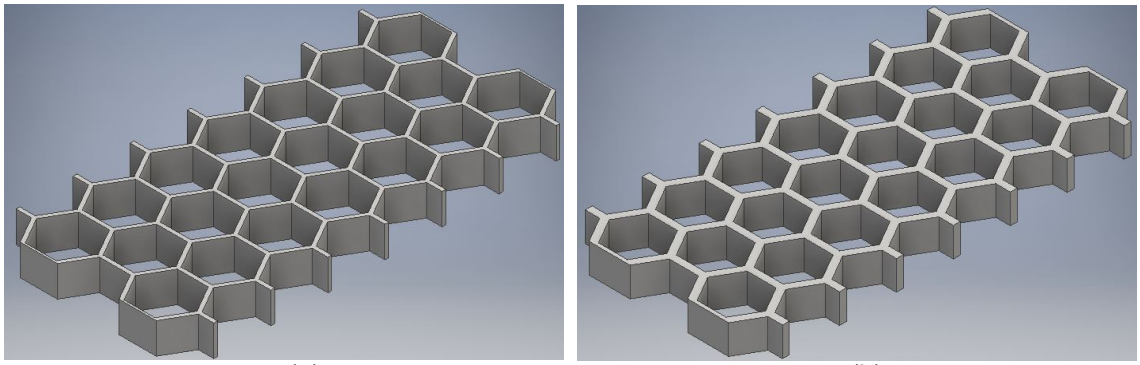

(a) (b)

Figure 3.7: CAD samples for the honeycomb bending test (a) honeycomb B, and (b) honeycomb C.

Table 3.3: Honeycomb bending parameters.

	Cell parameters		Module parameters					
	t (mm)	l (mm)	W (mm)	L(mm)	h (mm)	V_T (mm^3)	V_S(mm^3)	ρ (-)
Honeycomb D	0.8	10	126.84	62.77	10	7.96×10^4	6.88×10^3	0.086
Honeycomb A	1	10	128.24	63.46	10	8.14×10^4	8.64×10^3	0.106
Honeycomb B	1.2	10	129.64	64.15	10	8.32×10^4	1.04×10^4	0.125
Honeycomb C	2.4	10	138.04	68.31	10	9.43×10^4	2.16×10^4	0.229

3.1.2.2. Enamel configuration

The eight geometries created for the enamel samples are presented in the following sections, showing a table of the most characteristics parameters of cells and arrangements.

Compression test

Figure 3.8 and Figure 3.9 show the four samples with the enamel configurations created to perform this test and the respective features are exhibited in Table 3.4.

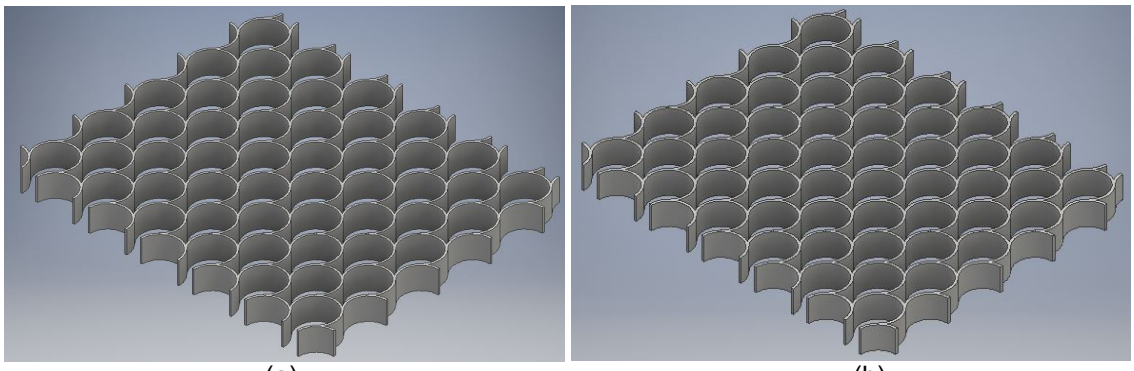

(a) (b)

Figure 3.8: CAD samples for the enamel compression test (a) enamel A, and (b) enamel B.

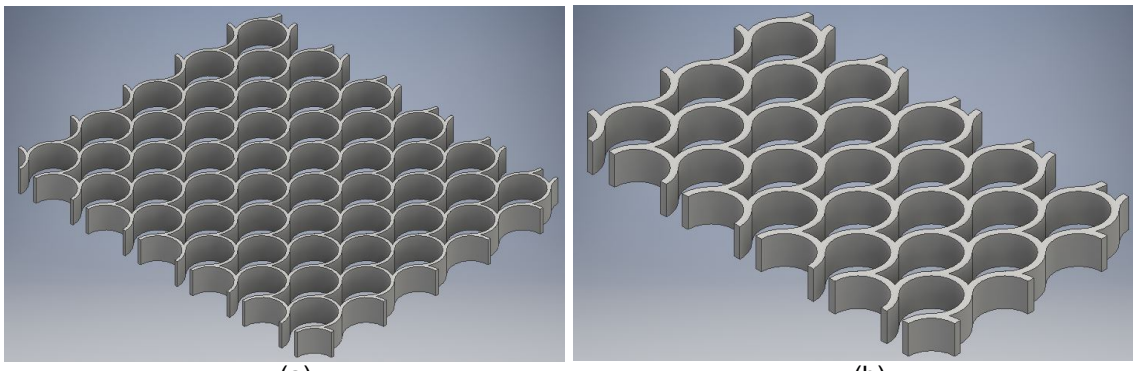

(a) (b)

Figure 3.9: CAD samples for the enamel compression test (a) enamel E and (b) enamel C.

Table 3.4: Enamel compression samples parameters.

	Cell parameters		Module parameters					
	t (mm)	r (mm)	W (mm)	L(mm)	h (mm)	V_T (mm3)	V_S(mm3)	ρ (-)
Enamel A	0.8	8.145	145.01	120.85	10	1.75×10^5	1.76×10^4	0.101
Enamel B	1	8.145	146.71	122.26	10	1.79×10^5	2.20×10^4	0.123
Enamel E	1.2	8.145	148.41	123.67	10	1.83×10^5	2.64×10^4	0.144
Enamel C	2	8.145	129.33	77.60	10	1.00×10^5	2.23×10^4	0.222

Three point bending test

The models built for the enamel bending tests are illustrated in Figure 3.10 and Figure 3.11. Table 3.5 contains all the geometric characteristics of the samples.

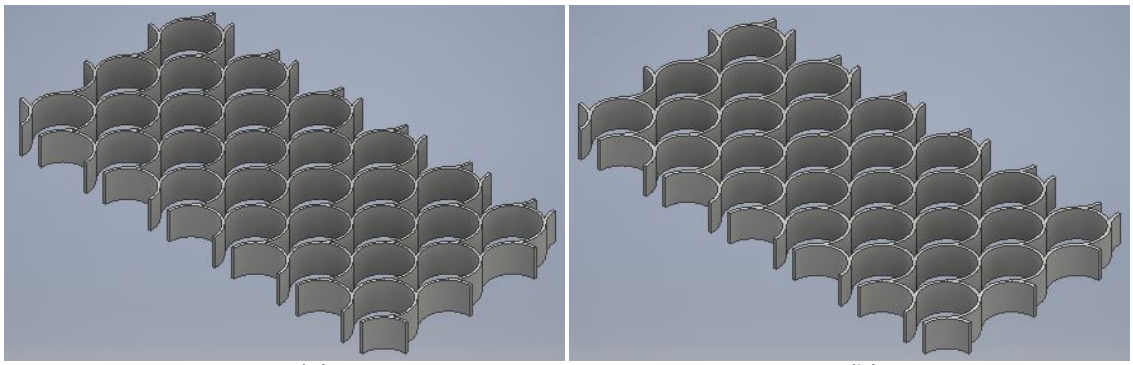

(a) (b)

Figure 3.10: CAD samples for the enamel bending test (a) enamel A, and (b) enamel B.

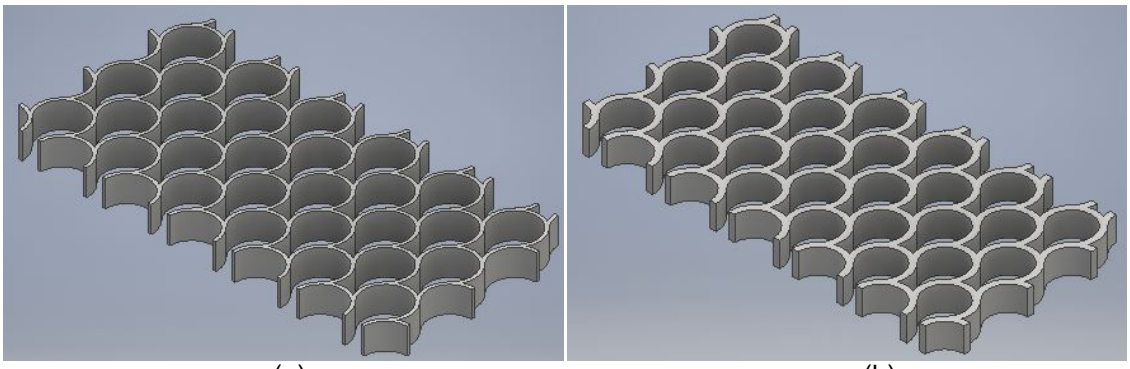

(a) (b)

Figure 3.11: CAD samples for the enamel bending test (a) enamel E, and (b) enamel C.

Table 3.5: Enamel bending samples parameters.

	Cell parameters		Module parameters					
	t (mm)	r (mm)	W (mm)	L(mm)	h (mm)	V_T (mm^3)	V_S(mm^3)	ρ (-)
Enamel A	0.8	8.145	145.01	72.51	10	1.05×10^5	1.06×10^4	0.101
Enamel B	1	8.145	146.71	73.36	10	1.08×10^5	1.32×10^4	0.123
Enamel E	1.2	8.145	148.41	74.20	10	1.10×10^5	1.59×10^4	0.144
Enamel C	2	8.145	155.20	77.60	10	1.20×10^5	2.68×10^4	0.222

The names of the samples modules, as it was commented before, are designated by the letters A, B, C and E, where in this case, letter A is for the lowest relative density and C for the highest relative density, as is indicated in Table 3.6.

The following table has a summary of the correspondence between letters and the relative density for honeycomb and enamel configurations.

Table 3.6: Letters associate an each relative density.

Letter	A	B	C	D	E
ρ (-)	≈ 0,10	≈ 0,12	≈ 0,22	≈ 0,08	≈ 0,14

3.1.2.3. Bamboo configuration

As it was highlighted before, two bamboo configurations were draw, bamboo_1 and bamboo_2, which are described in this section. To designate the bamboo structures, the first number means the number of the structure 1 or 2 and the second number indicates the initial value of the wall-cell thickness.

Compression test

Figure 3.12 represents the configuration bamboo_1 while Figure 3.13 shows configuration bamboo_2. Additionally, the parameters of the entire samples are summarised in Table 3.7 and the graded thicknesses of the cells are shown in Table 3.8.

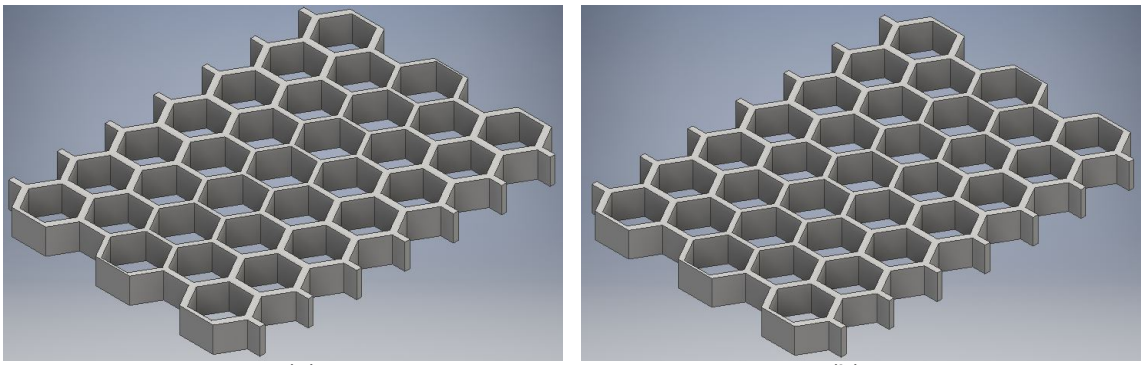

(a) (b)

Figure 3.12: CAD of bamboo configuration for compression test (a) bamboo_1_14, and (b) bamboo_1_16.

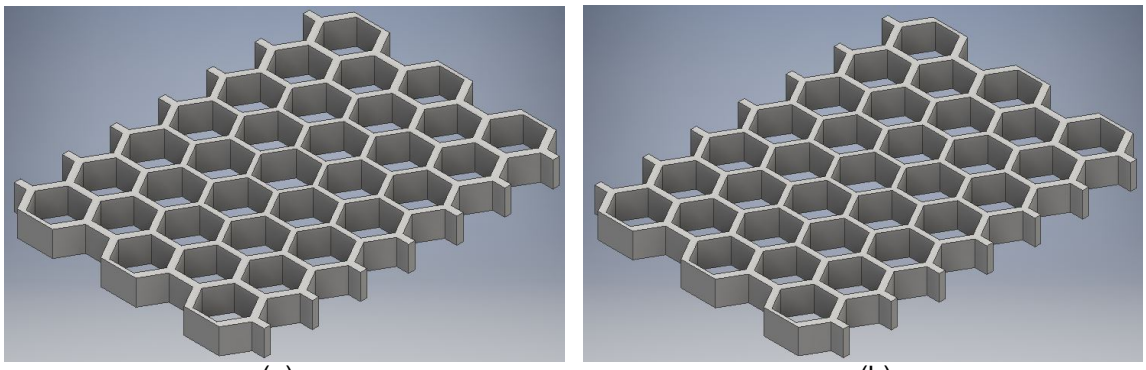

(a) (b)

Figure 3.13: CAD of bamboo configuration for compression test (a) bamboo_2_17, and (b) bamboo_2_18.

Table 3.7: Parameters of the bamboo compression samples.

	W (mm)	L(mm)	h (mm)	V_T (mm^3)	V_S(mm^3)	ρ (-)
Bamboo_1_14	135.24	100.39	10	1.36×10^5	2.78×10^4	0.205
Bamboo_1_16	135.24	100.39	10	1.36×10^5	2.75×10^4	0.202
Bamboo_2_17	135.24	100.39	10	1.36×10^5	3.05×10^4	0.225
Bamboo_2_18	135.24	100.39	10	1.36×10^5	2.93×10^4	0.216

Table 3.8: Graded wall thickness of the bamboo compression samples.

	Wall graded thickness			
	t_1 (mm)	t_2 (mm)	t_3 (mm)	t_4 (mm)
Bamboo_1_14	1.4	2	2.6	2
Bamboo_1_16	1.6	2	2.4	2
Bamboo_2_17	1.7	2	2.3	2.6
Bamboo_2_18	1.8	2	2.2	2.4

Three point bending test

The bamboo samples created to do the bending test are represented in Figure 3.14 for bamboo_1 and Figure 3.15 for bamboo_2.

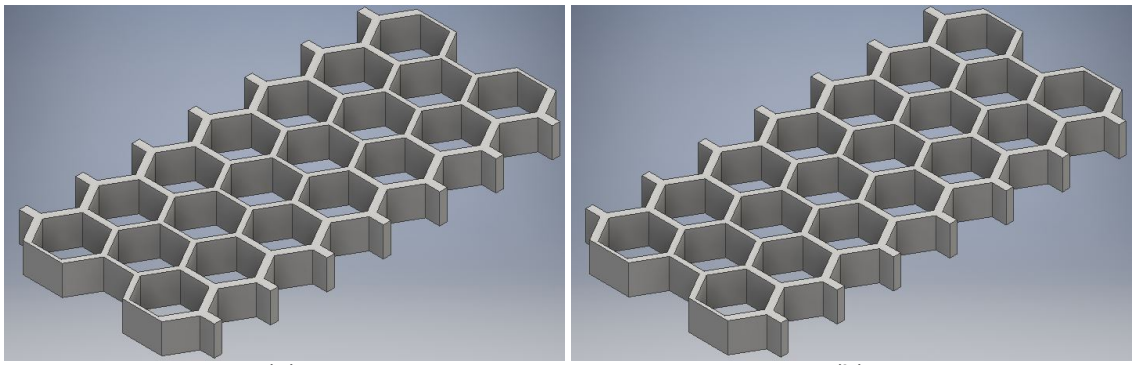

(a) (b)

Figure 3.14: CAD of bamboo arrangement for 3PB test (a) bamboo_1_14, and (b) bamboo_1_16.

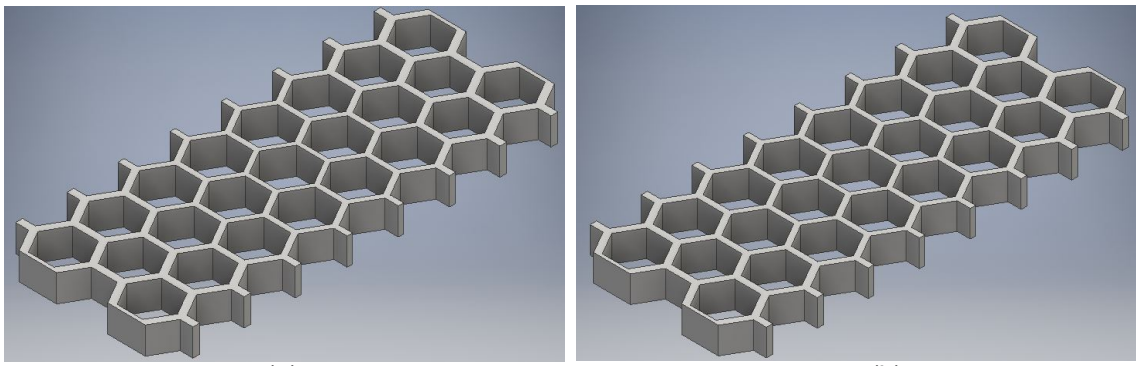

(a) (b)

Figure 3.15: CAD of bamboo configuration for 3PB test (a) bamboo_2_17, and (b) bamboo_2_18.

Finally, the parameters of the samples are summed up in Table 3.9 and in Table 3.10 the graded thickness of the walls are shown.

Table 3.9: Bamboo bending samples parameters.

	W (mm)	L(mm)	h (mm)	V_T (mm^3)	V_S (mm^3)	ρ (-)
Bamboo_1_14	135.24	66.92	10	9.05×10^4	1.77×10^4	0.196
Bamboo_1_16	135.24	66.92	10	9.05×10^4	1.78×10^4	0.196
Bamboo_2_17	154.56	66.92	10	1.03×10^5	2.30×10^4	0.222
Bamboo_2_18	154.56	66.92	10	1.03×10^5	2.21×10^4	0.213

Table 3.10: Graded wall thickness of the bamboo bending modules.

	Wall graded thickness			
	t_1 (mm)	t_2 (mm)	t_3 (mm)	t_4 (mm)
Bamboo_1_14	1.4	2	2.6	-
Bamboo_1_16	1.6	2	2.4	-
Bamboo_2_17	1.7	2	2.3	2.6
Bamboo_2_18	1.8	2	2.2	2.4

3.1.3. FEM

The numerical simulations were carried out using the software ABAQUS, version 6.14-1, a program that uses the finite elements method (FEM) to make all the calculations. The online ABAQUS guide [39] was used to clarify some parts of the applied methodology.

ABAQUS has a very intuitive interface divided in some modules where each one is explained in this section. This process is repeated for both tests and all configurations.

Module part

The module part is the module where the instance used in the simulations is created or imported. First of all, for both tests, the samples obtained with the CAD system software Autodesk Inventor were imported. Then the supports for the three point bending test and the plates for the compression test were created. In addition, for the compression test plates the inertias were assigned, being 0.275 Kg for the upper plate and 0.1 Kg for the lower plate.

Module property

The module property allows creating and assigning new materials to the part. In order to assign the material, the software required it to create a section with one material and then assign this section to the geometry.

As it was commented in section 3.1.1, the material used for all samples was PLA and its properties are shown in Table 3.1. However, bending test supports were assigned with a material having a higher Young's module with the aim of being able to transmit the forces without being deformed.

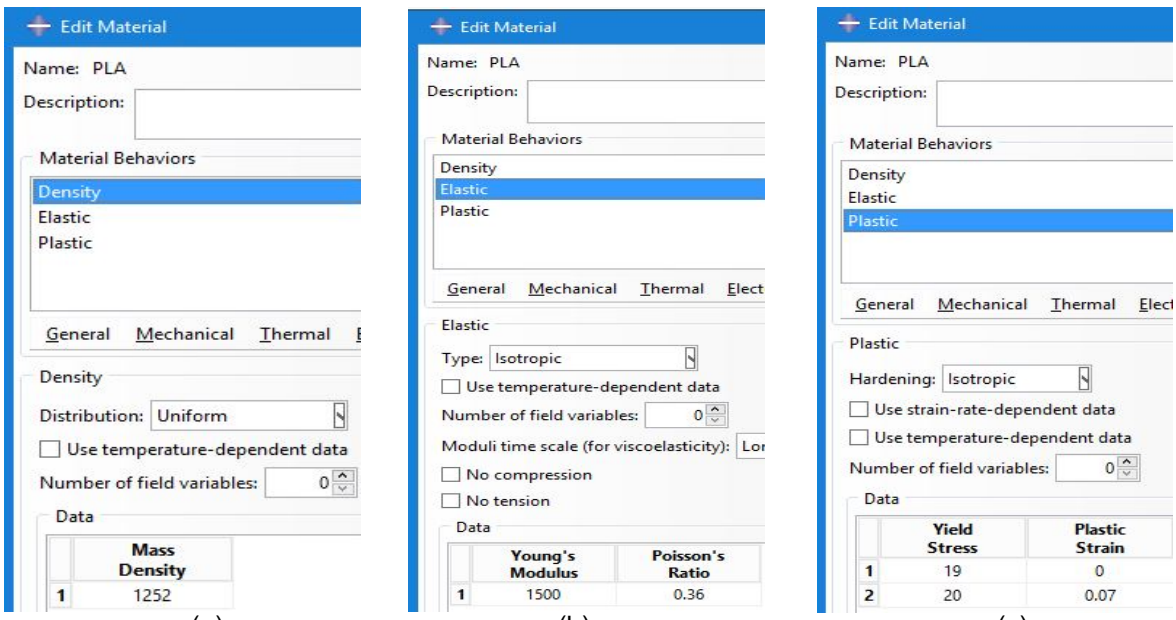

(a) (b) (c)

Figure 3.16: Create material properties: (a) density values, (b) elastic values, and (c) plastic values.

The following figures show the way to create and assign a section. Firstly, the software needed to know the category and the type of the section (Figure 3.17 (a)) and then, in the edit section (Figure 3.17 (b)) the material created in the previous step was assigned to this section. Once the section was created, in edit section assignment (Figure 3.17 (c)) the section with the correspondent material and the desired geometry was chosen.

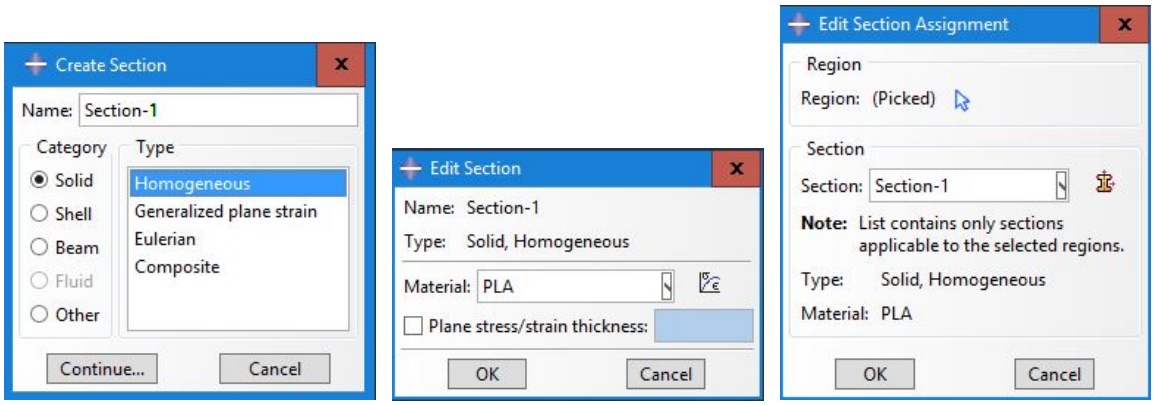

(a) (b) (c)

Figure 3.17: Steps to assign the material: (a) create section, (b) edit section, and c) edit section assignment.

This process is the same for both test modules and for the bending test supports. Only the plates of the compression test do not have a material assigned.

Module assembly

Once a material is assigned to each part, it is time to put all the parts together creating an instance in the module assembly. Figure 3.18 shows the assembly for the compression (a) and three point bending test (b).

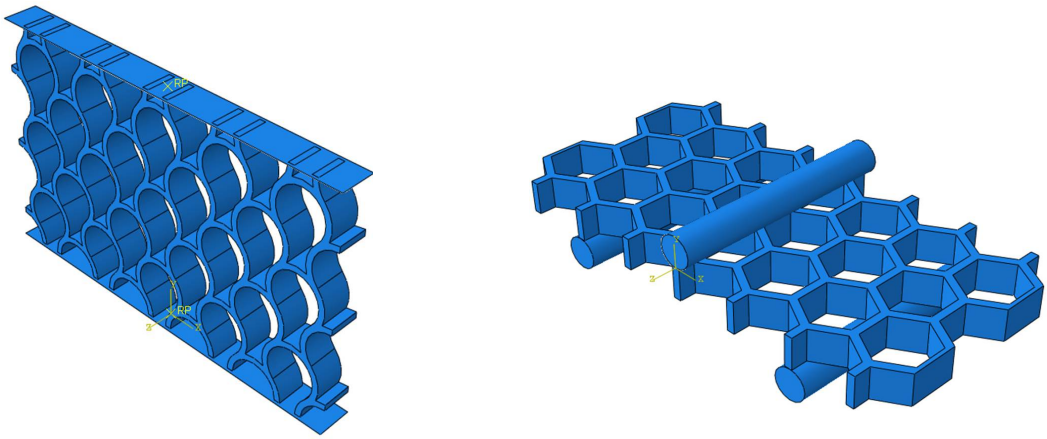

(a) (b)

Figure 3.18: Assembly for (a) compression test: enamel C and (b) three point bending test: honeycomb C.

Furthermore, the sets and the surfaces were created to be used in the interaction module.

Module step

In the module step two things were mainly defined. The first thing was create a step to select which kind of problem ABAQUS is going to solve. Figure 3.19 shows the options selected.

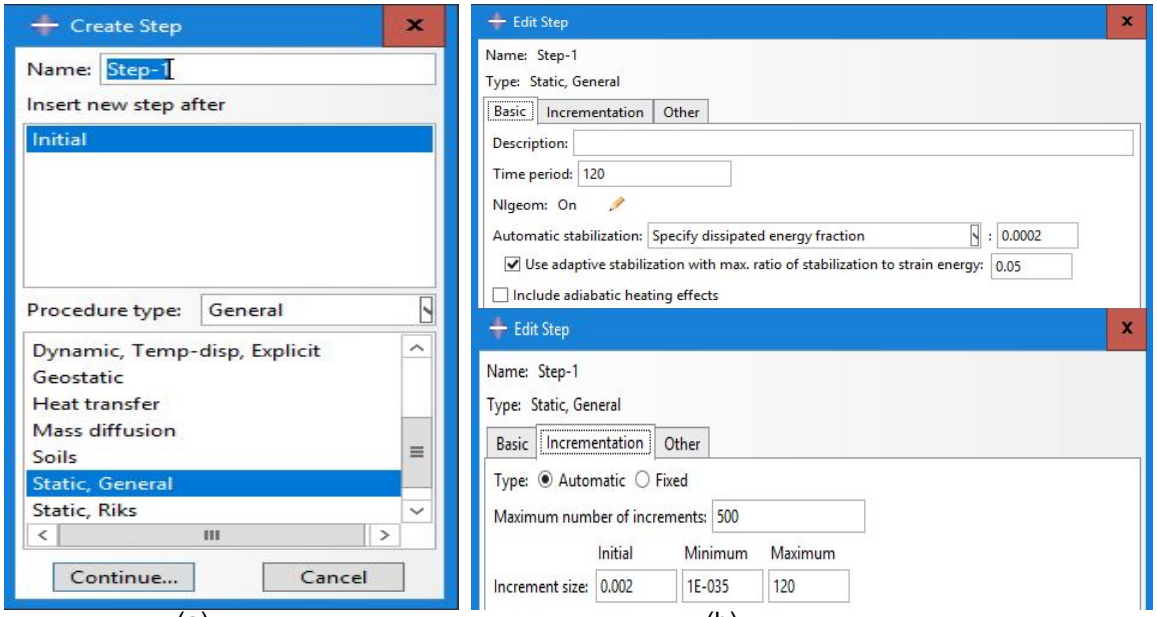

(a) (b)

Figure 3.19: Created step (a) problem to solve, and (b) configuration of the step.

The second thing was to define the output variables that were needed after the simulation. These variables were defined in the Field Output and in the History Output.

Module interaction

In this module the interaction between all instances as well as the constraints were established. For both tests, the interaction properties were created using the tool *create interaction property*. The surface-to-surface contact (standard) option was selected with the mechanical options: tangential behaviour with a friction formulation “penalty” with a friction coefficient of 0.2,and normal behaviour with a “hard” contact.

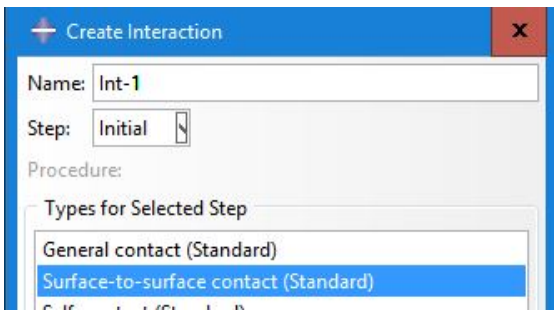

Figure 3.20: Create interaction with surface-to-surface contact type.

For the compression test it was necessary to create two interactions, between the upper and the lower plate with the module structure. For the bending test, three interactions were required: one for each contact between each support and the module cell.

In terms of the constraints two “tie” type constraints were created for the bending test to prevent the relative motion between the module cell and the upper and lower supports. For the compression test, three constraints were established: one “tie” type constraint between the lower plate and the module cell, and two of the type “rigid body” to designate the plate as a rigid body.

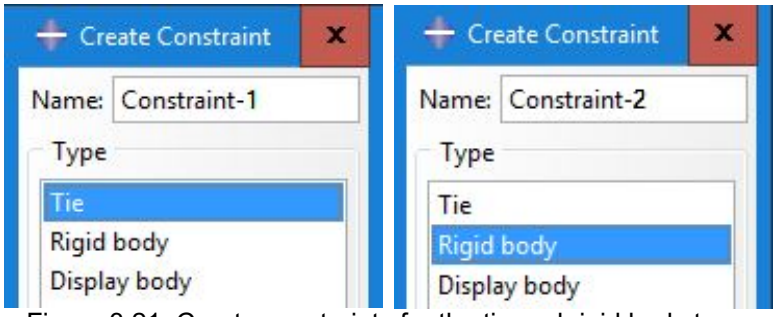

Figure 3.21: Create constraints for the tie and rigid body type.

Module load

The load module is used to define the boundary conditions. Two types of boundary conditions were used for both tests. The first one was for the lower supports in bending test and for the lower plate in compression plus the parts of the module that are in contact with the plate. A *symmetric/antisymmetric/encastre* type of boundary condition was applied as shown in Figure 3.22.

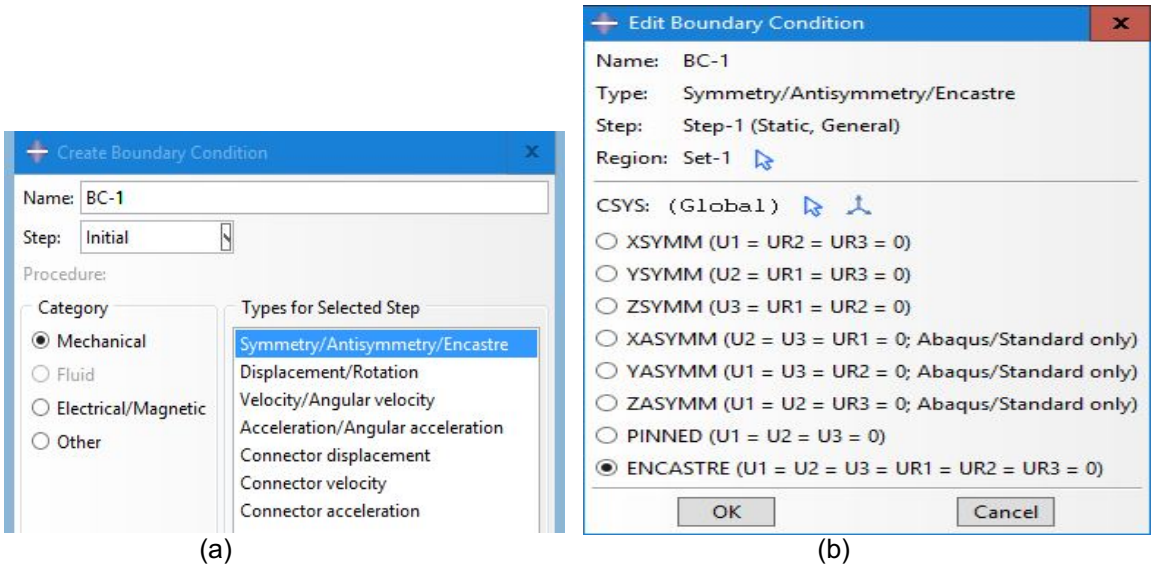

(a) (b)

Figure 3.22: Definition of symmetry boundary condition parameters: (a) creation and (b) edition.

The second boundary condition was used to impose a displacement in the model. For the bending test the upper support was selected to assign a displacement of -2.5 mm in the Y direction while for the compression test a displacement of -10 mm in the Y direction was applied in the upper plate. This boundary condition is a *Displacement/Rotation* type as shown Figure 3.23.

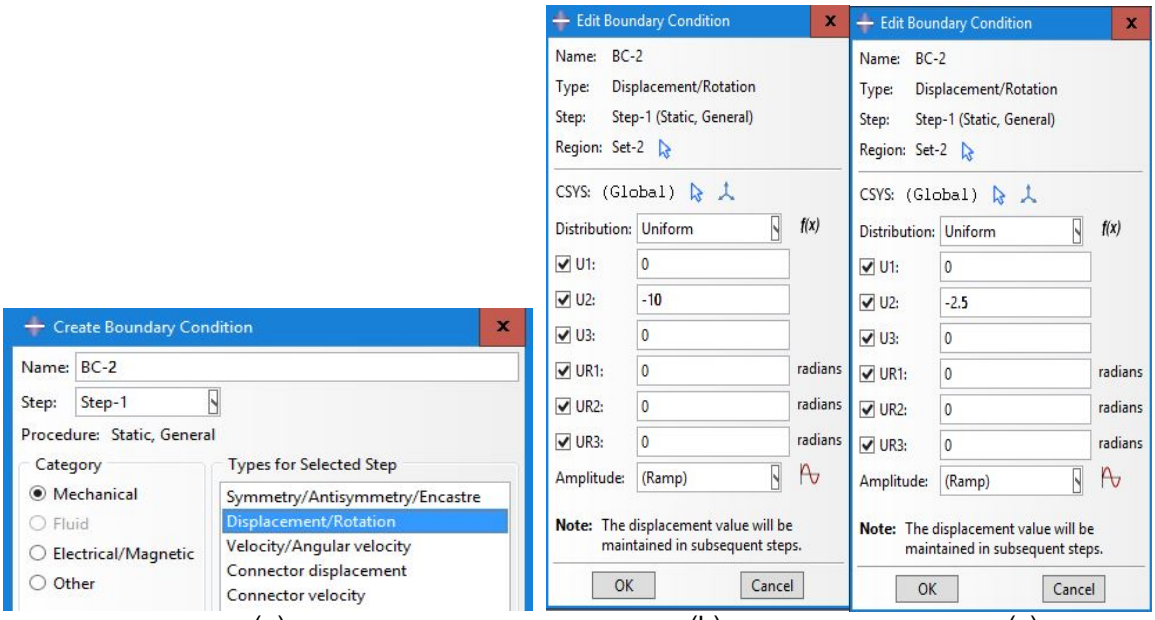

(a) (b) (c)

Figure 3.23: Definition of displacement boundary conditions parameters: (a) creation, (b) edition for compression test, and (c) edition for three point bending test.

Module mesh

The module mesh was used to define the mesh for every instance. The creation of the mesh was done in the tab global seeds, Figure 3.24, where the size and curvature control parameters were set. For all supports and plates, the approximate global size was constant with a value of 1.4 and 12 respectively. However, for the cellular modules, the approximate global size was different for each geometry and test. A mesh refinement study was made in the section 3.1.3.1, to verify the quality of the mesh.

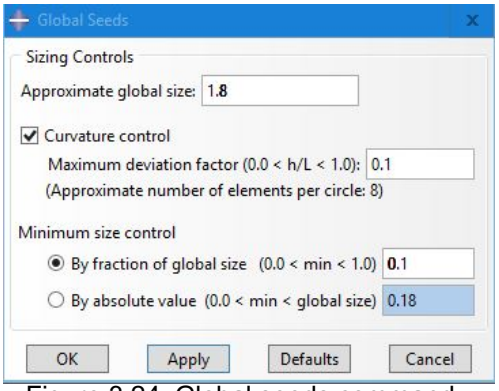

Figure 3.24: Global seeds command.

After this, the mesh was assigned to the instance with the command *Mesh Part* and finally, just for the compression test modules, a quadratic mesh was selected with the command *Assign Element Type.*

Module job

Finally, the module job is the last module where the program created was submitted to start the simulations. Once the simulation had finished, with the button *Results,* access to the module visualization was allowed to manage the obtained results.

To create the load-displacement plots, it was necessary to select the option *Create XY data* and choose the source *ODB field output* in the visualization module. In the variables box, the position of the variables *Unique nodal* was selected. To calculate the values of the force and displacement it was picked the value of the reaction force in the Y direction (RF2) and the displacement in the Y direction (U2). The node sets that encompass all the upper plate plus the structure points that are in contact with the plate for the compression test and for the 3PB test, the upper support were selected. However, for the displacement calculation it was only necessary to select one point from the top of the structure because it is the same in all the upper plate for the compression test and for the 3PB one point from the middle of the module top surface was chosen. Finally, in the option *Operate on XY data* the final load-displacement plot was made and exported to excel file.

3.1.3.1. Mesh refinement

In order to assign the size of the mesh for each configuration, a mesh sensitivity study was performed with a certain criteria to assess if there is not much variation in the stress values and seek a compromise between the refinement of the mesh (real value of the parameters) and the processing time spent in the calculation. If the parameter approximate global size is small, the program creates a mesh with more elements which means that the model is more realistic but the computational time required for the simulations to converge is also larger. However, to decrease the simulation time it is necessary to increase the parameter approximate global size, at the expense of having less precision in the model. For this reason, it is important to make a

mesh refinement study to find which is the maximum mesh size that will allow the simulation to converge in the minimum time necessary to provide realistic enough results.

To assign the global size of the mesh six studies were carried out, three for each test and one for each of the three configurations. The plots with the von Mises stress results in function of the global size of the mesh are shown.

From Figure 3.25 to Figure 3.30, different mesh sizes led to a range of values of stress. The value that differed less than 7% between the maximum and the minimum in the von Mises stress was taken as global size because it was considered stable and therefore, increasing the mesh size, the computational time will not provide significantly different stress.

Compression test

Figure 3.25 to Figure 3.27 exhibits the mesh refinement study for the honeycomb A, enamel B and bamboo_2_17.

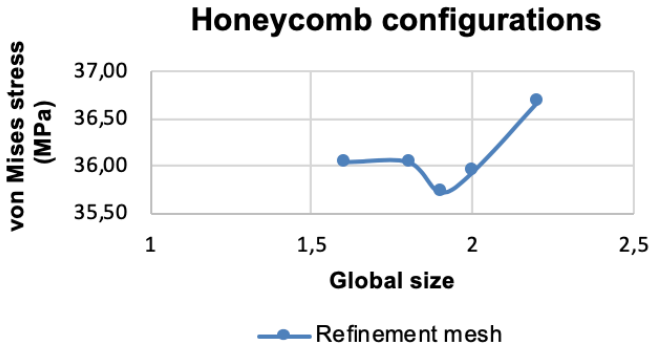

Figure 3.25: Mesh refinement for the honeycomb compression structures.

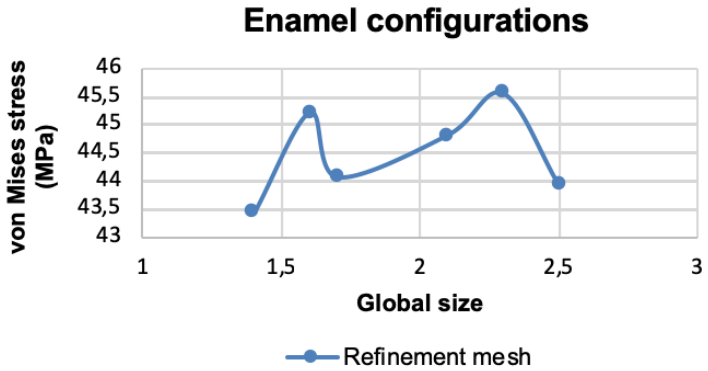

Figure 3.26: Mesh refinement for the enamel compression test.

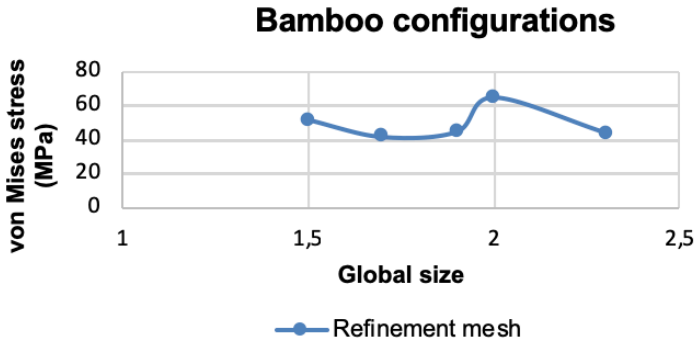

Figure 3.27: Mesh refinement for the bamboo compression arrangements.

For the honeycomb structure from 1.8 value of global size the stress converges to 36.05 MPa of von Mises stress and lower values of global size would not change the stress, so for this reason 1.8 was chosen as the global size. Following the same reasoning, for the enamel assembly the global size 1.7 was picked with a 44.08 MPa stress. Finally, for the bamboo arrangements the selected global size was 1.9 having a stress of 44.56 MPa.

Three point bending test

Figure 3.28 to Figure 3.30 represents the mesh refinement analysis for the three point bending test samples. Honeycomb A, enamel B and bamboo_1_16 were selected to do the study.

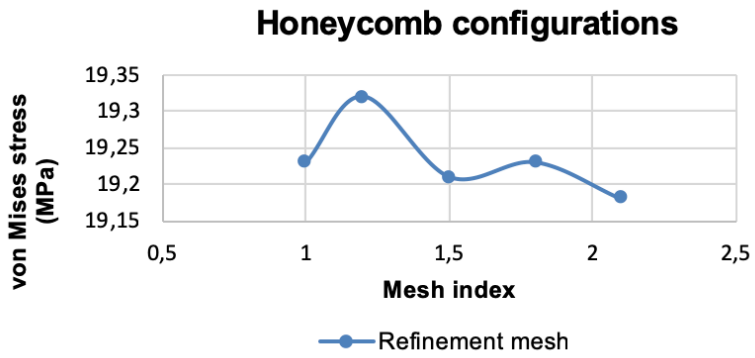

Figure 3.28: Mesh refinement for the honeycomb three point bending arrangements.

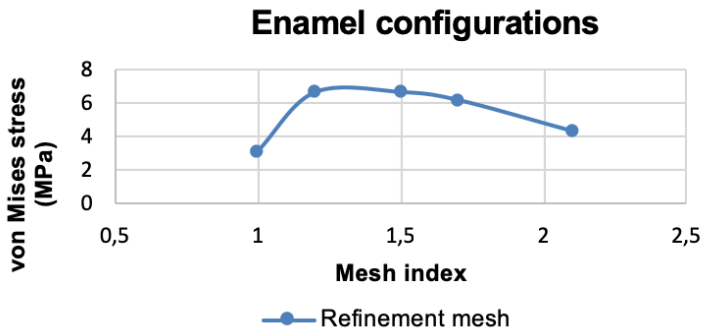

Figure 3.29: Mesh refinement for the enamel three point bending test.

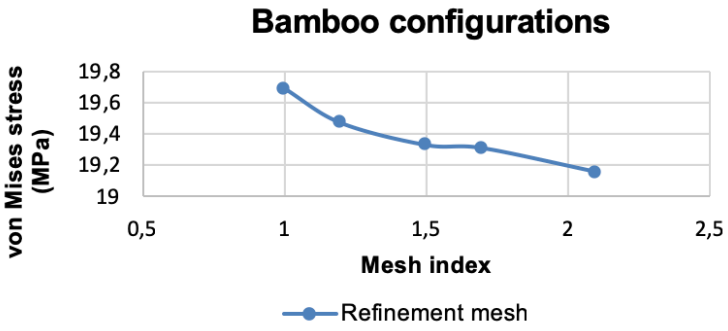

Figure 3.30: Mesh refinement for the bamboo three point bending structures.

In this case, for the honeycomb structure 1.8 it was chosen as the global size with a 19.23 MPa of stress. For the enamel arrangement it was selected a global size of 1.5 with 6.66 MPa of stress. Finally, for the bamboo assembly it was picked 1.7 as a global size with 19.31 MPa of stress.

To conclude, a summary table was created with the parameter of global size for each test and configuration.

Table 3.11: Global size for each test and configuration.

	Compression test	Three point bending test
Honeycomb	1.8	1.8
Enamel	1.7	1.5
Bamboo	1.9	1.7

3.2. Additive manufacturing

Selected samples were printed using FDM. The starting point of the 3D printing process is the CAD file where the geometry to build is made. In this thesis Autodesk Inventor was used. Then, the CAD file needs to be converted to stereolithography (STL) file in order to have the layer information of the samples that is going to be printed using the software CURA. Finally, the STL file was sent to the Ultimaker 3 3D printer (Figure 3.31) where the object was built layer by layer until the part is completed.

The material used to create the samples was PLA from the supplier ULTIMAKER with a printing temperature of 210 ºC and layer height of 0.15 mm. The built plate temperature was 80ºC. All parts were created at room temperature as the printer has no closed chamber. The printer speed to make the inner and outer wall was respectively 40 mm/s and 30 mm/s. The 3D printer had problems in the graded structure and the infill density parameter was not used since the filament arrived very hot to the nozzle preventing the correct print. Instead of using the infill density parameter, the command *Line Wall Count* with value 3 as an infill parameter was adopted. In this option, the printer follows the contours of the sample.

Non-graded structures were printed without apparent air gaps because the cell was selected to be a multiple of the size of the nozzle. However, this was not the case for the graded structures which were printed with slight air gaps inside the walls.

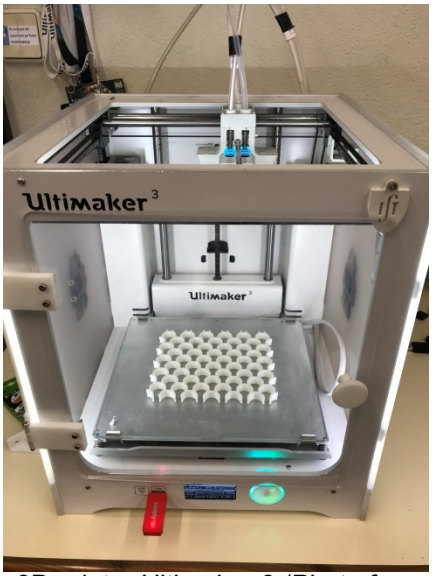

Figure 3.31: 3D printer Ultimaker 3 (Photo from the IST lab).

3.3. Experimental test

In order to validate the results obtained in the numerical simulations, four samples for each test were selected. For the compression test honeycomb C, enamel C, bamboo_1_14 and bamboo_2_18 were chosen and for the 3PB test honeycomb C, enamel C, bamboo_1_16 and bamboo_2_18 were picked. The criteria to select the samples was that all of them possessed approximately the same relative density and the structure had a wall thickness multiple of the size of the printing nozzle which is 0.4 mm. In Figure 3.32 and Figure 3.33 all the samples printed by FDM and experimentally tested are represented.

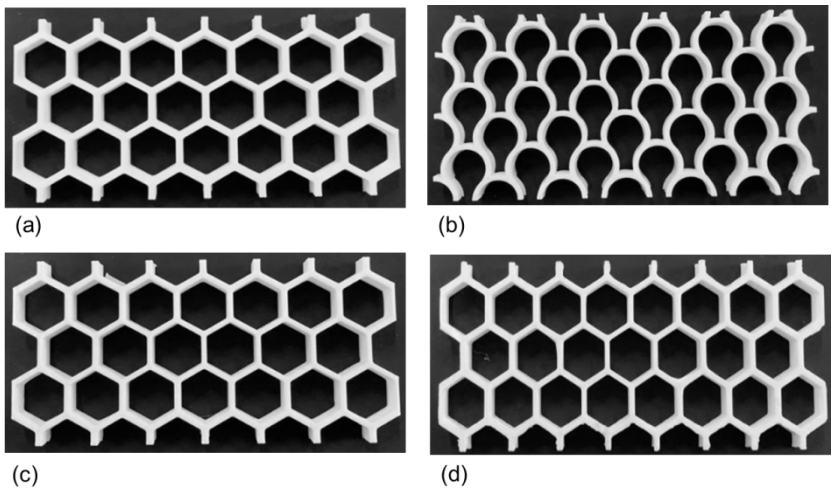

Figure 3.32: PLA samples before 3PB test, (a) honeycomb C, (b) enamel C, (c) bamboo_1_16, and (d) bamboo_2_18.

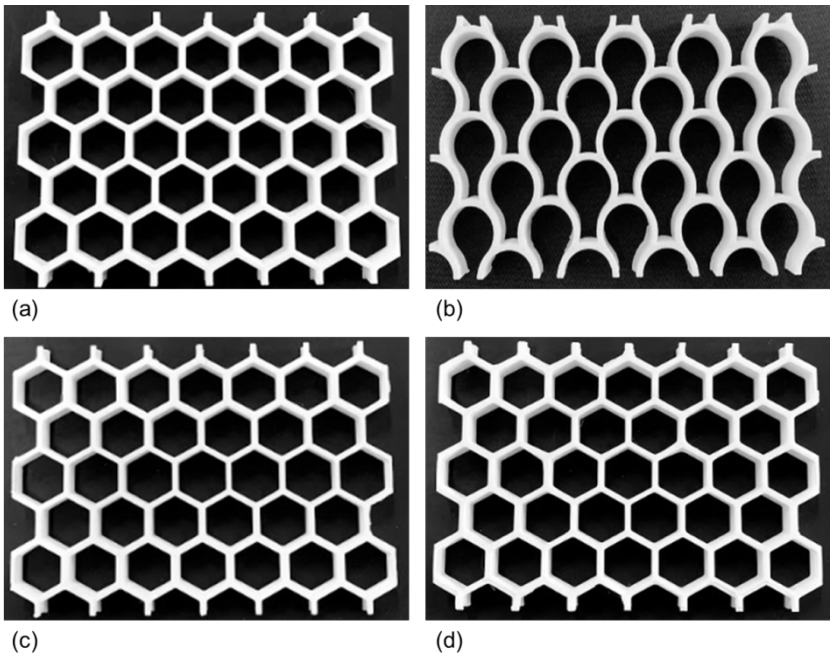

Figure 3.33: PLA samples before compression test, (a) honeycomb C, (b) enamel C, (c) bamboo_1_14, and (d) bamboo_2_18.

Before the tests were made, the dimensions of the modules were measured and are summarized in Table 3.12 and Table 3.13.

Table 3.12: Dimensions of the three point bending samples.

	W (mm)	L (mm)	h (mm)
Honeycomb C	139	68	10
Enamel C	156	78	10
Bamboo_1_16	135	68	10
Bamboo_2_18	155	68	10

Table 3.13: Dimensions of the compression samples.

	W(mm)	L(mm)	h (mm)
Honeycomb C	138	103	10
Enamel C	130	78	10
Bamboo_1_14	136	101	10
Bamboo_2_18	136	101	10

3.3.1. Compression and three point bending test set up

The compression tests were carried out according to the standard/normative ASTM D695 – 15 test (Standard Test Method for Compressive Properties of Rigid Plastics) [40]. Figure 3.34 shows a representative schema of the compression test.

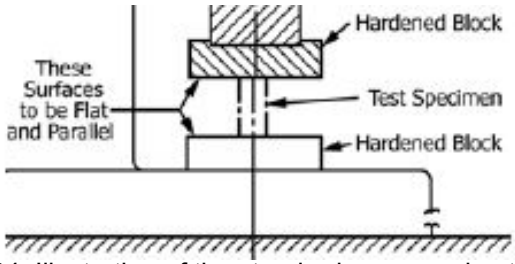

Figure 3.34: Illustration of the standard compression test [40].

Similarly, the three point bending test was performed following the standard/normative ASTM D790 – 17 (*Standard Test Methods for Flexural Properties of Unreinforced and Reinforced Plastics and Electrician Insulating Materials*) [41]. Figure 3.35 exhibits a schema of the three point bending test where P is the applied force and L is the support span which was taken as 80 mm for all tests.

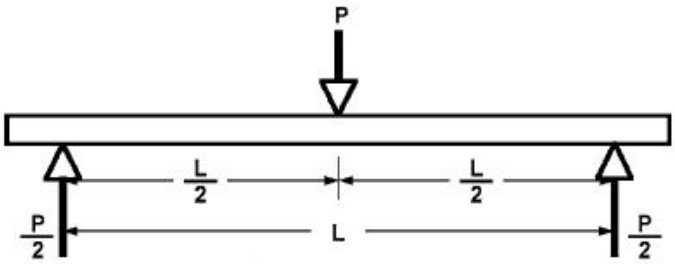

Figure 3.35: Loading diagram [41].

Figure 3.36 (a) and (c) show the set-up made in the experimental tests, whilst Figure 3.36 (b) and (d) represent the finite elements model. For the bending test the enamel structure is exhibited in Figure 3.36 (a) and (b) whereas for the compression test, the bamboo_2 is displayed in Figure 3.36 (c) and (d).

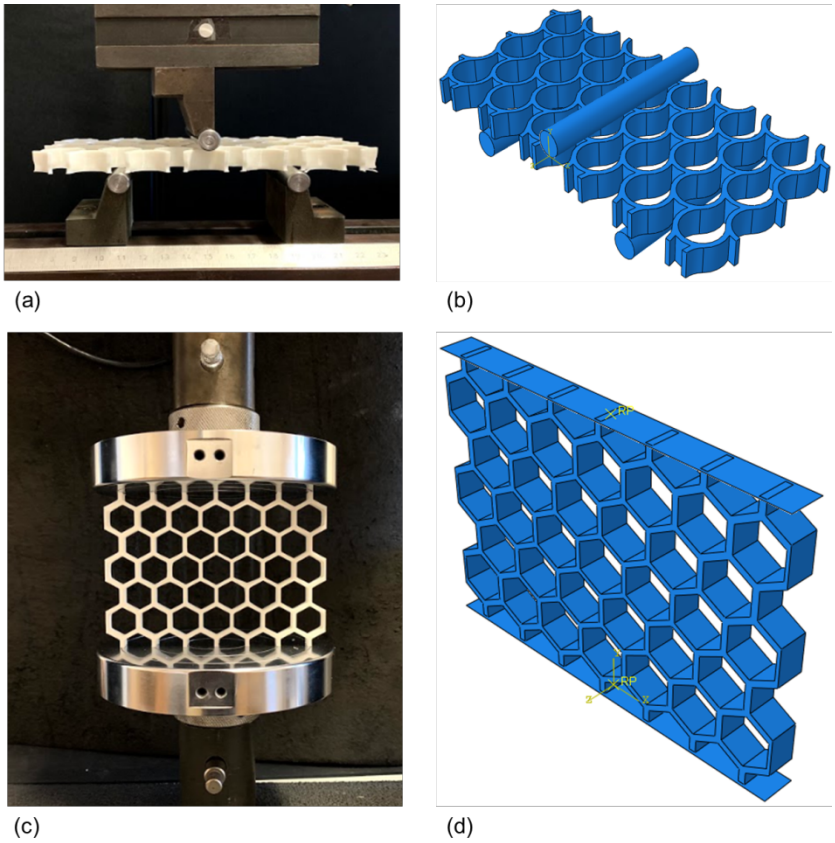

Figure 3.36: Experimental set-up for bending (a) and compression (c) test, and numerical models for 3PB (b) and compression test (d).

The equipment Instron 3369 was used during the experimental process for both tests, Figure 3.37 shows the photograph of the machine which has a load cell of 50 kN. For all tests, a 2.5 mm/min cross-head speed for the upper plate or support was defined.

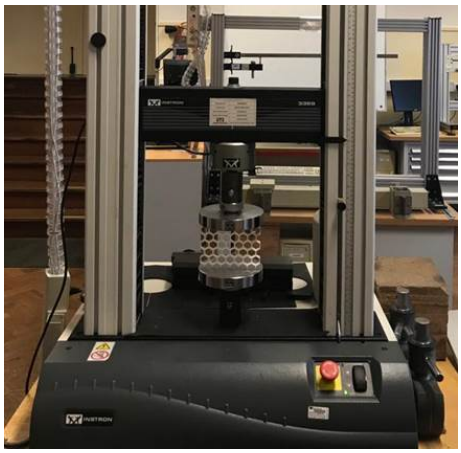

Figure 3.37: Instron 3369 equipment (Photo from the IST lab).

4. Results and discussion

4.1. FEM results

4.1.1. Compression test

The results from the numerical simulations for the compression test are shown in this section. The results for each one of the configurations considered are presented in terms of the von Mises stress, S (in MPa) and of the displacement, U (in mm). Firstly, the results are exhibited for the honeycomb structures with the relative densities of 0.086 (D), 0.106 (A), 0.125 (B) and 0.229 (C). The enamel arrangements results obtained with relative densities of 0.101 (A), 0.123 (B), 0.144 (E) and 0.222 (C) will be discussed next. Finally, the graded structure of bamboo with the two different assemblies is shown.

4.1.1.1. Honeycomb configuration

Figure 4.1 shows the von Mises stress results for the honeycomb configuration. The maximum value of stress was obtained for the case of the relative density ρ=0.229, labelled honeycomb C. In views of the colour plots presented in Figure 4.1, there is no clear direct relationship that linearly relates the relative density with the stress since the lowest relative density case (ρ=0.086) presents higher stress levels than those with relative densities ρ=0.106 and 0.125 but less than the configuration with the highest relative density of all the studied cases. This fact suggests that the maximum von Mises stress is highly dependent on the relative density.

Similarly, the displacement contours shown in Figure 4.2 do not reflect any linear proportionality between the displacement and relative density. The maximum value of displacement is achieved in the same configuration that the highest value of stress is attained, i.e. honeycomb C.

It has to be said that the stress scale of the honeycomb and enamel plots was modified in order to better see how the stress is distributed along the structure. For this reason, honeycomb D and C and enamel B and E have a maximum stress that exceeds the scale maximum but it cannot be seen in the figures.

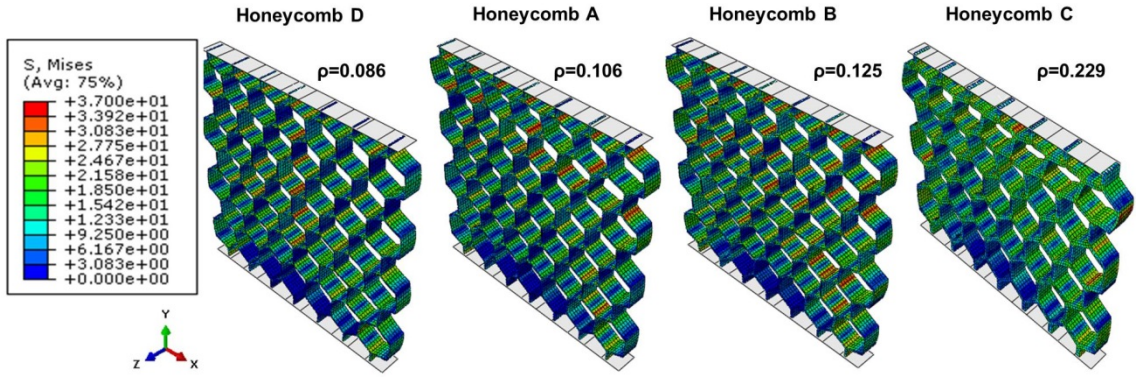

Figure 4.1: Finite element von Mises stress after compression test for honeycomb arrangements with different relative densities.

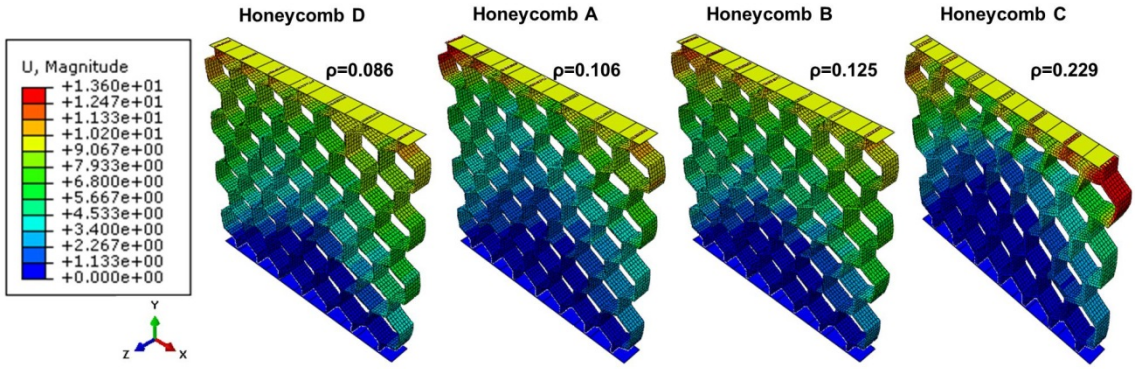

Figure 4.2: Finite element displacement after compression test for honeycomb assemblies with different relative densities.

Table 4.1: Maximum S and U values for each honeycomb configuration.

	ρ (-)	S-von Mises stress (MPa)	U-Displacement (mm)
Honeycomb D	0.086	44.25	11.57
Honeycomb A	0.106	36.05	13.00
Honeycomb B	0.125	36.45	11.80
Honeycomb C	0.229	47.15	13.57

4.1.1.2. Enamel configuration

Von Mises stress and displacement results for the enamel arrangements are respectively shown in Figure 4.3 and Figure 4.4. The highest value of stress is achieved for the case with relative density ρ=0.123, followed very close by the sample with density ρ=0.144. It is remarkable that for this configuration the maximum stress is not attained for the configuration with higher relative density.

Moreover, it seems interesting that the highest values of von Mises stress and displacement are not achieved for the same value of relative density, since enamel B shows the maximum stress while enamel E exhibits the largest displacement.

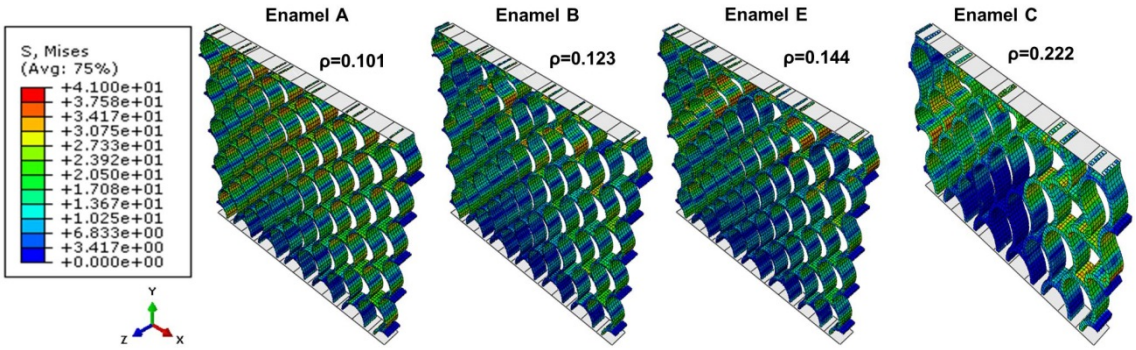

Figure 4.3: Finite element von Mises stress after compression test for enamel arrangements with different relative densities.

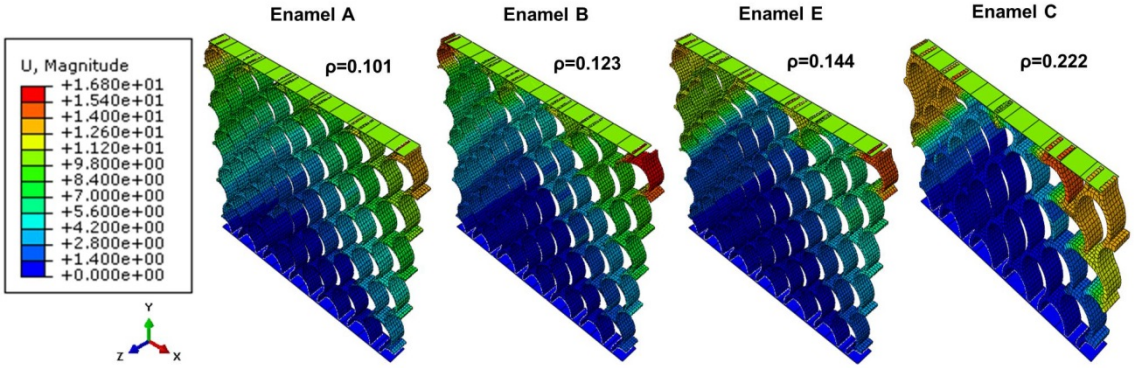

Figure 4.4: Finite element displacement after compression test for enamel configurations with different relative densities.

Table 4.2: Maximum S and U parameters value for each enamel configuration.

	ρ (-)	S-von Mises stress (MPa)	U-Displacement (mm)
Enamel A	0.101	38.43	14.07
Enamel B	0.123	44.08	16.67
Enamel E	0.144	43.39	16.75
Enamel C	0.222	49.87	14.45

Comparing the results of Table 4.2 with the ones of Table 4.1, for the common relative density between both configurations, the enamel arrangement is able to withstand a higher maximum stress, which indicates that exhibits higher strength.

4.1.1.3. Bamboo configuration

For all the samples, the studied bamboo structures have more or less the same relative density but as it is a graded configuration, the results change due to the different distribution of the thickness. Figure 4.5 shows the stress results and in views of the colour plots, it can be observed that for bamboo_1, the middle cell has more tension, being the maximum stress 50.29 MPa, as it is indicated in Table 4.3 for the model bamboo_1_14. Bamboo_2 has the stress distributed into more cells, having a maximum value of stress for the configuration with relative density ρ=0.216.

As it happened in enamel, the maximum values of von Mises stress and displacement are not attained for the same configuration, since bamboo_1_14 shows the maximum stress and bamboo_1_16 the highest displacement.

Finally, in Figure 4.6 it is easily seen that bamboo_1 has a larger displacement on the top cells than the bamboo_2 structure.

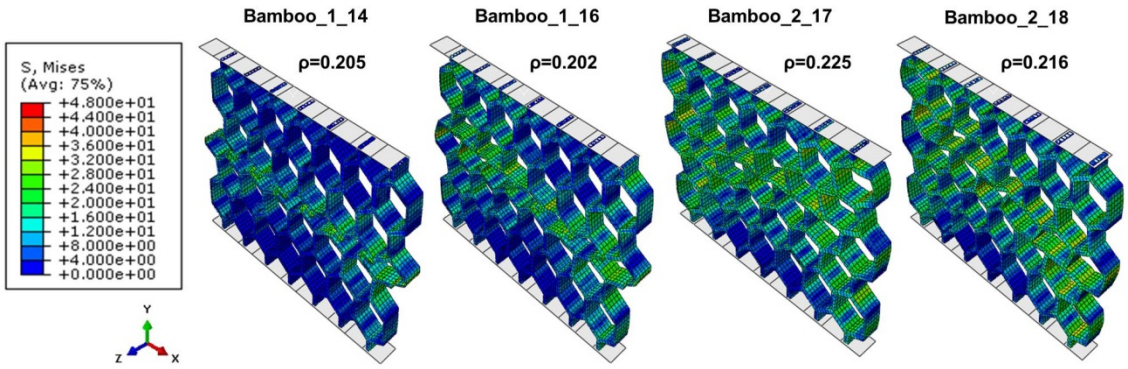

Figure 4.5: Finite element von Mises stress after compression test for bamboo arrangements with different relative densities.

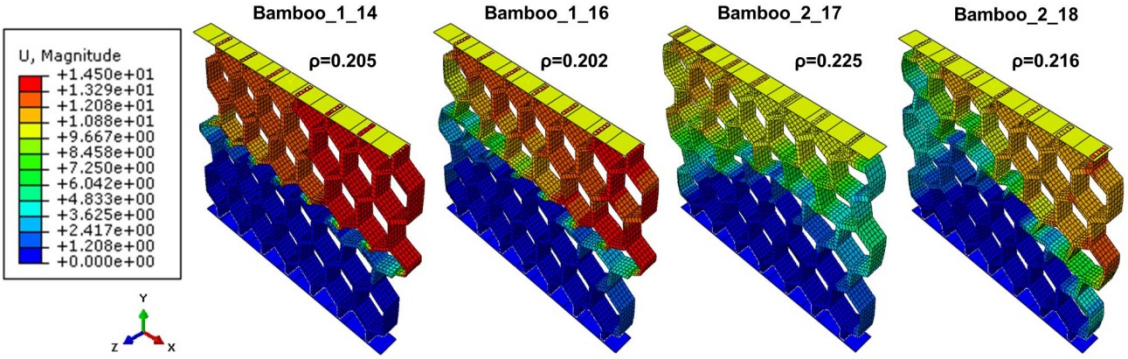

Figure 4.6: Finite element displacement after compression test for bamboo configurations with different relative densities.

Table 4.3: Maximum S and U parameters values for bamboo_1 and bamboo_2 configurations.

	ρ (-)	S-von Mises stress (MPa)	U-Displacement (mm)
Bamboo_1_14	0.205	50.29	14.25
Bamboo_1_16	0.202	44.50	14.43
Bamboo_2_17	0.225	44.56	11.47
Bamboo_2_18	0.216	47.89	12.36

4.1.2. Deformation shape

In this section the way that the arrangements deform under compression loads is analyzed. In this plane view the deformation shape can be better seen. For all samples, the figures will presented as follows: figure (a) is the shape of the configuration before testing, while (b) and (c) respectively exhibits the von Mises stress and the displacement after compression. All the figures are in the X_1-X_2 plane, previously defined, but in the ABAQUS software the axis are denoted by (X-Y).

4.1.2.1. Honeycomb

Figure 4.7 to Figure 4.10, represent the shape of the honeycomb configurations. It presents the aspect of the classic in-plane deformation for elastomeric honeycomb where the cell walls bend due to the loads in the X_2 direction. The lower plate is fixed and the upper plate is the responsible to provide the displacement to the module. Because of this, it can be appreciated that there is more deformation in the cells of the upper part than in the lower part of the structure. In addition, it was recognized that the highest values of stress were found closer to the triple junction of the cell.

Honeycomb D

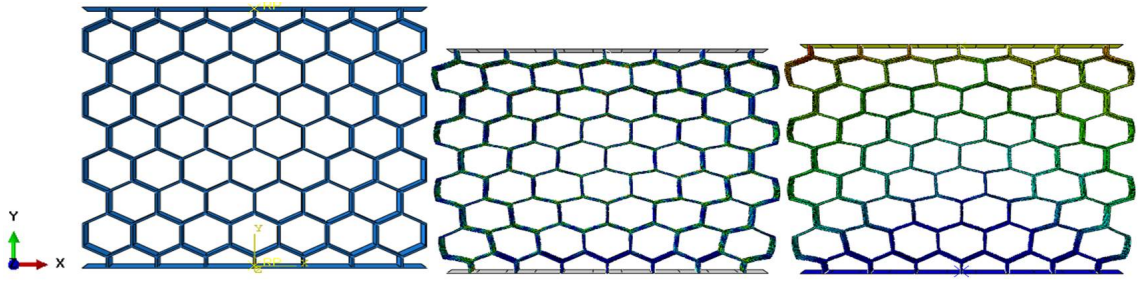

(a) (b) (c)

Figure 4.7: Structure with ρ=0.086, (a) undeformed honeycomb, (b) von Mises stress, and (c) deformation.

Honeycomb A

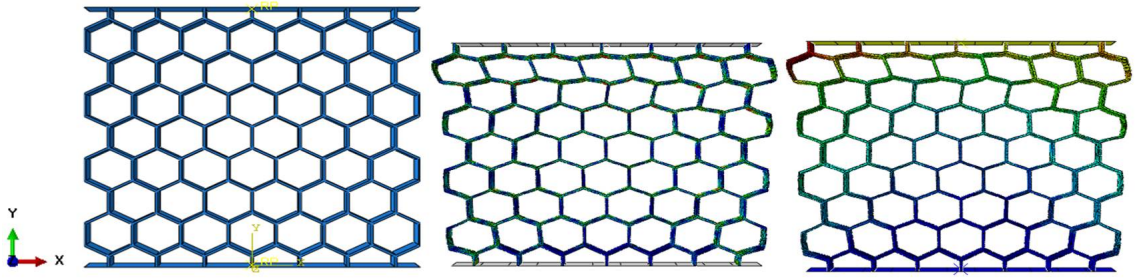

(a) (b) (c)

Figure 4. 8: Structure with ρ=0.106, (a) undeformed honeycomb, (b) von Mises stress, and (c) deformation.

Honeycomb B

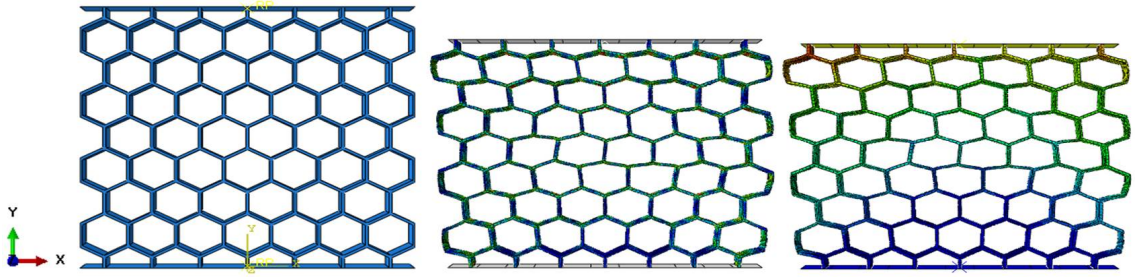

(a) (b) (c)

Figure 4.9: Structure with ρ=0.125 (a) undeformed honeycomb, (b) von Mises stress, and (c) deformation.

Honeycomb C

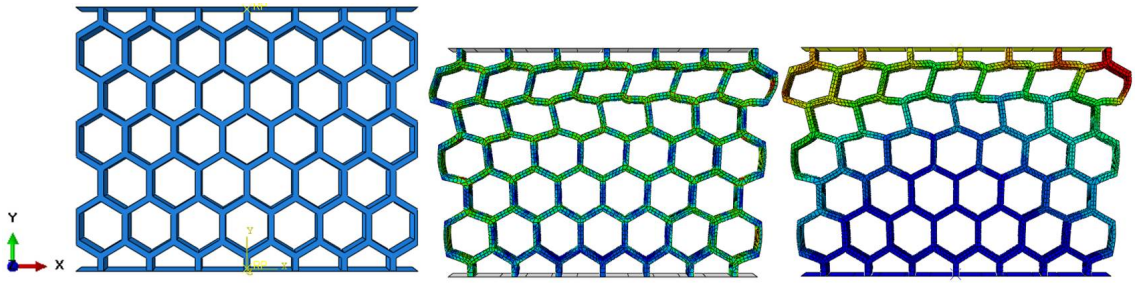

(a) (b) (c)

Figure 4.10: Structure with ρ=0.229, (a) undeformed honeycomb, (b) von Mises stress, and (c) deformation.

As it can be seen in the previous figures the relative density plays an important role in the deformation shape. There is a clear relationship between the relative density and the maximum strain. With lower relative densities, the maximum strain (ε) is larger. The maximum strains for the different relative densities are shown in the next table.

Table 4.4: Maximum strain for the honeycomb arrangements.

	D	A	B	C
ε	0.080	0.066	0.057	0.048

4.1.2.2. Enamel

Similar deformation is suffered by the enamel structures. The upper part is exposed to larger deformation. It can be appreciated that the cells in the periphery have larger displacement. Figure 4.11 to Figure 4.14 show the deformation shape of this arrangement.

Enamel A

(a) (b) (c)

Figure 4.11: Structure with ρ=0.101, (a) undeformed enamel, (b) von Mises stress, and (c) deformation.

Enamel B

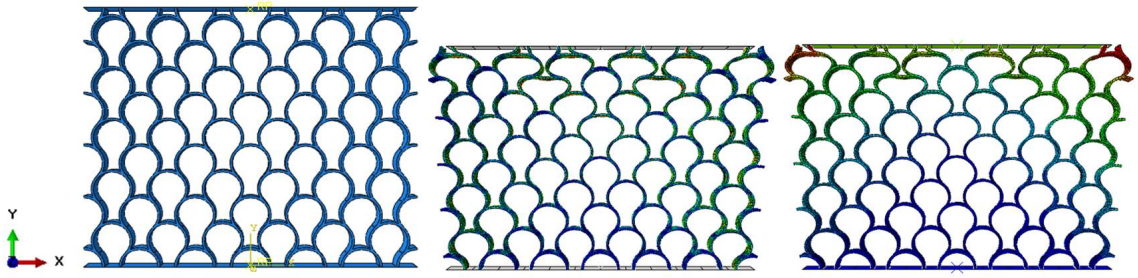

(a) (b) (c)

Figure 4.12: Structure with ρ=0.123 (a) undeformed enamel (b) von Mises stress, and (c) deformation.

Enamel E

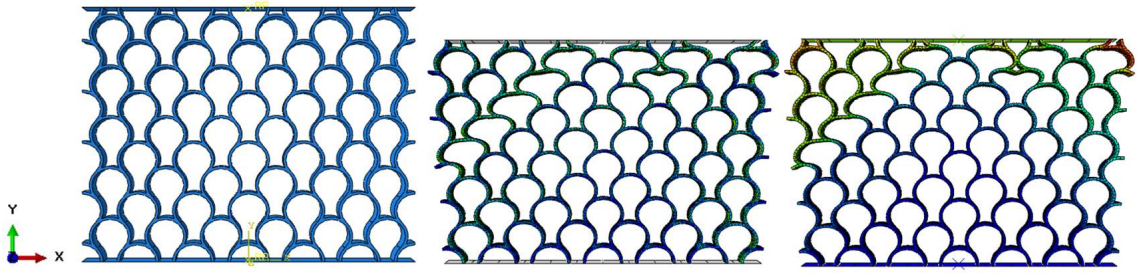

(a) (b) (c)

Figure 4.13: Structure with ρ=0.144 (a) undeformed enamel (b) von Mises stress, and (c) deformation.

Enamel C

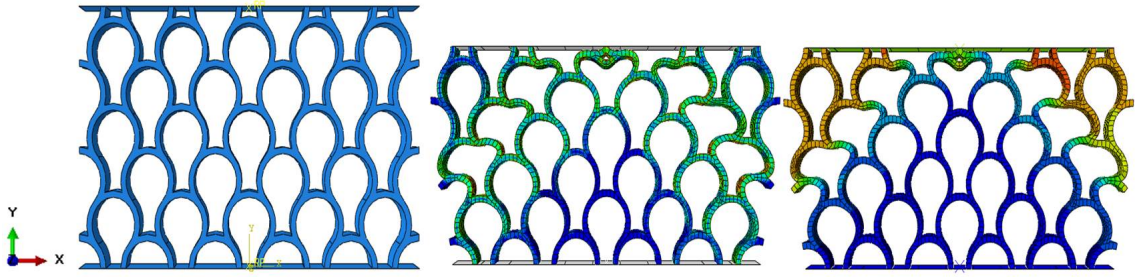

(a) (b) (c)

Figure 4.14: Structure with ρ=0.222, (a) undeformed enamel, (b) von Mises stress, and (c) deformation.

As it happened in the honeycomb configuration, the relative density is very important for the deformation shape. As the relative density increases, the maximum strain decreases. Table 4.1 shows the maximum strain for each structure.

Table 4.5: Maximum strain for the enamel arrangements.

	A	B	E	C
ε	0.070	0.062	0.057	0.047

4.1.2.3. Bamboo

For the bamboo configuration the deformation shape is different depending on whether the study sample is the bamboo_1 or bamboo_2. Figure 4.15 to Figure 4.18 exhibit the deformation for both structures.

For the bamboo_1 arrangement, one can see that the middle cells, corresponding to the lower wall thickness cells, are completely deformed. As these cells are less thick they buckle in the first place, and divide the module into two different parts, the upper part with more deformation and the lower part with less deformation. The middle layer acts as a barrier to the propagation of the deformation.

Regarding the bamboo_2 assembly, it can be observed that the cell in the middle (which has less thickness) suffers more deformation than the other cells. As it happened in the honeycomb configuration, the maximum stress is found near the triple junction.

Bamboo_1_14

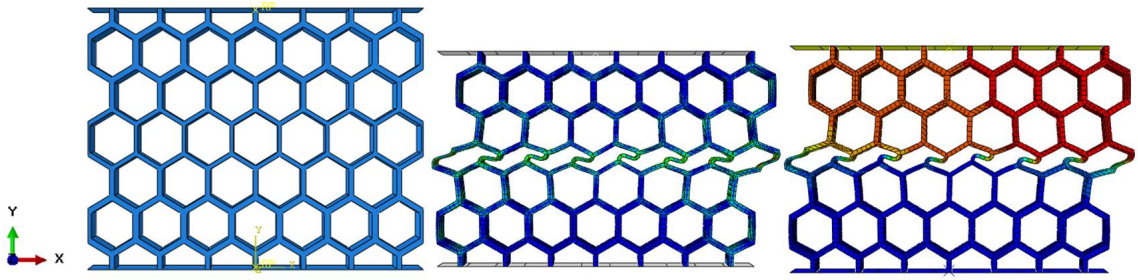

Figure 4.15: Structure with ρ=0.205, (a) undeformed bamboo_1, (b) von Mises stress, and (c) deformation.

Bamboo_1_16

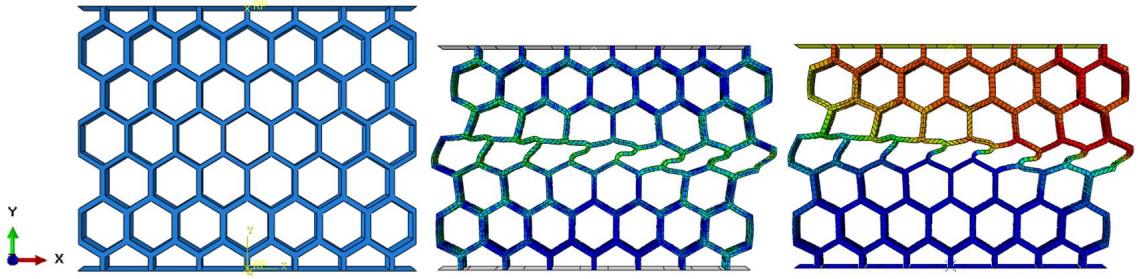

Figure 4.16: Structure with ρ=0.202, (a) undeformed bamboo_1, (b) von Mises stress, and (c) deformation.

Bamboo_2_17

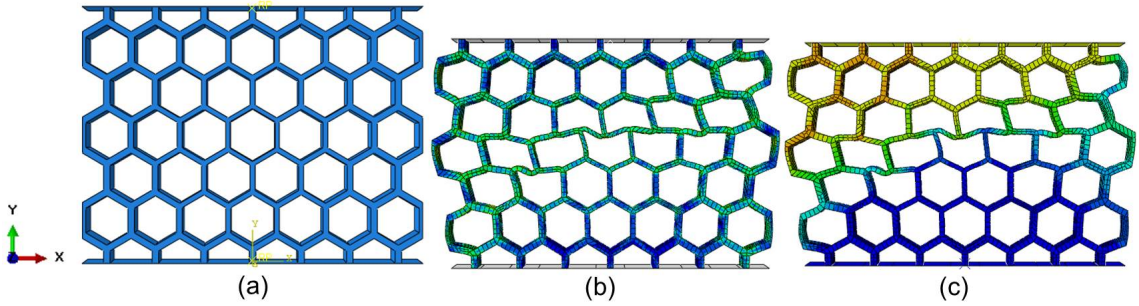

Figure 4.17: Structure with ρ=0.225, (a) undeformed bamboo_2, (b) von Mises stress, and (c) deformation.

Bamboo_2_18

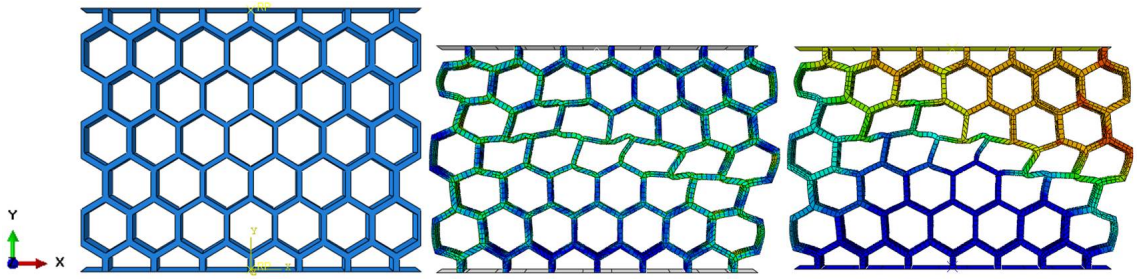

(a) (b) (c)

Figure 4.18: Structure with ρ=0.216, (a) undeformed bamboo_2, (b) von Mises stress, and (c) deformation.

Table 4.6 shows that for bamboo_1 structure the maximum strain changes despite of the fact that both structures have more or less the same relative density. The distribution of the wall thickness plays a key role in the distribution and the maximum strain. Additionally, it can be seen that the bamboo_2 structure attains a larger strain more than bamboo_1 arrangement does.

Table 4.6: Maximum strain for the bamboo arrangements.

	B_1_14	B_1_16	B_2_17	B_C_18
ε	0.034	0.040	0.046	0.046

4.1.2.4. Analysis and discussion of the results

Once the results were obtained from the numerical simulations the load-displacement curves for each test and configuration were created to have an overview of the structure behavior and study the effect that the relative density has on it. Figure 4.19 to Figure 4.22 present the load-displacement curves calculated for all configurations and all the relative densities.

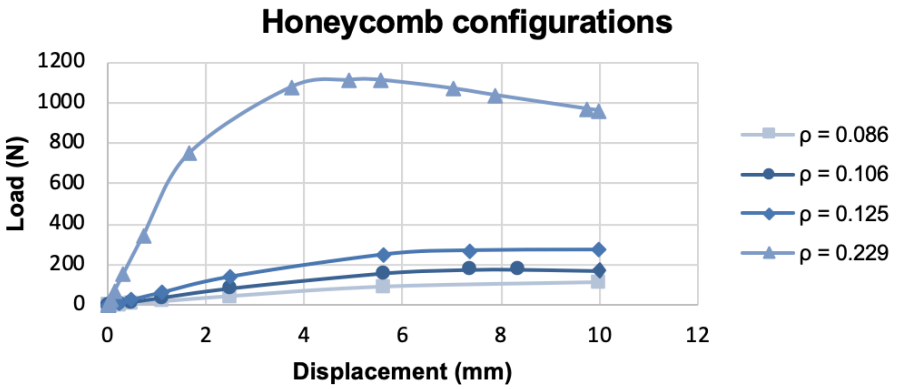

Figure 4.19: Load-displacement curves for the honeycomb compression samples.

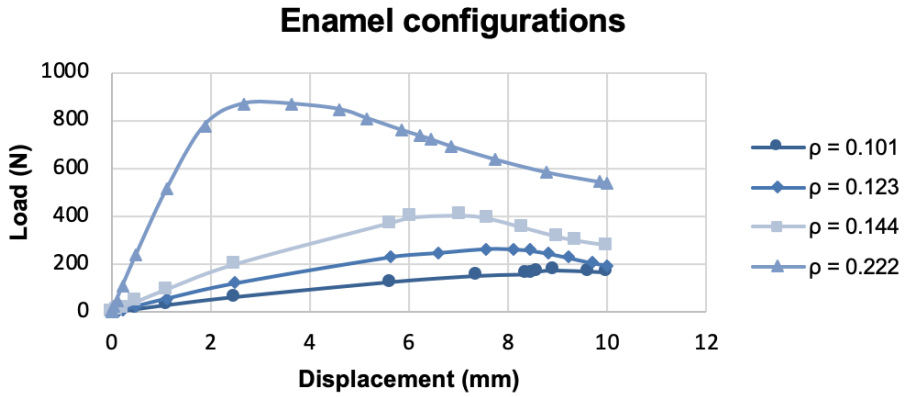

Figure 4.20: Load-displacement curves for the enamel compression arrangements.

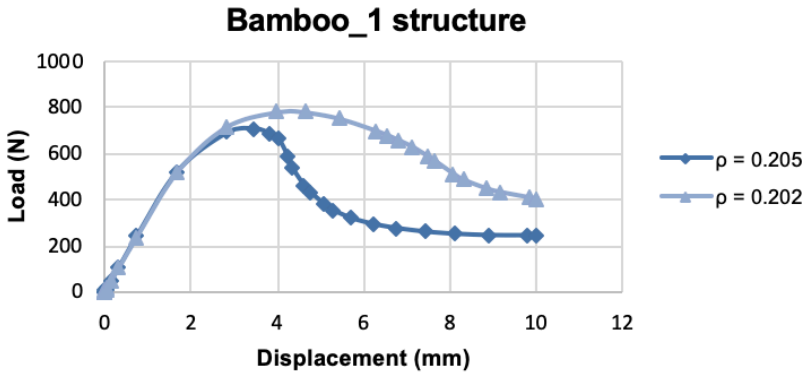

Figure 4.21: Load-displacement curves for the compression bamboo_1 structure.

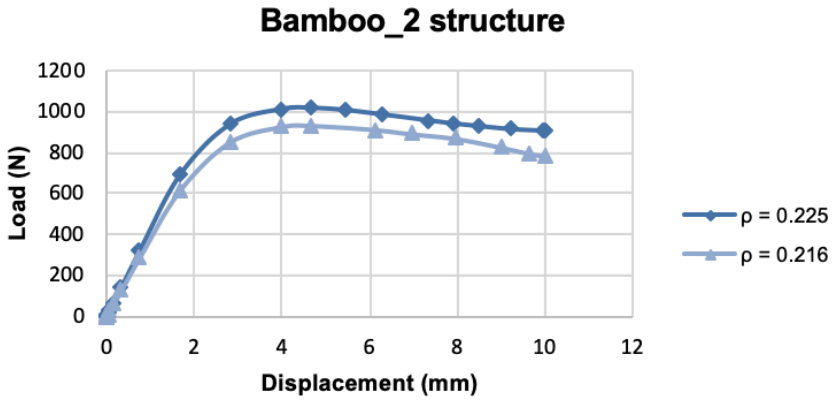

Figure 4.22: Load-displacement curves for the compression bamboo_ 2 structure.

All the plots have a linear part continued by a nonlinear zone which is thought to be associated to the damage.

Doubling the relative density average from 0.10 to 0.22 increases the applicable load over 5 times for honeycomb (Figure 4.19) and enamel configurations (Figure 4.20). The enamel load-displacement curves present a maximum that is shifted towards the left hand-side of the curve as the density increases. Comparing the results obtained during this research to the existing literature, Figure 2.4 and Figure 2.5 presented in section 2.1.2.1 one could see a similar distribution, indicating that the maximum observed in the enamel load-displacement distribution corresponds to the end of the linear elastic section and the starting point of the plateau region. Comparing Figure 4.19, Figure 4.20 and Figure 2.5 one can deduce that the honeycomb configuration has not reached its displacement corresponding to the end of plateau zone for the densities under consideration.

Regarding the bamboo structure, for the bamboo_2 configuration the behaviour is the same for both studied cases, being the maximum load slightly larger for higher relative density. In the first assembly i.e. bamboo_1, for almost the same relative density, the curve has a common initial load increment. However, despite the similar densities, the shape of the load-displacement distribution largely differs since in one case it follows the same trend that was mentioned for honeycomb and enamel structures, and in the other case it shows a curve that had not been seen before for any of the study cases. Another fact worth to highlight is that in this case the reduction in load after the maximum is 50%, a much larger difference than those observed earlier.

To compare the three configurations together and analyse the most important parameters, Table 4.7 was created to present the maximum von Mises stress (σ_{vM}), the initial stiffness (K) which is the initial slope of the load-displacement curve, and the energy absorbed until maximum load (E_a) divided by the relative density (ρ). In this way, all the parameters were normalized by the relative density.

Table 4.7: Normalized numerical simulation results by the relative density for the compression test.

	ρ (-)	σ_{vM}/ρ (MPa)	K/ρ (N/mm)	E_a/ρ (J)
Honeycomb D	0.086	512.46	208.37	6.386
Honeycomb A	0.106	339.49	318.64	6.959
Honeycomb B	0.125	290.70	449.53	7.873
Honeycomb C	0.229	206.26	1981.54	11.947
Enamel A	0.101	382.04	57.79	6.772
Enamel B	0.123	358.67	404.38	8.191
Enamel E	0.144	300.66	566.37	9.873
Enamel C	0.222	224.64	1925.99	7.095
Bamboo_1_14	0.205	245.18	1544.05	5.971
Bamboo_1_16	0.202	219.98	1565.62	7.656
Bamboo_2_17	0.225	198.10	1855.04	10.478
Bamboo_2_18	0.216	222.21	1724.78	10.033

For the honeycomb, enamel and bamboo_2 structure one can perceive the same response, as the relative density increases, the maximum stress decreases, but the stiffness and the energy absorbed increase. The values of the parameters are slightly different for bamboo_1 structure taking into account that bamboo_1_14 and bamboo_1_16 have the same relative density. The reason of this difference could be due to the way that the geometry changes in each structure.

Comparing the two non-graded structures (honeycomb and enamel) for the densities around 0.10 (A), 0.12 (B) and 0.22 (C), it is observed that enamel can withstand higher stress, which indicates that enamel exhibits higher strength than honeycomb. Regarding the stiffness, honeycomb has higher values than enamel reaching the maximum for the density C. The energy absorbed is quite similar between these two arrangements. Finally, the maximum stress is achieved for the density D, and the higher initial stiffness and the energy absorbed values are reached for the maximum density studied C.

4.1.3. Three point bending test

The results for the three point bending test numerical simulations are shown in this section. As it was done for the compression test, the results for each of the configurations considered are presented in terms of the von Mises stress, S (in MPa) and the displacement, U (in mm). Initially, the results are exhibited for the honeycomb arrangements with the relative densities of 0.086 (D), 0.106 (A), 0.125 (B) and 0.229 (C). The enamel structures with relative densities of 0.101 (A), 0.123 (B), 0.144 (E) and 0.222 (C) will be discussed next. Finally, the graded structure of bamboo with the two different assemblies is shown. The upper support placed at the middle point of the configuration was deleted to better observe the whole module.

4.1.3.1. Honeycomb configuration

Figure 4.23 exhibits the stress results for the honeycomb structures. The maximum value of stress was obtained for the case of the relative density ρ=0.229 (C). However, for all the samples, the values of the von Mises stress are quite similar, as shown in Table 4.8. It can be observed that the maximum stress is reached where the structure has contact with the support and closer to the triple junction. Analysing the colours of Figure 4.23 one can say that for the samples D, A and B the stresses are higher in the lower part of the module which is in contact with the lower supports than in the upper part of the module which is in contact with the upper support.

Furthermore, as shown in Figure 4.24, the displacement is larger in the middle of the module where the load is applied. The maximum value of the displacement was achieved in the sample with relative density ρ=0.125 (B).

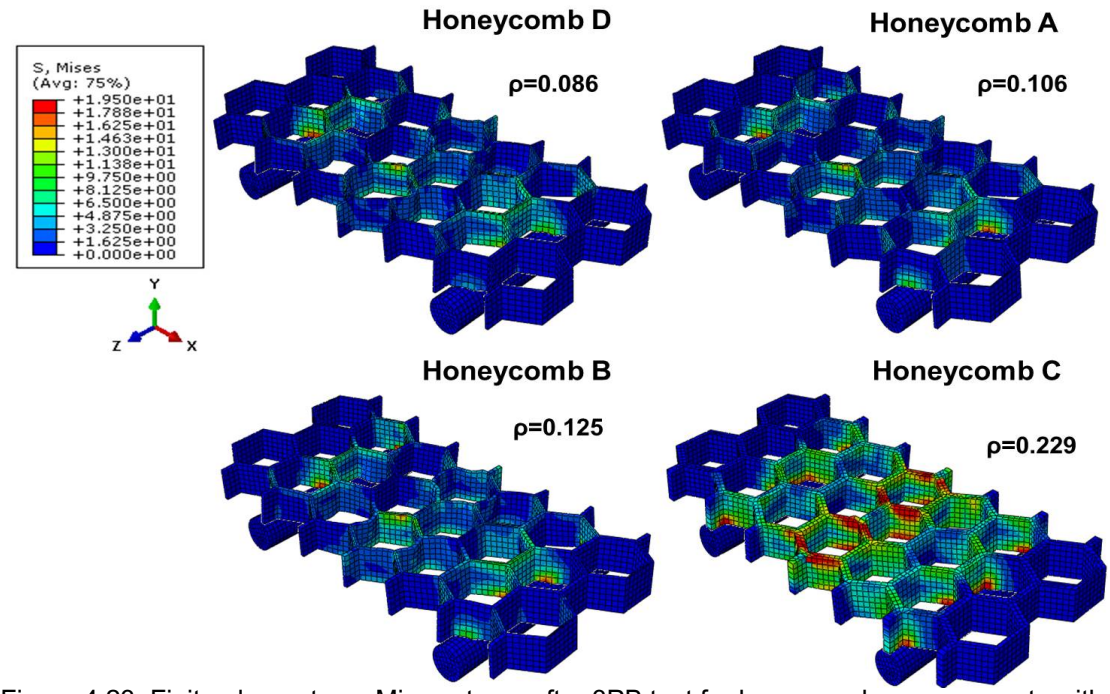

Figure 4.23: Finite element von Mises stress after 3PB test for honeycomb arrangements with different relative densities.

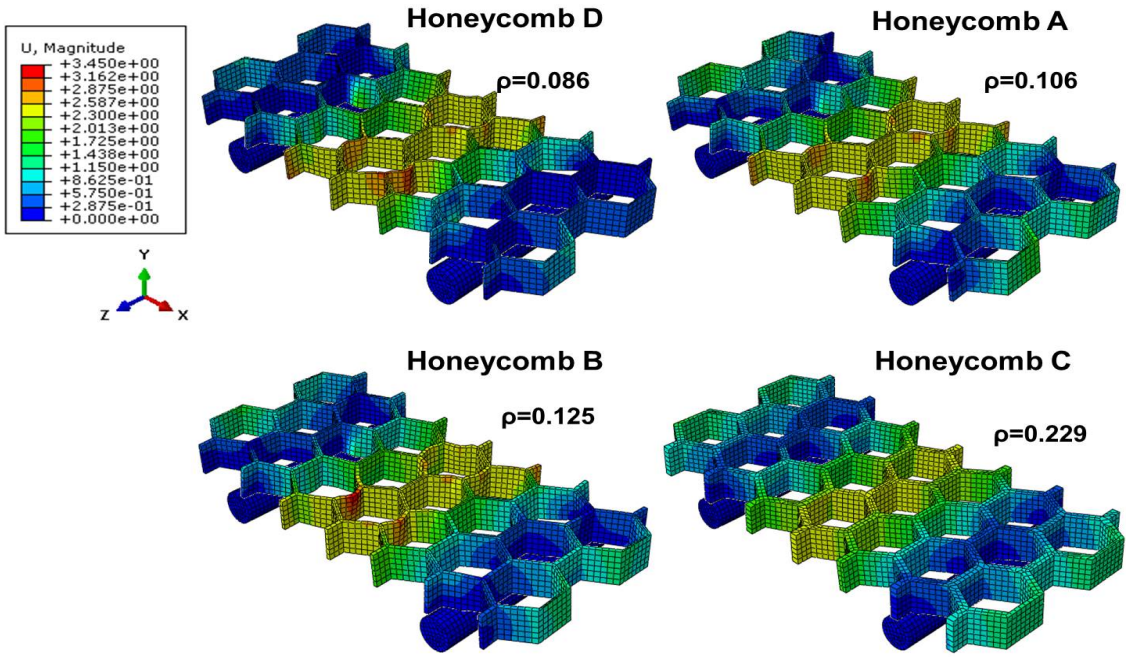

Figure 4.24: Finite element displacement after 3PB test for honeycomb assemblies with different relative densities.

Table 4.8: Von Mises stress (S) and displacement (U) for honeycomb configurations.

	ρ (-)	S-von Mises stress (MPa)	U-Displacement (mm)
Honeycomb D	0.086	19.08	3.18
Honeycomb A	0.106	19.23	3.00
Honeycomb B	0.125	19.26	3.45
Honeycomb C	0.229	19.50	2.56

4.1.3.2. Enamel configuration

Von Mises stress and displacement results for the enamel configuration are respectively shown in Figure 4.25 and Figure 4.26. Enamel samples with low relative density (A, B and E) have a low capacity of stress support in comparison with other configurations but, there is a huge increment of the stress when the density increases from 0.144 (E) to 0.222 (C) having the last configuration a stress value of 19.11 MPa (Table 4.9). As enamel C supports three times higher stress than the other structures, another scale of values was created. It is interesting to comment that the predominant colour in the stress figure is blue. This predominance of the blue colour means that most of the module is not under stress when the load is applied and there are small focalized areas that have the maximum load.

Once more, the displacements are quite similar between all the samples being larger in enamel A and the maximum value was not achieved in the same sample where the maximum stress is attained.

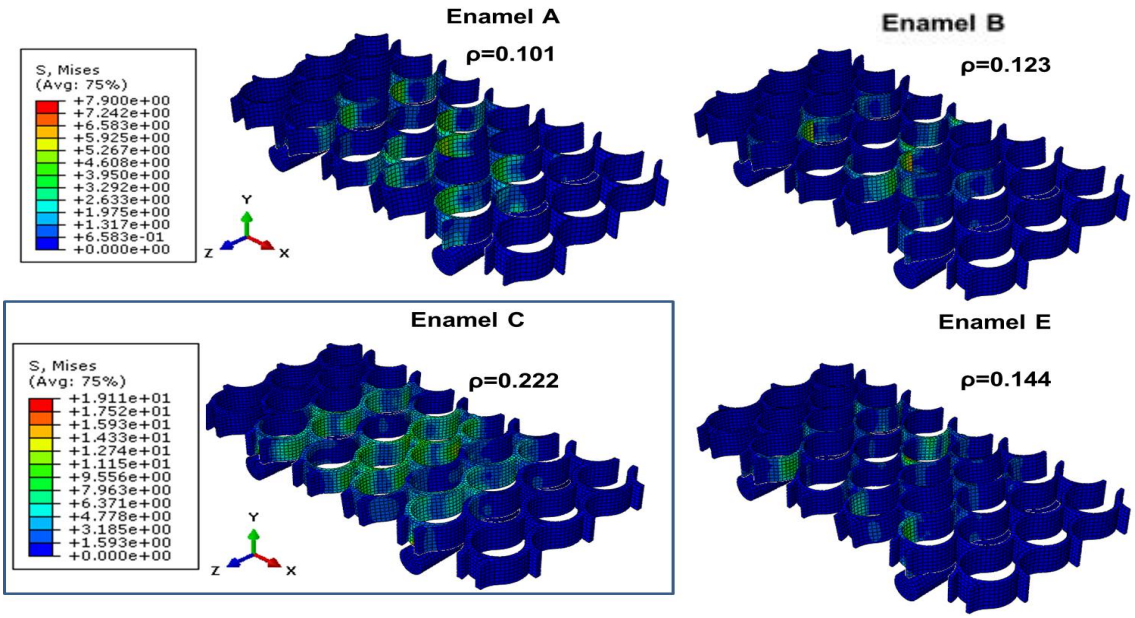

Figure 4.25: Finite element von Mises stress after 3PB test for enamel arrangements with different relative densities.

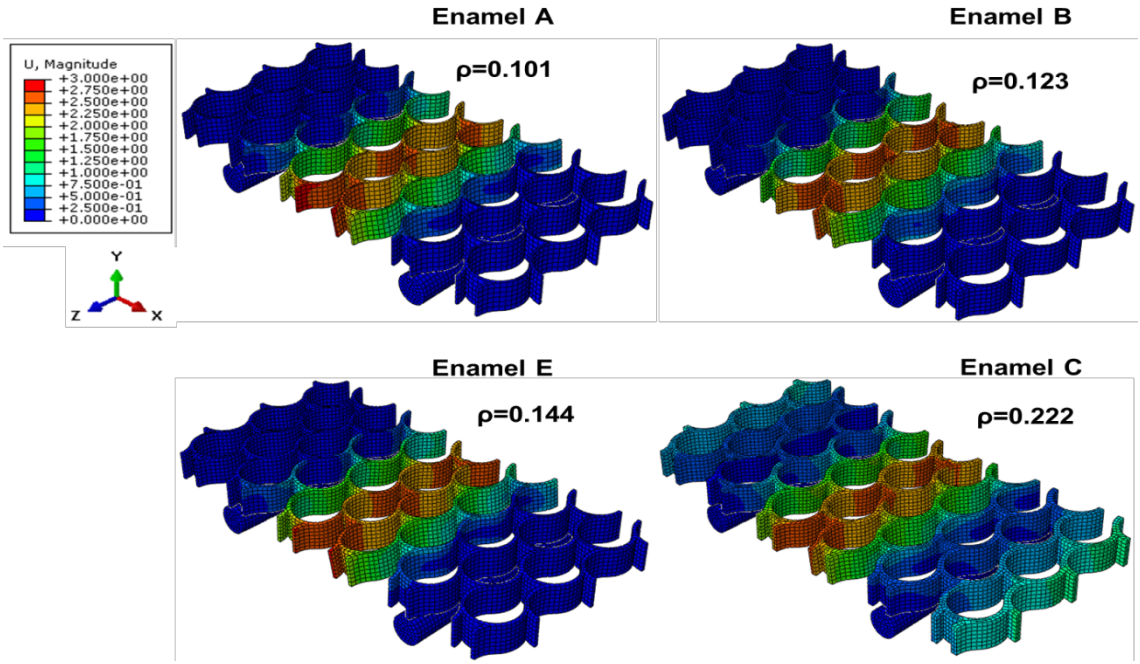

Figure 4.26: Finite element displacement after 3PB test for enamel assemblies with different relative densities.

Table 4.9: Von Mises stress (S) and displacement (U) for enamel configurations.

	ρ (-)	S-von Mises stress (MPa)	U-Displacement (mm)
Enamel A	0.101	7.85	2.98
Enamel B	0.123	6.66	2.73
Enamel E	0.144	6.16	2.91
Enamel C	0.222	19.11	2.67

4.1.3.3. Bamboo configuration

The stress value for the bamboo structure is almost the same for the four samples, being a bit larger in the bamboo_1 structure with the value of 19.31 MPa (Table 4.10). Analysing Figure 4.27, one can observe that as it happened in the honeycomb configuration, the maximum stress was attained where the structure is in contact with the supports and closer to the triple junction.

Finally, Figure 4.28 shows that the maximum value of the displacement is attained in the middle of the module and the highest displacement is reached in bamboo_1_16.

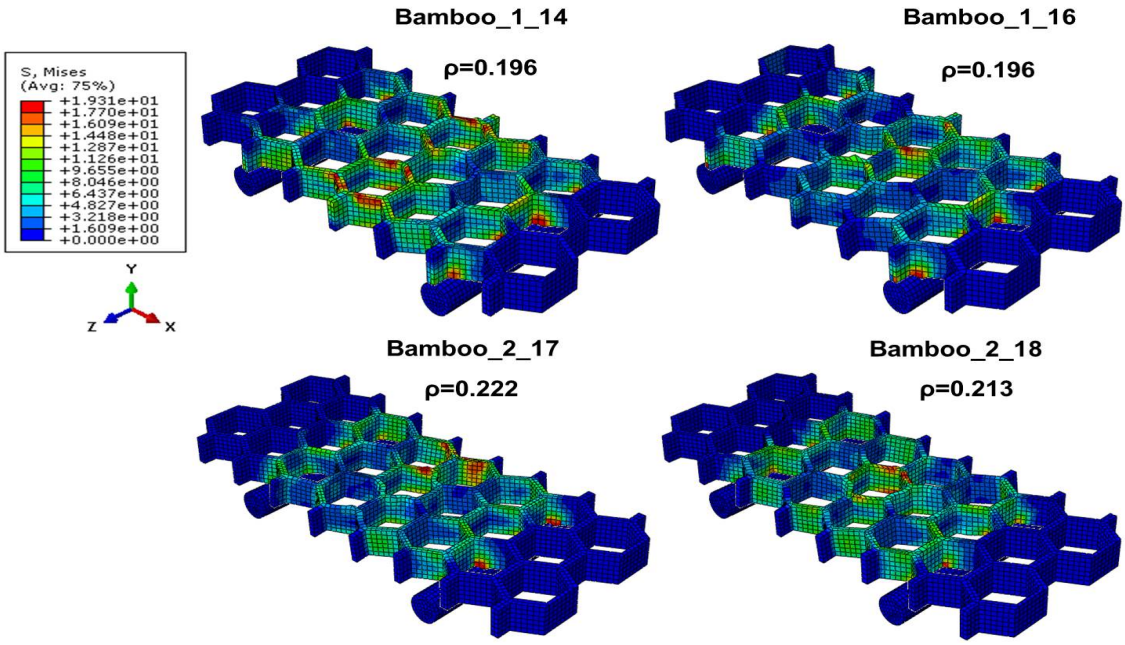

Figure 4.27: Finite element von Mises stress after 3PB test for bamboo configurations with different relative densities.

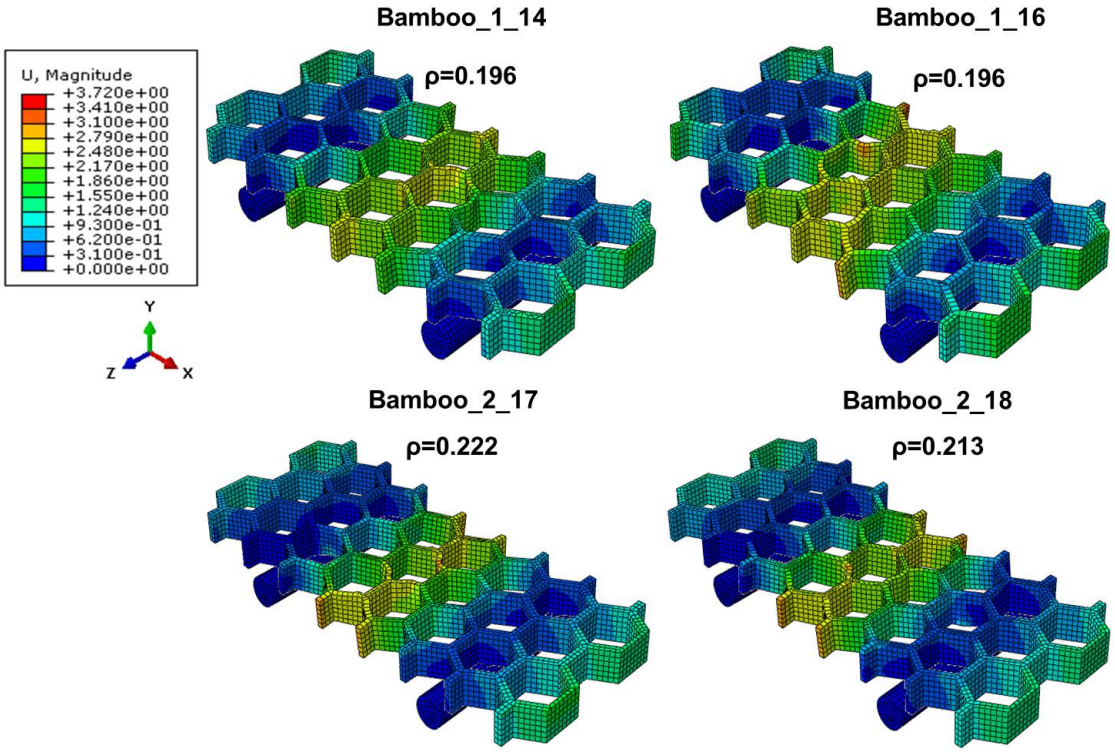

Figure 4.28: Finite element displacement after 3PB test for bamboo arrangements with different relative densities.

Table 4.10: Von Mises stress (S) and displacement (U) for bamboo configurations.

	ρ (-)	S-von Mises stress (MPa)	U-Displacement (mm)
Bamboo1_14	0.196	19.31	2.90
Bamboo1_16	0.196	19.31	3.72
Bamboo2_17	0.222	19.16	3.12
Bamboo2_18	0.213	19.19	3.16

4.1.3.4. Analysis and discussion of the results

As it was done with the compression test, the same process was followed to analyse the final results after the numerical simulations. The load-displacement curves for each configuration and relative density are represented in the next plots. In this way it can easily be seen how the relative density influences the mechanical behaviour.

As shown in Figure 4.29 (a) and Figure 4.30 (a) with just an increase of 0.1 in the relative density, the load rises from almost 50 N to more than 300 N, in the honeycomb arrangements and 5.3N to almost 80N in enamel configuration. To appreciate the slight differences between the lower relative cases, another plot without the higher density (C) has been included with a lower scale Figure 4.29 (b) and Figure 4.30 (b).

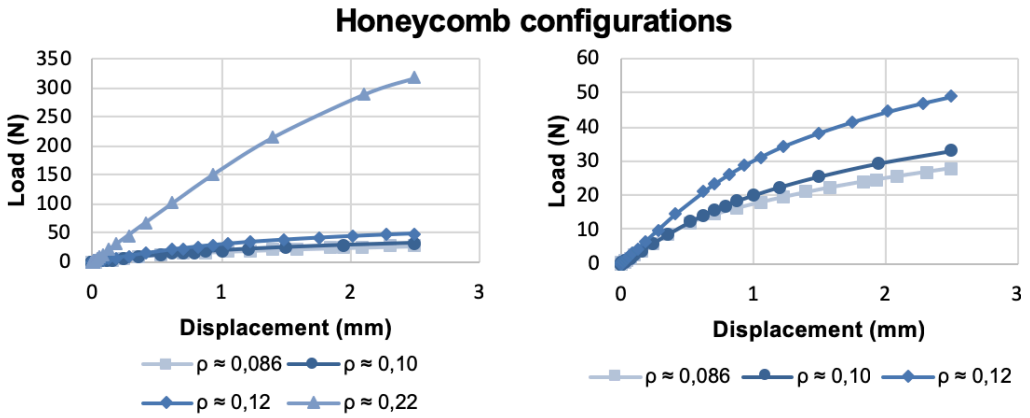

Figure 4.29: Load-displacement plot for, (a) honeycomb bending samples and, (b) honeycomb bending samples without C density.

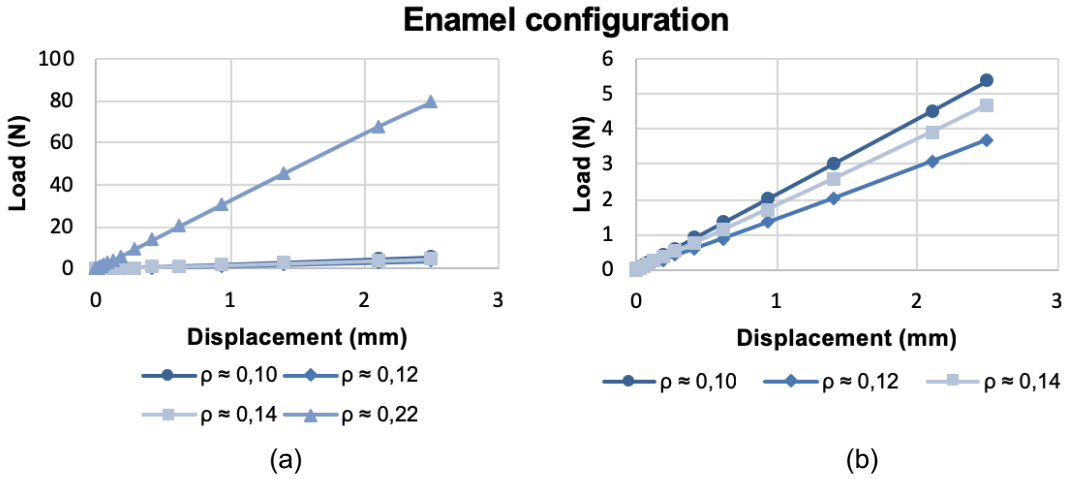

Figure 4.30: Load-displacement plot for, (a) enamel bending samples and (b) enamel bending samples without C density.

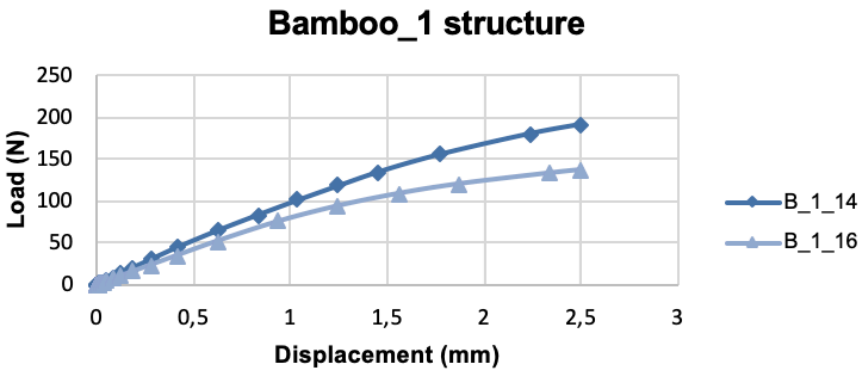

Figure 4.31: Load-displacement plot for the bending bamboo_1 structure.

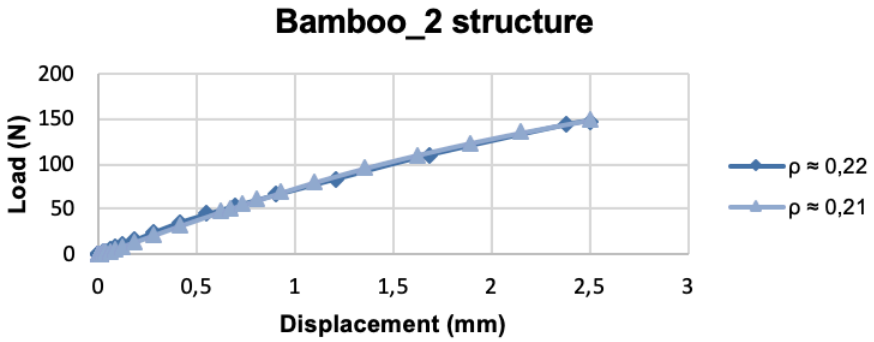

Figure 4.32: Load-displacement plot for the bending bamboo_2 structure.

For every configuration there is an elastic-linear response. Honeycomb is the arrangement that can reach the highest load value, experiencing a large increment of this load when the density change from 0.12 (B) to 0.22 (C). In honeycomb, as the relative density increases, there is a gain in the load. Nevertheless, this mentioned relation does not happen in the enamel assembly as it can be seen in Figure 4.30 (b). Enamel with 0.10 (A) has higher load value than 0.12 (B) and 0.14 (E). In comparison with the other two configurations enamel does not have a good response in bending situations.

In the middle of the load spectrum are the bamboo structures (Figure 4.31 and Figure 4.32). The two bending bamboo_1 structures have the same relative density 0.196, being this the reason why the name is in the plot rather than the relative density. Having the same density, the sample that starts with thickness of 1.4 mm reaches a slightly higher load. This indicates, as it happened in compression test, that the increase of the cell walls in bamboo_1 structure plays an important role. As it can be observed in bamboo_2 structure with a slight difference in the relative density, the curve is the same.

To analyse the most important parameters and compare the three configurations Table 4.11 was created. The maximum von Mises stress (σ_{vM}), the initial stiffness (K) and the energy absorbed (E_a) until maximum load were normalized by the relative density.

Table 4.11: Normalized numerical simulation results by the relative density for the 3PB test.

	ρ (-)	σ_{vM}/ρ (MPa)	K/ρ (N/mm)	E_a/ρ (J)
Honeycomb D	0.086	220.97	234.13	0.405
Honeycomb A	0.106	181.09	206.36	0.389
Honeycomb B	0.125	153.60	263.02	0.487
Honeycomb C	0.229	85.31	593.77	1.732
Enamel A	0.101	78.08	21.30	0.067
Enamel B	0.123	54.21	11.88	0.038
Enamel E	0.144	42.69	12.85	0.041
Enamel C	0.222	85.97	144.01	0.446
Bamboo_1_14	0.196	98.60	508.26	1.223
Bamboo_1_16	0.196	98.47	417.68	0.876
Bamboo_2_17	0.222	86.34	279.31	0.834
Bamboo_2_18	0.213	89.89	302.43	0.874

For honeycomb structures, as the relative density increases the maximum stress decreases but the stiffness and the energy absorbed enhance. This response cannot be observed in the other two structures.

Comparing the maximum stress, bamboo_1 structure has the highest values whereas for the relative density around 0.22 (C), honeycomb presents the lower value. However, the maximum value of stiffness and energy absorbed is attained for honeycomb with a density (C).

It is remarkable that the enamel arrangements when compared against the other configurations does not have a good response in bending situations. For instance, the energy absorbed shows very low values.

4.2. Experimental results

Some selected samples were printed in PLA by FDM technique and experimentally tested under compression and bending tests. The data was extracted from the machine with the software Bluehill. The load-displacement curve was obtained and afterwards the most important parameters for each test were calculated.

Experimental and finite elements results have been compared in these two sections for each test and for the selected PLA samples.

4.2.1. Compression

Figure 4.33 shows the results obtained for the compression test, experimentally (a) and with FE simulations (b). The load-displacement distributions for each case are included side by side for ease of comparison.

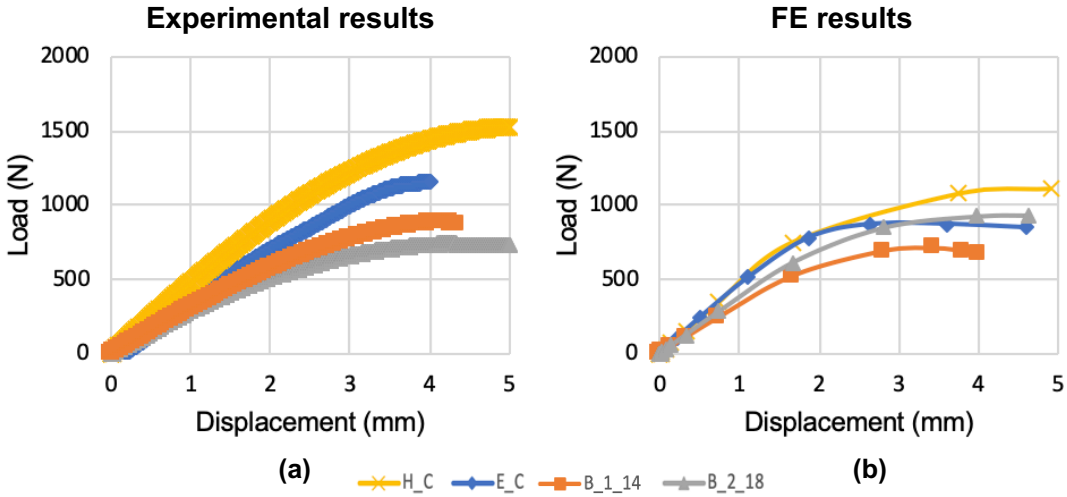

Figure 4.33: Load-displacement curves for (a) compression experimental results, and (b) compression FE results.

From the load-displacement curves the initial stiffness (K), the energy absorbed (E_a), the maximum stress (σ_{max}) and the maximum strain (ε) were calculated. Table 4.12 and Table 4.13 show the values of these parameters normalized by the relative density. Table 4.12 displays the experimental results whilst Table 4.13 summarises the finite elements results.

Table 4.12: Experimental results for compression tests.

	ρ (-)	K/ρ (N/mm)	E_a/ρ (J)	σ_{max} (MPa)	ε
Honeycomb C	0.229	1957.69	16.351	1.05	0.049
Enamel C	0.222	1732.08	10.392	1.23	0.071
Bamboo_1_14	0.205	1414.32	8.565	0.65	0.043
Bamboo_2_18	0.216	1215.73	6.830	0.54	0.050

Table 4.13: FE results for compression tests.

	ρ (-)	K/ρ (N/mm)	E_a/ρ (J)	σ_{max} (MPa)	ε
Honeycomb C	0.229	1981.54	11.947	0.81	0.048
Enamel C	0.222	1925.99	7.095	0.67	0.047
Bamboo_1_14	0.205	1544.05	5.971	0.53	0.034
Bamboo_2_18	0.216	1724.78	10.033	0.69	0.046

Figure 4.33 (a) and (b), show that the load-displacement curves for experimental and FE results presents the same trend, with the honeycomb sample being the structure that reaches more capacity of load support in both cases. However, there are discrepancies between the experimental and computational results both in terms of trends and absolute values. It should be noted that the experimental data displays higher load values than the FE results. Indeed, in Figure 4.33 (a) the honeycomb configuration appears to be the one able to withstand the highest load for a given displacement, followed by the enamel, the bamboo_1 structure and bamboo_2 configuration. On the contrary, FE results in Figure 4.33 (b) suggest that the bamboo_1 assembly carries the lowest load, with negligible differences between the bamboo_2 arrangement and the enamel configuration. An interesting fact to highlight is that experimentally, the enamel maximum displacement before failure was much lower than the bamboo structures (4mm) although for higher load whilst the FE method predicted equal values of maximum load and displacement for enamel and bamboo_2. Differences between both plots and tables can be due to the manufacturing process and the differences in the material that was used in the FE simulations and that was used to print the samples.

Figure 4.34 shows the samples after the compression test allowing to do an analysis of the failed samples by visual inspection. For the enamel instance, the finally failure does not appear in the same place where the maximum stress is attained in the numerical simulations. The same happened with the honeycomb configuration, as it broke in the corner instead of the triple junction where the maximum stress appeared in the simulations. These differences may be due to the printed samples defects such as air gaps or tilt of the walls. Although the final failure did not match the FE predictions, the deformation of the samples is similar.

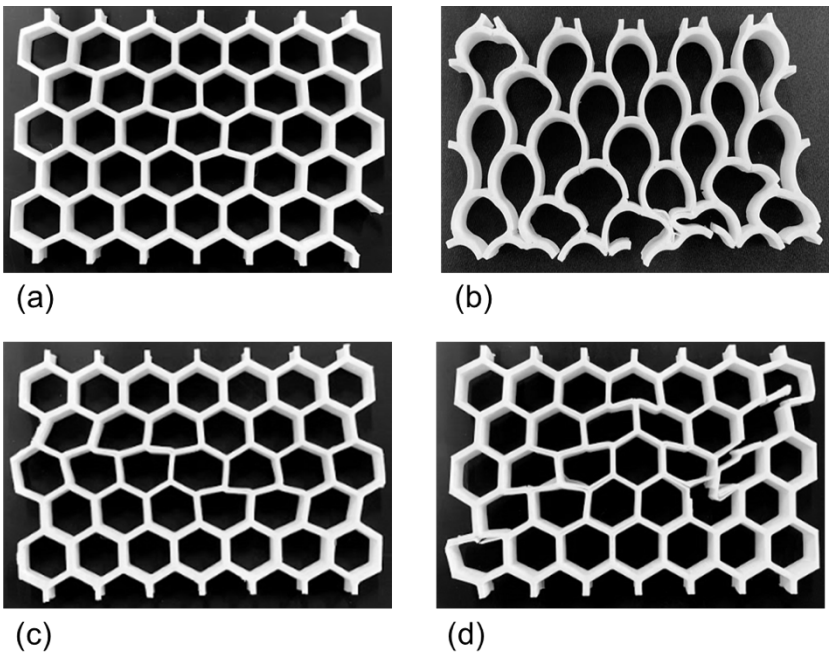

Figure 4.34: PLA samples after compression test, (a) honeycomb C, (b) enamel C, (c) bamboo_1_14, and (d) bamboo_2_18.

4.2.2. Three point bending

Figure 4.35 (a) and (b), show the experimental and the finite elements results obtained for the three point bending test.

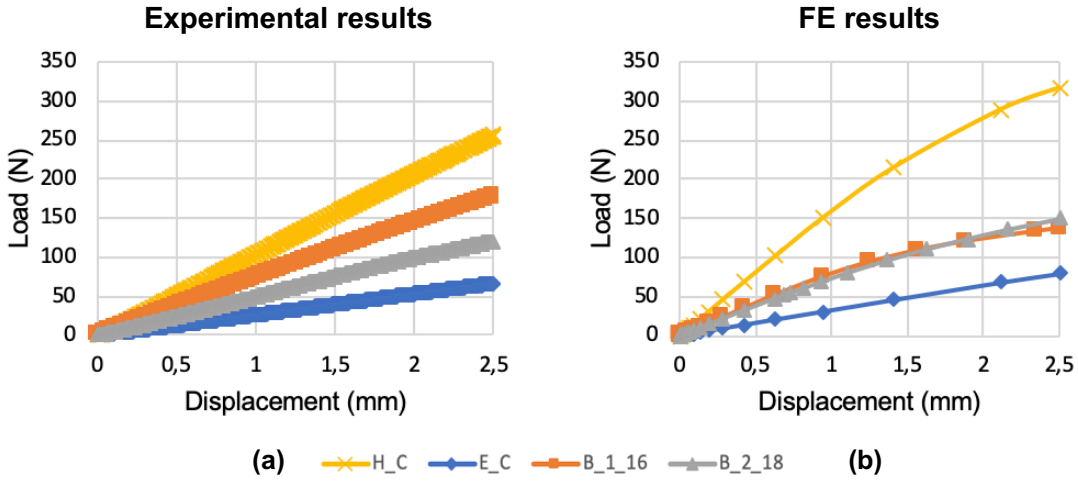

Figure 4.35: Load-displacement curves for (a) 3PB experimental results, and (b) 3PB FE results.

From the load-displacement curves the initial stiffness (the slope of the linear region) and the energy absorbed until maximum load were calculated. These two parameters are included in Table 4.14 where they can be compared to the FE results.

Table 4.14: Experimental and FE results for 3PB test.

		Experimental		FE	
	ρ (-)	K/ρ (N/mm)	E_a/ρ (J)	K/ρ (N/mm)	E_a/ρ (J)
Honeycomb C	0.229	453.65	1.401	593.77	1.732
Enamel C	0.222	320.79	0.378	144.01	0.446
Bamboo_1_16	0.196	252.14	1.134	417.68	0.876
Bamboo_2_18	0.213	126.29	0.708	302.43	0.874

Load-displacement curves exhibit the same response for both plots, experimental and FE, corroborating that honeycomb has the best behaviour under the conditions of the bending test and enamel is the configuration with lower capacity of load support. Despite an apparent overprediction of the load from the FE results (apart from the bamboo_1 structure), since the other configurations attain more load in the FE results than in the experimental results. It seems that the material problem commented in the compression test does not affect the bending test as both experimental and FE results are of the same order of magnitude, with the differences being attributable to the manufacturing process where the material is not printed homogenously having some air gaps inside the walls.

Finally, in Figure 4.36 one can see the failed samples after the three point bending test. For honeycomb, enamel and bamboo_1 structure the failure starts at the points where the FE shows higher stress. However for bamboo_2 arrangement, the failure occurs in the middle of the wall meaning that the failure was caused due to the air gaps.

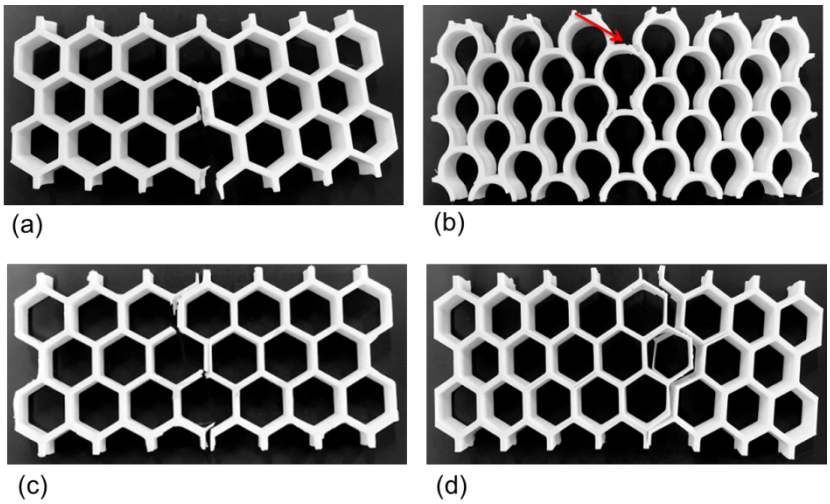

Figure 4.36: PLA samples after 3PB test, (a) honeycomb C, (b) enamel C, (c) bamboo_1_16, and (d) bamboo_2_18.

5. Conclusions

Conclusions

This dissertation analyses the features of two new core structures based on bioinspired natural materials obtained by simulations and by experiments. Among all natural sources, enamel and bamboo were selected to study their characteristics and compare them with the classic honeycomb. Compression and three point bending tests were carried out to predict the failure behaviour in both the numerical simulation and experimental tests. Generally, a good agreement was found between FE results and experimental results. For the three configurations analysed and for both tests, the mechanical properties show a strong dependency on the core geometry and the relative density.

For instance, enamel arrangements have good response in the compression test with a maximum load of the same order of magnitude than honeycomb configuration achieved. However, under the same conditions, for the bending test, enamel has low load capacity even for the highest relative density where the load undergoes a large increase with respect to the other relative densities.

Regarding the bamboo structure, as it is a graded configuration it can be appreciate that the results of both tests change due to the different distribution of the thickness despite all configurations having a similar relative density. For compression test, the bamboo_2 assemblies have the same order of magnitude as the honeycomb and enamel, nevertheless, bamboo_1 structure has less capacity of compression load. For the three point bending test, the bamboo structure have an intermediate load capacity, being between honeycomb, which has double bending load capacity, and enamel which has half of the bending load capacity, respect the bamboo structure.

The maximum strain calculated in the compression test shows that for the three configurations and the same average relative density, all of them have more or less the same strain value being a little bit less for the bamboo_1 structure.

Finally, this study provides evidence to conclude that for the same relative density, the bioinspired structures may compete with the traditional core structures in what concerns to strength, stiffness and energy absorption.

Future work

In this study was designed, numerically simulated, and experimentally tested two new configurations based on bioinspired natural materials in order to be compared with the classic and most common structure, the honeycomb arrangement. Future work on this area will consist of finding new bioinspired structures in order to analyse and study the mechanical properties and features under a compression and 3PB tests. In addition, it would be interesting to carry out a parametric study with the studied structures with the aim to establish a hierarchical architecture that could potentially rank the influence of each one of the design variables on the mechanical properties.

Bibliography

[1] L.J. Gibson, M.F. Ashby, Cellular Solids: Structure and properties, Cambridge University Press, 1997. doi:10.1557/mrs2003.79.

[2] W. Becker, Closed-form analysis of the thickness effect of regular honeycomb core material, Compos. Struct. 48 (2000) 67–70. doi:10.1016/S0263-8223(99)00074-4.

[3] I.G. Masters, K.E. Evans, Models for the elastic deformation of honeycombs, Compos. Struct. 35 (1996) 403–422. doi:10.1016/S0263-8223(96)00054-2.

[4] H. Araújo, M. Leite, A. Ribeiro, A. Deus, L. Reis, M.F. Vaz, The effect of geometry on the flexural properties of cellular core structures, Proc. Inst. Mech. Eng. Part L J. Mater. Des. Appl. (2018). doi:10.1177/1464420718805511.

[5] A. Uzal, F.O. Sonmez, F.E. Oz, K. Cinar, N. Ersoy, A composite sandwich plate with a novel core design, Compos. Struct. 193 (2018) 198–211. doi:10.1016/j.compstruct.2018.03.047.

[6] Hexcel Composites, Honeycomb sandwich design technology, 1995. doi:AGU 075b.

[7] F. Campbell, Structural Composite Materials. ASM International., 2010.

[8] T. Bitzer, Honeycomb Technology, Springer, Dublin, USA, 1997. doi:10.1007/978-94-011-5856-5.

[9] W. Ronan, V.S. Deshpande, N.A. Fleck, The tensile ductility of cellular Solids: The role of imperfections, Int. J. Solids Struct. 102–103 (2016) 200–213. doi:10.1016/j.ijsolstr.2016.10.004.

[10] J. Kramberger, M. Šraml, S. Glodež, Computational study of low-cycle fatigue behaviour of lotus-type porous material, Int. J. Fatigue. 92 (2016) 623–632. doi:10.1016/j.ijfatigue.2016.02.037.

[11] R.F. Gibson, Principles of Composite Material Mechanics, 1994. doi:10.1074/jbc.M409278200.

[12] U.G.K. Wegst, H. Bai, E. Saiz, A.P. Tomsia, R.O. Ritchie, Bioinspired structural materials, Nat. Mater. 14 (2015) 23–36. doi:10.1038/nmat4089.

[13] M.A. Meyers, P.Y. Chen, A.Y.M. Lin, Y. Seki, Biological materials: Structure and mechanical properties, Prog. Mater. Sci. 53 (2008) 1–206. doi:10.1016/j.pmatsci.2007.05.002.

[14] M.S. Aziz, A.Y. El Sherif, Biomimicry as an approach for bio-inspired structure with the aid of compu tation, Alexandria Eng. J. 55 (2016) 707–714. doi:10.1016/j.aej.2015.10.015.

[15] P. Fratzl, Biomimetic materials research: What can we really learn from nature's structural materials?, J. R. Soc. Interface. 4 (2007) 637–642. doi:10.1098/rsif.2007.0218.

[16] J.M. Rensberger, Mechanical adaptation in enamel, in: Tooth Enamel Microstruct., Koenigswal, Balkema, 1997: pp. 237–257.

[17] D. Haines, Physical properties of human tooth enamel and enamel sheath material under load, J. Biomech. 1 (1968) 117–118. doi:10.1016/0021-9290(68)90014-6.

[18] J. Ge, F.Z. Cui, X.M. Wang, H.L. Feng, Property variations in the prism and the organic sheath within enamel by nanoindentation, Biomaterials. 26 (2005) 3333–3339. doi:10.1016/j.biomaterials.2004.07.059.

[19] L.H. He, N. Fujisawa, M. V. Swain, Elastic modulus and stress-strain response of human enamel by nano-indentation, Biomaterials. 27 (2006) 4388–4398.

doi:10.1016/j.biomaterials.2006.03.045.

[20] B.R. Lawn, J.J.-W. Lee, H. Chai, Teeth: Among Nature's Most Durable Biocomposites, Annu. Rev. Mater. Res. 40 (2010) 55–75. doi:10.1146/annurev-matsci-070909-104537.

[21] S. Amada, Y. Ichikawa, T. Munekata, Y. Nagase, H. Shimizu, Fiber texture and mechanical graded structure of bamboo, Compos. Part B Eng. 28 (1997) 13–20. doi:10.1016/S1359-8368(96)00020-0.

[22] P. Van Der Lugt, Design interventions for stimulating bamboo commercialization, Delft Univ, Rotterdam, 2008.

[23] J. Vogtländer, P. Van Der Lugt, H. Brezet, The sustainability of bamboo products for local and Western European applications. LCAs and land-use, J. Clean. Prod. 18 (2010) 1260–1269. doi:10.1016/B978-0-12-375688-6.10082-9.

[24] U.G.K. Wegst, Bending efficiency through property gradients in bamboo, palm, and wood-based composites, J. Mech. Behav. Biomed. Mater. 4 (2011) 744–755. doi:10.1016/j.jmbbm.2011.02.013.

[25] N. Matheson, J. Schmidt, J. Travis, Isolation and properties of an angiotensin II-cleaving peptidase from mesquite pollen., Am. J. Respir. Cell Mol. Biol. 12 (1995) 441–448. doi:10.1165/ajrcmb.12.4.7695924.

[26] L.J. Gibson, P.G. Dixon, The structure and mechanics of Moso bamboo material, J. R. Soc. Interface. 11 (2014). doi:10.1098/rsif.2014.0321.

[27] D. Grosser, W. Liese, On the anatomy of Asian bamboos, with special reference to their vascular bundles, Wood Sci. Technol. 5 (1971) 290–312. doi:10.1007/BF00365061.

[28] T. Tan, N. Rahbar, S.M. Allameh, S. Kwofie, D. Dissmore, K. Ghavami, W.O. Soboyejo, Mechanical properties of functionally graded hierarchical bamboo structures, Acta Biomater. 7 (2011) 3796–3803. doi:10.1055/s-0043-109481.

[29] K. Ghavami, Bamboo as reinforcement in structural concrete elements, Cem. Concr. Compos. 27 (2005) 637–649. doi:10.1016/j.cemconcomp.2004.06.002.

[30] A.A. Yazdi, A. Popma, W. Wong, T. Nguyen, Y. Pan, J. Xu, 3D printing: an emerging tool for novel microfluidics and lab-on-a-chip applications, Microfluid. Nanofluidics. 20 (2016) 1–18. doi:10.1007/s10404-016-1715-4.

[31] J.P. Kruth, Material Incress Manufacturing by Rapid Prototyping Techniques, CIRP Ann. - Manuf. Technol. 40 (1991) 603–614. doi:10.1016/S0007-8506(07)61136-6.

[32] B.N. Turner, R. Strong, S.A. Gold, A review of melt extrusion additive manufacturing processes : I . Process design and modeling, 3 (2014) 192–204. doi:10.1108/RPJ-01-2013-0012.

[33] M.H. Michalski, J.S. Ross, The shape of things to come: 3D printing in medicine, JAMA - J. Am. Med. Assoc. 312 (2014) 2213–2214. doi:10.1001/jama.2014.9542.

[34] Ian Gibson · David Rosen Brent Stucker, Additive Manufacturing Technologies, 2015. doi:10.1520/F2792-12A.2.

[35] K. Modjarrad, S. Ebnesajjad, Handbook of Polymer Applications in Medicine and Medical Devices, Elsevier, 2013. doi:10.1016/C2012-0-07906-9.

[36] D. Garlotta, Journal of Environmental Polymer Degradation, 9 (2002) 63–84.

[37] E.T.H. Vink, D.A. Glassner, J.J. Kolstad, R.J. Wooley, R.P. O'Connor, ORIGINAL RESEARCH: The eco-profiles for current and near-future NatureWorks® polylactide (PLA) production, Ind. Biotechnol. 3 (2007) 58–81. doi:10.1089/ind.2007.3.058.

[38] J. Fernandes, A.M. Deus, L. Reis, M.F. Vaz, M. Leite, Study of the influence of 3D printing parameters on the mechanical properties of PLA, Proc. Int. Conf. Prog. Addit. Manuf. 2018–May (2018) 547–552. doi:10.25341/D4988C.

[39] Simulia, Abaqus Analysis User's Guide, (n.d.). doi:http://abaqus.software.polimi.it/v6.14/books/usb/default.htm.

[40] ASTM D695-15, Standard Test Method for Compressive Properties of Rigid Plastics, 2008. doi:10.1520/D0695-10.2.

[41] ASTM International, D 7264 Standard Test Method for Flexural Properties of Polymer Matrix Composite Materials, ASTM Stand. i (2007) 1–11. doi:10.1520/D7264.